UNIVERSIDADE DE LISBOA

INSTITUTO SUPERIOR TÉCNICO

Scalable Production of Extracellular Vesicles Derived from Mesenchymal Stromal Cells for Cancer-Targeted Drug Delivery

Miguel de Almeida Fuzeta

Supervisor: Doctor Cláudia Alexandra Martins Lobato da Silva

Co-supervisors: Doctor Diana Maria Diez Gaspar

Doctor Nuno Filipe Santos Bernardes

Thesis approved in public session to obtain the PhD Degree in Bioengineering

Jury final classification: Pass with Distinction

2021

TÉCNICO LISBOA

UNIVERSIDADE DE LISBOA

INSTITUTO SUPERIOR TÉCNICO

Scalable Production of Extracellular Vesicles Derived from Mesenchymal Stromal Cells for Cancer-Targeted Drug Delivery

Miguel de Almeida Fuzeta

Supervisor: Doctor Cláudia Alexandra Martins Lobato da Silva

Co-supervisors: Doctor Diana Maria Diez Gaspar

Doctor Nuno Filipe Santos Bernardes

Thesis approved in public session to obtain the PhD Degree in Bioengineering

Jury final classification: Pass with Distinction

Jury

Chairperson: Doctor Joaquim Manuel Sampaio Cabral, Instituto Superior Técnico, Universidade de Lisboa

Members of the committee:

Doctor Pieter Vader, University Medical Center Utrecht, The Netherlands

Doctor Cláudia Alexandra Martins Lobato da Silva, Instituto Superior Técnico, Universidade de Lisboa

Doctor Fábio Monteiro Fernandes, Instituto Superior Técnico, Universidade de Lisboa

Doctor Ana Margarida Pires Fernandes-Platzgummer, Instituto Superior Técnico, Universidade de Lisboa

Doctor Rita Leonor Álvares Cabral de Figueiredo Fior Sousa Soares, Champalimaud Centre for the Unknown, Champalimaud Foundation

Doctor Joana Simões Correia, Exogenus Therapeutics

Funding institutions: Fundação para a Ciência e Tecnologia

European Research Council

2021

Abstract

Extracellular vesicles (EVs) have been the focus of great attention over the last decade for their promising application both as intrinsically therapeutic agents in regenerative medicine and as drug delivery vehicles. In particular, mesenchymal stromal cells (MSC) have been regarded as a promising source for the production of EVs for biomedical applications, considering their intrinsic beneficial therapeutic properties, favorable safety profile and good expansion capacity when cultured *ex vivo*. In spite of the promising potential of EVs for therapeutic applications, robust and scalable manufacturing processes for EV production are still lacking.

In this work, a serum-/xeno-free (S/XF) microcarrier-based culture system was implemented in a Vertical-Wheel™ bioreactor, employing a human platelet lysate culture supplement, towards the scalable production of MSC-derived EVs (MSC-EVs). EVs were produced using MSC isolated from three different human tissue sources (bone marrow (BM), adipose tissue (AT) and umbilical cord matrix (UCM)). When compared to static culture systems (i.e. T-flasks), the bioreactor system improved EV manufacturing yields (5.7-fold increase overall) and stimulated the secretion of more EVs per cell (3-fold increase overall), after EV isolation using a commercial precipitation kit.

The functional activity of both BM and UCM MSC-EVs was studied in conditions closely translatable to a clinical setting. MSC were cultured under S/XF conditions using planar systems, and a scalable and selective EV isolation method based on size exclusion chromatography (SEC) was applied. Both BM and UCM MSC-EVs revealed a similar pro-angiogenic activity, by improving sprouting of endothelial spheroids in a 3D *in vitro* model, leading to 1.9-fold increase in total sprouting length per spheroid.

Lastly, SEC-isolated MSC-EVs were surface-modified with the p28 peptide to develop anti-cancer drug delivery systems (DDS). This peptide derived from the bacterial protein azurin is able to preferentially enter a variety of cancer cells. Here we observed that p28 increased EV uptake into breast cancer cells by 2.4-fold, revealing the possibility to functionalize MSC-EVs with p28 for the development of novel EV-based DDS for cancer therapy.

Overall, it was demonstrated throughout this thesis the possibility of using manufacturing strategies closely translatable to clinical settings to obtain MSC-EVs applicable both for regenerative medicine, by demonstrating their inherent pro-angiogenic capacity, as well as for drug delivery, due to the possibility to modify these MSC-EVs with a cancer-targeting peptide.

Keywords: extracellular vesicles, mesenchymal stromal cells, scalable production, drug delivery systems, anti-cancer therapy

Resumo

As vesículas extracelulares (EVs) têm tido especial destaque na última década pelas suas aplicações promissoras tanto como agentes intrinsecamente terapêuticos em medicina regenerativa, bem como veículos para entrega de fármacos. Em particular, as células estromais mesenquimais (MSC) têm sido consideradas uma fonte promissora para a produção de EVs para aplicações biomédicas, tendo em conta as suas propriedades terapêuticas inerentes, um perfil de segurança favorável e uma boa capacidade de expansão quando cultivadas *ex vivo*. Apesar do potencial promissor das EVs para aplicações terapêuticas, ainda estão em falta processos de produção escaláveis e robustos.

Neste trabalho, foi implementado um sistema de cultura baseado em "microcarriers" num bioreactor "Vertical-Wheel™", em condições de cultura sem soro nem componentes de origem xenogénica (S/XF), utilizando como suplemento de cultura um lisado de plaquetas humanas, tendo em vista a produção escalável de EVs produzidas por MSC (MSC-EVs). Foram produzidas EVs utilizando MSC isoladas a partir de três fontes de tecido humano diferentes (medula óssea (BM), tecido adiposo (AT) e matriz do cordão umbilical (UCM)). Quando comparado com sistemas de cultura estáticos (i.e. T-flasks), o sistema implementado no bioreactor aumentou o rendimento de produção de EVs (5.7 vezes no global), tendo inclusivamente estimulado a secreção de uma quantidade superior de EVs por cada célula (3 vezes superior no global), após isolamento de EVs recorrendo a um kit de precipitação comercial.

A actividade funcional de MSC-EVs tanto de BM como de UCM foi estudada em condições passíveis de serem transpostas para um contexto clínico. As MSC foram cultivadas em condições S/XF em sistemas planares e foi aplicado um método de isolamento de EVs escalável e selectivo, baseado em cromatografia de exclusão molecular (SEC). Tanto as MSC-EVs com origem em BM como em UCM apresentaram uma actividade pro-angiogénica semelhante, aumentando a formação de protrusões celulares em esferoides de células endoteliais num modelo 3D *in vitro*, levando a um aumento do comprimento total destas protrusões por esferoide em 1.9 vezes.

Por fim, MSC-EVs isoladas por SEC foram modificadas à superfície com o péptido p28 para desenvolver sistemas de entrega de fármacos anti-cancerígenos. Este péptido derivado da proteína bacteriana azurina tem a capacidade de entrar preferencialmente em vários tipos de células de cancro. Neste trabalho observámos que o p28 aumentou em 2.4 vezes a internalização de EVs em células de cancro de mama, revelando a possibilidade de utilizar MSC-EVs decoradas com p28 para o desenvolvimento de novos sistemas de entrega de fármacos baseados em EVs para terapia de cancro.

No global, ao longo desta tese foi demonstrada a possibilidade de usar estratégias de produção passíveis de serem transpostas para um contexto clínico, por forma a obter MSC-EVs aplicáveis tanto para medicina regenerativa, demonstrando a sua capacidade pro-angiogénica inerente, bem como para entrega de fármacos, devido à possibilidade de modificar estas MSC-EVs com péptidos direccionados para células de cancro.

Palavras-chave: vesículas extracelulares, células estromais mesenquimais, produção escalável, sistemas de entrega de fármacos, terapia anti-cancro

Acknowledgements

In the next few pages I would like to acknowledge all the people that, in a way or another, have contributed for this PhD thesis. Either for having a major role in the development of this work, for helping me out when I needed their collaboration or simply for being part of my life, the people mentioned in these paragraphs have had a positive impact upon me and made this PhD possible.

I want to thank my supervisors (from IST) Cláudia Lobato da Silva and Nuno Bernardes for all the guidance and for giving me the freedom to pursue my ambitions. For sharing my passion for science and for always giving a great support and encouragement in all my scientific endeavors, from writing papers, to participating in conferences and to going abroad for part of my PhD thesis. I thank Cláudia for teaching me much more than science but more importantly how to develop my scientific work and establish good interactions with members of the work environment. I also thank her for making situations look simpler than I thought before and for always making me feel calmer after our meetings when I was feeling more stressed. I thank Nuno for our long debates and scientific discussions as well as for helping me whenever I was struggling with unforeseen experimental challenges. I feel very lucky to have supervisors with whom I share a great empathy and to have created not only a great professional relationship but also one of friendship.

I thank Professor Joaquim Cabral for making this work possible by accepting me at SCERG. For all his key leading roles at iBB, at SCERG and in the MIT Portugal Program, which made it possible for me to follow my dream of studying Bioengineering. For always supporting my work, for sharing my fascination with bioprocessing and bioengineering and for having inspired me since my first year as a Biological Engineering student at IST.

I thank my supervisor Diana Gaspar (previously iMM Lisboa, currently GenIbet) for her decisive initiative in the foundation of this project and for all her support and encouragement. I thank my PhD colleague Filipa Oliveira (iMM) for, together with Diana, sharing their previous knowledge on working with extracellular vesicles, enabling the establishment of this research area in IST. I also thank Diana and Filipa for performing AFM and zeta potential characterization of EVs. I extend my gratitude to Professor Miguel Castanho (iMM) for giving me the opportunity to be part of his research group, as well as to all the members of his group for welcoming me.

I would like to thank all the members of SCERG that have made this work possible for their collaboration and for the great working environment we are fortunate to have in our group. To Ana Fernandes-Platzgummer for her crucial role in this project, by helping and supporting in all stem cell-related work and in the development of bioprocessing strategies for EV manufacturing. Also for sharing my enthusiasm for constantly improving our lab and acquiring

new equipment to make increasingly more interesting experiments. I also thank to Raquel Cunha for together with Ana collaborating in our EV group workforce, for her great contribution to support the implementation of this research area in our group.

I thank Carlos Rodrigues for introducing me to Vertical-Wheel bioreactors during MIT Portugal PhD classes and for playing an important role in disseminating the use of these bioreactors in our group, as well as for our enjoyable interactions throughout these years.

I thank previous SCERG members Diogo Pinto and Marta Costa for introducing me to working with stem cells and for teaching me so much in the lab and about the life of a PhD student. Also to Cátia Bandeiras for our collaboration in my first ever research paper and for the great interaction we had as office partners.

I want to thank my Lab 3 colleagues that have been working together with me over the past years Carina Manjua, André Branco, Marília Silva, Sara Bucar, Cristiana Ulpiano and Sara Morini for their help and companionship. Thanks for not only being amazing colleagues but also for becoming great friends. A special word to André for the partnership in our book chapter odyssey and for the many years of friendship since the beginning of our Biological Engineering degree. I also extend this gratitude to my long-term colleague Diogo Nogueira for his constant help and availability ever since I first arrived at SCERG, for our shared enthusiasm for science and other non-scientific matters, for always giving me the motivation to push forward and for being a great friend.

I thank Ana Catarina Costa for her amazing work together with me during her Master's thesis as well as afterwards, making a crucial contribution for the success of this PhD thesis. I am also grateful to Jaqueline Garcia for her vital support in managing the lab, going above and beyond to assure we have the best possible conditions to develop our work. To all the other SCERG members, I want to express my gratitude for these years sharing great moments together.

I thank Ana Rita Garizo, Andreia Pimenta and Dalila Mil-Homens for our interactions and for their help during my working periods at IST-Alameda. To Professor Arsénio Fialho for bringing the field of cancer therapy research to IST, making it possible for me to develop this PhD.

I want to thank José Paulo Farinha from CQE-IST and the members of his group for supporting me on the use of the NTA equipment, which was a key piece of my PhD.

I would like to acknowledge William Milligan and Rong-Jeng Tseng (AventaCell Biomedical Corp.) for scientific discussions and support regarding the use of human platelet lysate-based culture supplements (UltraGRO™), as well as Brian Lee and Sunghoon Jung (PBS Biotech) for scientific discussions and for their support regarding the use of Vertical Wheel™ bioreactors. I thank them for fostering great partnerships with our research group, supporting fruitful collaborations between academia and industry.

I would like to thank all the team that welcomed me at UMC Utrecht in The Netherlands. To Professor Joost Sluijter and Pieter Vader for so kindly receiving me at their research groups, for supervising and guiding my work there and for really allowing me to take my PhD project to the next level during this period, resulting in the work presented in Chapters 3 and 4 of this thesis. To my fellow PhD colleagues Marieke Roefs, Simon van de Wakker and Margarida Viola for exceedingly teaching me so many new techniques and for openly sharing their experience with me. To two great Master students Wilte Olijve and Marjolein Rozeboom for sharing many experiments with me. On a more personal level, I really want to thank this group of people for their friendship and for helping and supporting me during some troubled times caused by the pandemic. I also want to thank Sander Kooijmans and Olivier de Jong for their help at crucial moments during my research work there. I thank Professor Raymond Schiffelers for openly chatting with me when we met at an EACR congress in Cambridge and for putting me in touch with Joost and Pieter, making this collaboration possible. I also want to thank everyone at both the Experimental Cardiology Lab and CDL Research for welcoming me.

I thank to the members of my Thesis Commission (CAT) Rita Fior (Champalimaud Foundation) and Fábio Fernandes (iBB-IST) for their valuable inputs and contribution throughout my PhD. To Rita for our long-lasting friendship in science and to Fábio for our insightful interactions about EVs.

I thank Inês Ferreira and Rita Oliveira (CEDOC, Universidade NOVA de Lisboa) for their help and support unraveling the often challenging Western blots of EVs.

I thank to my MIT Portugal colleagues for sharing so many adventures during the first year of the PhD program, filled with classes, projects and amusing moments throughout Portugal.

I would also like to acknowledge Fundação para a Ciência e a Tecnologia (FCT), Portugal, for my PhD scholarship (SFRH/PD/BD/128328/2017) and the MIT Portugal Program.

Thank you to my college friends Carolina, Sabino, Rogério and Andreia whose friendship I deeply cherish. To all of my great friends Vasques, Prescott, Ginja, Rui, Pombeiro, Souto, Maria Medina, João Pires, João Vasques, Joana Dias and Zahra for their long-standing friendship. They say friends are the family you choose and I truly consider all of you to be extremely important in my life. I know you will always be there for me as I will for you.

To my girlfriend and life partner Rafaela for all of her love and for always being there for me. Thank you for always listening to me when I was excited about science and my work, as well as for encouraging me when I was feeling down. You mean the world to me. I also thank Rafaela's family, particularly her parents Luísa and Tiago for welcoming me as part of their own family and for always showing their support for me.

To my parents Helena and António, words are not enough to express my gratitude. Thank you for your love, for transmitting me good values, for encouraging me to pursue my dreams,

for opening my mind, for making me the man I am today. To my grandparents Aurora, Marcelino, Ondina and Celestino for their example of struggle and perseverance, and who will always be stars guiding my way through life.

Table of contents

List of tables

List of figures

List of abbreviations

αMEM	Minimum Essential Medium Eagle alpha
AFM	atomic force microscopy
ALIX	ALG‑2 interacting protein X
AT	adipose tissue
ATMP	advanced therapy medicinal products
ATP	adenosine triphosphate
BACE1	beta secretase 1
BACS	buoyancy-activated cell sorting
BBB	blood-brain barrier
BCA	bicinchoninic acid
BM	bone marrow
BMP-2	bone morphogenetic protein-2
BSA	bovine serum albumin
BSP	bone sialoprotein
CAR	chimeric antigen receptor
CCL2	C-C Motif Chemokine Ligand 2
CD	cluster of differentiation
CDK2	cyclin dependent kinase 2
CFD	computational fluid dynamics
CFU-F	colony-forming unit-fibroblasts
CIBN	CRY-interacting protein
CIP	clean-in-place
CM	conditioned medium
CML	chronic myeloid leukemia
CNS	central nervous system
COVID-19	coronavirus disease-19
CPC	cardiomyocyte progenitor cells
CPP	cell-penetrating peptide
DAPI	4′,6-diamidino-2-phenylindole
DC	dendritic cell
DDS	drug delivery system
DMEM	Dulbecco's Modified Eagle’s Medium
DMPE	1,2-Dimyristoyl-sn-glycero-3-phosphoethanolamine
DMSO	dimethyl sulfoxide
ECM	extracellular matrix

EDTA	ethylenediaminetetraacetic acid
EGF(R)	epidermal growth factor (receptor)
EMA	European Medicines Agency
EMMPRIN	extracellular matrix metalloproteinase inducer
EMT	epithelial-to-mesenchymal transition
ERK1/2	extracellular signal-regulated kinase 1/2
ESCRT	endosomal sorting complex required for transport
EU	European Union
EV	extracellular vesicle
FACS	fluorescence activated cell sorting
FAK	focal adhesion kinase
FBS	fetal bovine serum
FDA	Food and Drug Administration
FGF	fibroblast growth factor
GAG	glycosaminoglycans
GAPDH	glyceraldehyde 3-phosphate dehydrogenase
GBM	glioblastoma multiforme
GMP	good manufacturing practice
GPI	glycosylphosphatidylinositol
GTP(ase)	guanosine triphosphate
GvHD	graft versus host disease
HCT	hematopoietic cell transplantation
HEK	human embryonic kidney
HER2	human epidermal growth factor receptor 2
HGF	hepatocyte growth factor
HLA	human leukocyte antigen
HMEC	human microvascular endothelial cells
hPL	human platelet lysate
HRP	horseradish peroxidase
HSPC	hematopoietic stem/progenitor cells
IBA1	ionized calcium binding adaptor molecule 1
IFATS	International Federation for Adipose Therapeutics and Science
IL3	interleukin 3
ILV	intraluminal vesicles
iPSC	induced pluripotent stem cell
ISCT	International Society for Cellular Therapy
JNK	c-Jun N-terminal kinase

Lamp2b	lysosome-associated membrane protein 2
LDH	lactate dehydrogenase
LDL	low-density lipoprotein
lncRNA	long non-coding RNA
MACS	magnetic activated cell sorting
MAPK	mitogen-activated protein kinase
MDR	multidrug resistant
MFI	median fluorescence intensity
MHC	major histocompatibility complex
MIF	migration inhibitory factor
miRNA	micro RNA
mRNA	messenger RNA
MSC	mesenchymal stromal cell(s)
MSC-EVs	mesenchymal stromal cell-derived extracellular vesicles
MVB	multivesicular bodies
MVE	multivesicular endosomes
MWCO	Molecular weight cut-off
NF-κB	nuclear factor kappa light chain enhancer of activated B cells
NK	natural killer
NRP-1	neuropilin 1
NTA	nanparticle tracking analysis
OP	osteopontin
PB	peripheral blood
PBS	phosphate-buffered saline
PDAC	pancreatic ductal adenocarcinoma
PDB	Protein Data Bank
PDGF(R)	platelet-derived growth factor (receptor)
PE	phosphatidylethanolamine
PEG	polyethylene glycol
PES	polyethersulfone
PI3K	Phosphatidylinositol-3-kinase
PMO	phosphorodiamidate morpholino oligomer
PPR	particle to protein ratio
PS	phosphatidylserine
PSMA	prostate-specific membrane antigen
PTD	protein transduction domain
PVDF	polyvinylidene fluoride

RIPA	radioimmunoprecipitation assay
RPMI	Roswell Park Memorial Institute
RVG	rabies viral glycoprotein
S/XF	serum-/xeno(geneic)-free
SD	standard deviation
SDS	sodium dodecyl sulfate
SEC	size exclusion chromatography
SEM	standard error of the mean
SFCA	surfactant-free cellulose acetate
SIP	steam-in-place
siRNA	small interfering RNA
SNARE	soluble N-ethylmaleimide-sensitive fusion attachment protein receptor
SPION	superparamagnetic iron oxide nanoparticles
STAT3	signal transducer and activator of transcription 3
SUB	single-use bioreactors
TACS	traceless affinity cell selection
TBS	tris-buffered saline
TBST	TBS with 0.1% Tween-20
TEI	Total Exosome Isolation
TFF	tangential flow filtration
TGF	transforming growth factor
Th1	T helper type 1
TME	tumor microenvironment
TSG101	tumor susceptibility gene 101 protein
UCB	umbilical cord blood
UCM	umbilical cord matrix
USA	United States of America
VEGF(R)	vascular endothelial growth factor (receptor)
VWBR	Vertical-Wheel™ bioreactor
WCL	whole cell lysate

1. Introduction

This chapter is partially published as: de Almeida Fuzeta M., de Matos Branco A.D., Fernandes-Platzgummer A., da Silva C.L., Cabral J.M.S. (2019) Addressing the Manufacturing Challenges of Cell-Based Therapies. In: Advances in Biochemical Engineering/Biotechnology. Springer, Berlin, Heidelberg.

1.1. Mesenchymal stromal cells: manufacturing challenges for cell-based therapies

1.1.1. The birth of cell therapies

Exciting developments in the cell therapy field over the last decades have led to an increasing number of clinical trials and the first cell products receiving marketing authorization. In fact, cell-based therapies offer unprecedented levels of therapeutic potential, already radically changing the landscape of medical care.

The development of cellular therapies began with the establishment of hematopoietic cell transplantation (HCT). Early work in murine models led to the observation that supralethal radiation could be survived if affected mice were infused with a bone marrow (BM) graft[1]. BM aspirates containing hematopoietic stem/progenitor cells (HSPC) were able to migrate to the affected BM after radiation-derived myeloablative treatment and reconstitute the entire hematopoietic system.

After proving to treat radiation injury, BM transplantation was considered as a possible treatment for leukemia. In 1956, Barnes and colleagues were able to infuse normal BM grafts on leukemic mice as a proof of concept[2]. Knocking out a murine hematopoietic system also meant eliminating its blood-related malignancies. Transplants of healthy grafts would then repopulate the BM and form a new hematopoietic system. By transposing this knowledge to humans, Thomas and colleagues were the first to successfully perform HCT in human acute leukemia patients, paving the way towards showing the feasibility of cell therapies[3].

1.1.2. MSC as a new paradigm for paracrine cell therapy

Following initial developments in HCT, the BM was once more the source for the discovery of yet another promising stem cell population, named mesenchymal stem cells (MSC) by Caplan in 1991[4]. The foundations for the discovery of these stem cells can be traced back to the nineteenth century, when studies on the BM transplantation to heterotopic anatomical sites resulted in *de novo* generation of ectopic bone and marrow[5,6]. However, it was only later that the work of Tavassoli and Crosby clearly provided evidence of an inherent osteogenic potential associated with the BM[7]. In the 1960s-1970s, Friedenstein and colleagues isolated and characterized a sub-population of adherent spindle-shaped cells from mouse BM that were responsible for the previously described osteogenic potential[8,9]. Moreover, they also demonstrated that BM cell suspensions could generate colony-forming unit-fibroblasts (CFU-F). These cells were then later designated as “mesenchymal stem cells” and shown to have multilineage differentiation potential, including the osteogenic, adipogenic and chondrogenic lineages[4,10].

Over the following decades, questions were raised over the usage of the term ‘‘mesenchymal stem cells’’ and alternative nomenclatures have been proposed by different authors. This is due to unfractionated plastic-adherent marrow cells being quite heterogeneous and current data being insufficient to characterize them as stem cells. In order to address the inconsistency in the nomenclature and account for the biological properties of these cells, the International Society for Cellular Therapy (ISCT) proposed that plastic-adherent cells described as mesenchymal stem cells should be termed multipotent mesenchymal stromal cells, maintaining the acronym MSC[11].

The controversy in the appropriate nomenclature is accompanied by the inconsistency between investigators on the set of characteristics that define MSC. Laboratories have developed different methods of isolation and expansion, as well as different approaches to characterize these cells. Thus, an appropriate comparison between studies may be difficult to achieve. In order to address this issue, the ISCT has proposed minimal criteria to define human MSC: i) adherence to plastic; ii) expression of CD73, CD90, CD105 and lack the expression of CD14 or CD11b, CD79α or CD19, CD34, CD45 and HLA-DR; iii) osteogenic, adipogenic and chondrogenic differentiation potential under standard culture conditions[12]. Similarly, minimal criteria for the definition of adipose tissue (AT)-derived stromal/stem cells have also been recently established by a combined panel from ISCT and the International Federation for Adipose Therapeutics and Science (IFATS)[13].

MSC present additional characteristics that make them attractive for therapeutic purposes, other than their ability to give rise to different mesenchymal phenotypes. The secretion of a broad range of bioactive molecules, such as growth factors, cytokines and chemokines, render them with immunomodulatory and trophic activities, acting both in a paracrine and autocrine manner[14,15]. MSC trophic activity relies on bioactive factors that assist in repair and regeneration processes. MSC are able to inhibit scarring (fibrosis) and apoptosis, promote angiogenesis and support growth and differentiation of progenitor cells into functional regenerative units[14,15].

The panoply of beneficial effects ascribed to MSC has made them the second most studied cells in clinical trials, immediately after HSPC[16], with over 900 clinical trials taking place worldwide, receiving a special focus in China, Europe and United States of America (USA) (Figure 1.1) (clinicaltrials.gov, accessed on 29th May 2019, using the search term “mesenchymal stem cell OR mesenchymal stromal cell”). MSC are promising candidates for the treatment of a wide range of diseases, which is clearly observed from the great diversity of conditions targeted in clinical trials. Musculoskeletal diseases, immune system diseases, wounds and injuries, central nervous system diseases and vascular diseases are the top 5 conditions with the highest numbers of undergoing clinical trials worldwide. In addition to

HSPC and MSC, many other cell types are being studied in clinical trials including lymphocytes, dendritic cells, hepatocytes and endothelial cells[16].

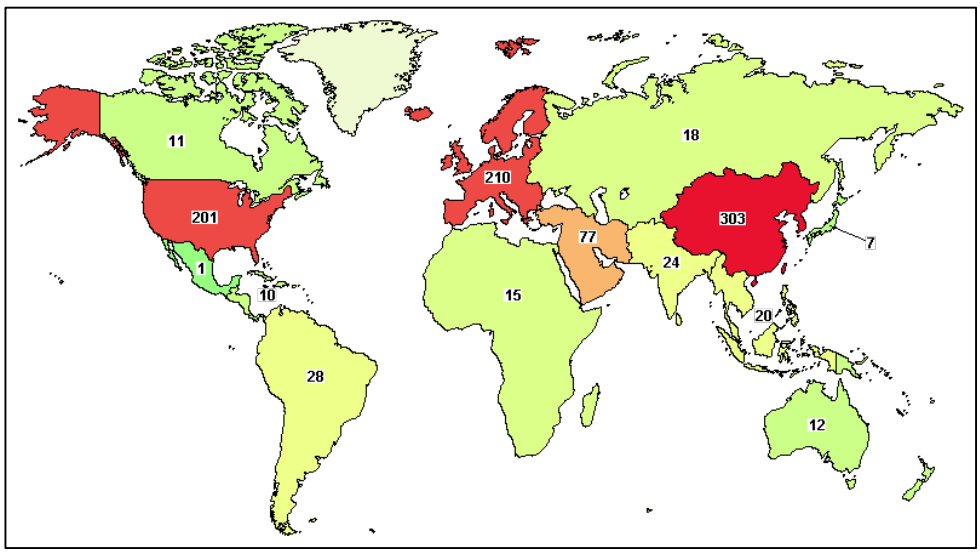

Figure 1.1 - Worldwide distribution of clinical trials obtained from "clinicaltrials.gov" on 29th May 2019, using the terms "mesenchymal stem cell OR mesenchymal stromal cell".

1.1.3. Clinical application and challenges of cell-based therapies

Since 2009, twelve cell-based therapies have been approved and received marketing authorization in the European Union (EU) and USA combined (Table 1.1)[17–19]. The first successfully approved product was ChondroCelect, from TiGenix, despite being withdrawn in 2016 due to commercial reasons. This product consisted in autologous cartilage cells expanded *ex vivo* to treat knee cartilage defects. Holoclar (Chiesi Farmaceutici) was the first approved stem cell product (2015), consisting in *ex vivo* expanded autologous human corneal epithelial cells containing stem cells to treat severe limbal stem cell deficiency. Other approved products include the first CAR-T cell therapies for liquid cancers, Kymriah (Novartis) and Yescarta (Kite Pharma), approved in 2017 in the USA and in 2018 in the EU and more recently, Alofisel (Takeda Pharma) that consists in expanded allogeneic AT-derived MSC to treat perianal fistulas in patients with Crohn's disease.

Due to their uniqueness, cell therapies have earned their own category in regulatory agencies with special directives concerning approval candidature. Cell-based therapies are considered advanced therapy medicinal products (ATMP), defined by the European Medicines Agency (EMA) as medicines for human use that are based on genes, tissues or cells, offering groundbreaking new opportunities for the treatment of disease and injury[18].

In spite of the establishment of guidelines and regulations applying to cell therapies, a number of unresolved issues remain, making the regulatory path toward clinical approval a challenge[20]. Certain important requirements often lack in clarity and regulation is not specific enough. This results in products where the appropriate classification is not entirely certain[21,22]. Furthermore, discrepancies between regulatory agencies from different countries hinders

companies trying to reach the market at an international level[22]. The challenging regulatory environment contributes to the need to endure over long time periods before reaching the market. Often, cell products only gain market access 15 - 20 years after the company was founded[22]. Nevertheless, the regulatory environment is gradually improving. In order to continue this path and make wise development choices, it will be crucial to promote a crosstalk between scientists, companies developing cell therapies and regulators[22].

Table 1.1 - Cell-based therapies that received MA in the USA and EU by September 2018[17–19].

Product (MA holder)	Product description	Therapeutic indication	Date approved
Alofisel (Takeda Pharma A/S)	Expanded allogeneic mesenchymal adult stem cells extracted from adipose tissue	Perianal fistulas in patients with Crohn's disease	2018 (EU)
Yescarta (Kite Pharma)	Autologous T cells genetically modified by retroviral transduction to encode an anti-CD19 chimeric antigen receptor (CAR)	Large B-cell lymphoma	2018 (EU) 2017 (USA)
Kymriah (Novartis)	Autologous T cells genetically modified using a lentiviral vector to encode an anti-CD19 CAR	Acute lymphoblastic leukemia; large B-cell lymphoma	2018 (EU) 2017 (USA)
Spherox (co.don AG)	Spheroids of human autologous matrix-associated chondrocytes	Knee cartilage defects	2017 (EU)
Strimvelis (Orchard Therapeutics)	Autologous $CD34^+$ cells transduced with an engineered retroviral vector encoding the human adenosine deaminase sequence	Severe combined immunodeficiency	2016 (EU)
Zalmoxis (MolMed)	Allogeneic T cells genetically modified to express a truncated form of the human low affinity nerve growth factor receptor and the herpes simplex I virus thymidine kinase	Control mechanism for graft-versus-host disease after hematopoietic cell transplantation	2016 (EU)
Holoclar (Chiesi Farmaceutici)	*Ex vivo* expanded autologous human corneal epithelial cells containing stem cells	Severe limbal stem cell deficiency	2015 (EU)
Provenge (Dendreon)	Autologous peripheral-blood mononuclear cells activated with prostatic acid phosphatase granulocyte-macrophage colony-stimulating factor	Metastatic prostate cancer	2013 (EU) (withdrawn from EU in 2015) 2010 (USA)
Maci (Vericel)	Autologous cultured chondrocytes	Knee cartilage defects	2016 (USA) 2013 (EU) (suspended in EU in 2014)
GINTUIT (Organogenesis)	Allogeneic cultured keratinocytes and fibroblasts in bovine collagen	Mucogingival conditions	2012 (USA)
Laviv (Fibrocell Technologies)	Autologous fibroblasts	Severe nasolabial fold wrinkles	2011 (USA)
ChondroCelect (TiGenix)	Autologous cartilage cells expanded *ex vivo* expressing specific marker proteins	Knee cartilage defects	2009 (EU) (withdrawn in 2016)

MA – marketing authorization; USA – United States of America; EU – European Union.

Although this millennium has been marked with considerate advances, with regulatory victories for several ATMP, cell therapy development has a long and considerable track record. Recent success is due to much effort in the past uncovering and understanding all the obstacles that stood between the establishment of therapeutic options based on cells. HCT

was decisive as a vehicle of problem-solving and thus has deserved its recognition as a foundation for cell therapy development[23].

With multiple cell-based therapies already reaching the market, one of the most pressing issues will be addressing the challenges in manufacturing these products. Most cell-based therapies are costly and target widespread medical conditions. The robust and scalable cell manufacturing for the cost-effective delivery of safe and potent cell-derived ATMP (either with autologous origin (i.e. cells from the patient) or allogeneic) relies on process engineering tools to understand the impact of cellular features (biological, biochemical, etc) on cell product function and performance, and how process variables influence the critical quality attributes of the cell product. In general, the manufacturing process of cell-based therapies, consists in several stages: tissue collection, cell isolation, culture and expansion (upstream processing), cell harvest, separation and purification (downstream processing) and finally product formulation and storage (Figure 1.2). The main advances made in the field and future challenges will be addressed in this section, with a particular focus on upstream processing, considering the particular relevance of these stages in the context of this thesis.

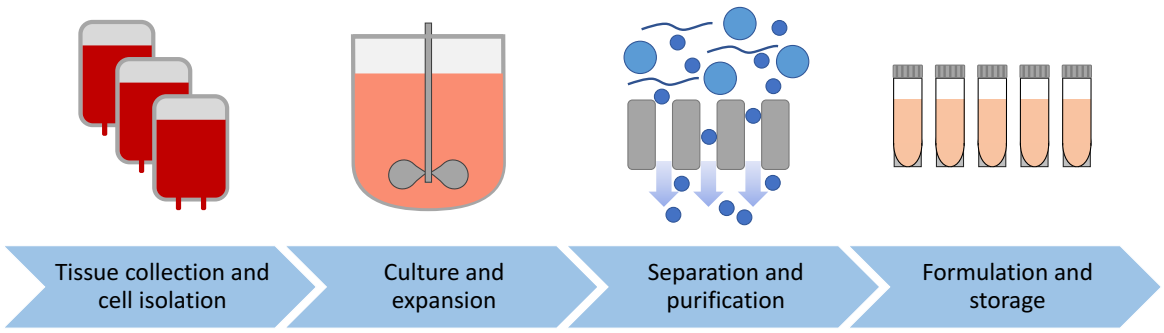

Figure 1.2 - Manufacturing process for cell-based therapeutic products.

1.1.4. Source and isolation of cells for therapeutic use

From a manufacturing perspective, cell-based therapies have transformed cells and tissues themselves into a bioprocess raw material. Consequently, securing their supply is an unprecedented initial challenge in a production pipeline, differing from previously established engineered cell factories. For instances, cell retrieval from human tissues can be problematic. Although the appropriation of biological waste can minimize this issue, some cell sources may be very difficult to reach, while potentially posing health risks for a donor or patient. Thus, management of this supply chain has a level of complexity that is very case-specific, depending on the cellular component of the therapy[24].

1.1.4.1. Sources and tissue collection

Cell-based therapies depend primarily on obtaining the appropriate material from which cells with possible therapeutic application can be isolated. So far, multiple human tissues have been used as sources to obtain cells with therapeutic potential[25].

Home to the hematopoiesis process, the BM harbors multiple cell types that closely interact together, forming the so called BM hematopoietic niche, encompassing bone, osteoblasts, osteoclasts, HSPC, MSC, macrophages, blood vessels and extracellular matrix (ECM)[26]. However, the harvesting of BM requires an invasive procedure, allowing a relatively small cell yield, which declines with donor age[27,28]. For example, MSC frequency in a BM aspirate is only 0.001% to 0.01%[10].

AT obtained from subcutaneous tissue represents an abundant source for isolating MSC reliably using simple techniques. Liposuction, the technique generally used for harvesting AT, has the advantage of being less invasive than BM aspiration and is associated with high MSC isolation yields[29]. Specifically, liposuction allowed a yield of stromal vascular cells of $0.5x10^6$ - $0.7x10^6$ cell/g AT and between 0.4% and 1.9% of the cells were able to adhere and proliferate in culture[29]. Moreover, liposuction material is considered medical waste, thus being an attractive alternative source. The expansion potential, differentiation capacity, and immunophenotype of MSC derived from AT are nearly identical to those isolated from BM[28].

Neonatal tissues, such as the umbilical cord and placenta, are promising alternative sources to adult ones. The umbilical cord is a rich source of HSPC[30,31] and has been shown to be a rich source of MSC[32]. For example, about 0.6 million MSC were obtained per gram of umbilical cord[33]. Harvesting the umbilical cord requires a painless and non-invasive procedure. The umbilical cord is considered medical waste and is usually discarded after birth, thus being an attractive alternative source. Within the umbilical cord, MSC can be isolated from the umbilical cord blood (UCB) as well as from the Wharton's Jelly, the connective tissue surrounding umbilical vessels[34]. Most studies are performed with MSC derived from the Wharton's Jelly, which is commonly referred as the umbilical cord matrix (UCM). Umbilical cord-derived MSC expand at a higher rate when compared to BM- and AT-derived MSC[28,35].

Possibly due to their broad definition, MSC have been successfully isolated from a number of tissues other than the previously mentioned, including synovial membrane[36], placenta[37], dental pulp[38], brain, liver, kidney, lung, muscle, thymus and pancreas[39].

Notably, cells show different therapeutic capacity depending on the source they were isolated from. For example, MSC isolated from BM, AT and UCM revealed different ability to suppress peripheral blood (PB) natural killer (NK), B and T cells, when co-cultured with phytohemagglutinin-stimulated PB mononuclear cells[40].

1.1.4.2. Isolation of target cell populations

Depending on the nature of a specific cell therapy, assuring source availability and succeeding in tissue collection may be enough to proceed to the following bioprocessing stage. For minimally manipulated cell products, such as HCT, heterogeneous populations are isolated and directly infused into the patient. However, newer and more advanced cell

therapies are becoming ever more population specific. Thus, bulk populations that normally result from harvesting procedures need funneling techniques that isolate a desired cell type[41].

Still, the most commonly used method to isolate MSC is very simplistic, relying solely on the ability that MSC have to adhere to plastic surfaces[12]. After tissue collection, cells are plated on polystyrene-based tissue culture flasks. MSC will adhere to the plastic surface while contaminating cells, such as the ones from hematopoietic lineages, are washed away after medium change and passaging[42,43]. Typically, when MSC are obtained from tissues such as UCM, AT or synovial membrane, these can be either enzymatically digested using collagenase solutions[29,43,44] or simply plated directly onto plastic surfaces as explants[45–47].

More sophisticated techniques can be used to isolate specific cell populations following tissue collection, typically relying on affinity-based and centrifugation-based separations. Although affinity-based separation has gained significant momentum in cell therapy manufacturing, centrifugation techniques are still part of typical bioproduction processes. Several Sepax (originally developed by BIOSAFE, now GE Healthcare) cell processing systems, have brought a fully closed and automated centrifugation unit to cell therapy production pipelines[48]. More advanced centrifugation platforms combine different physical forces to achieve higher isolation recovery and purity. Terumo BCT has established a continuous centrifugation system (Elutra®) that joins centrifugal forces with counterflow[49]. By achieving cell population separation based on size and density, these platforms are able to reach much higher resolution in separation[50].

Cell isolation through affinity is an ever-growing alternative due to its separation criteria being based on biological instead of physical characteristics. Cell population immunophenotype is commonly used to isolate specific cells from their original sources, such as HSPC ($CD34^+$ selection)[51,52] and MSC (Stro-1^+ selection)[53,54]. Typically mediated by antibody-antigen interactions, fluorescence activated cell sorting (FACS) and magnetic activated cell sorting (MACS) occupy leading roles in affinity-based separation. Through fluorescent labelled antibodies, FACS is able to separate cell populations based on their surface marker expression. This technology allows for multiple marker selection with high selectivity due to single-cell analysis[55]. MACS shares the same separation criteria as FACS (i.e. immunophenotype) but achieves cell sorting with antibodies coupled to magnetic particles.

Comparing both techniques, FACS presents better selectivity and subpopulation purity, but the respective cell sorter is not inherently prepared for a clinical setting[56]. An expensive hardware system combined with lack of parallelization, sterility issues and time-consuming protocols are some constraints that contribute against its translation. Due to its column-based system, MACS is able to separate cells at a much faster rate with possibility for parallel operation and is compatible with current good manufacturing practice (cGMP) guidelines. Still,

lack of bead detachment from cells after isolation is a significant drawback for MACS as a cell therapy bioprocessing unit.

Focusing on their translation, improved versions of the original platforms have been developed. New platforms for FACS such as WOLF (NanoCellect Biomedical) and On-chip Sort (On-chip Biotechnologies) include disposable microfluidic cartridges that allow for a closed circuit, minimizing contamination risks[55]. Closed versions of MACS (e.g. CliniMACS Plus® by Miltenyi Biotec and CTS™ DynaMag™ by ThermoFisher) have been developed for clinical scale cell isolation[57,58]. Other systems such as the MACSQuant Tyto (Miltenyi Biotec) system has been developed focusing on improved sorting speeds[55].

Novel approaches for affinity-based cell isolation have also been investigated. Since cell therapies possess more stringent safety criteria, delivering cells without any by-products due to bioprocessing is crucial. Therefore, antibody removal after affinity separation is of considerable interest. Traceless affinity cell selection (Fab-TACS®) available in an automated commercial device (FABian® by IBA Lifesciences) is an innovative technology that explores a reversible antibody-antigen interaction to allow isolated cells to be released from a capture column without any separation by-product or trace[59]. Another technique called buoyancy-activated cell sorting (BACS™) developed by Akadeum Life Sciences combines centrifugation and affinity-based separation. Undesired cells are captured by glass-shelled microbubbles (negative selection). These microbubbles are separated from the remaining cells populations through centrifugation by flotation[60,61].

Isolation of a target cell population can have different impact depending on a specific cell therapy, with products ranging from bulk and heterogeneous populations to very selective subpopulations with a defined phenotype. Adequate selection of a separation method is also dependent on the prioritization of opposing purification concepts, such as purity and recovery[24].

1.1.5. Cell production

The relatively low frequency of cells with therapeutic potential within the native tissues, followed by harvesting procedures and eventually successive isolation steps, yield a substantially low number of cells in the end. Therefore, in order to use these cells in a clinical context, it is usually required additional steps of manipulation and propagation *ex vivo*, which depend on choosing the appropriate culture medium conditions, physicochemical parameters and culture platforms[62].

1.1.5.1. Culture medium formulation

The maintenance and propagation of animal cells *in vitro* require a cell culture medium, supplying nutrients and inorganic salts, as well as providing the appropriate physicochemical conditions. Generally, medium components include glucose (carbon source), amino acids

(nitrogen source), vitamins (cofactors), inorganic salts (maintains electrolyte balance), sodium bicarbonate (buffer, to maintain pH at 7.4), sodium chloride (adjusts osmotic pressure), antibiotics (prevent microorganism contamination), phenol red (visual pH indicator), growth factors and hormones (growth stimulation)[63,64]. These components are provided in commercially available basal medium formulations, such as Eagle´s medium and derivatives (e.g. Dulbecco's modified Eagle's medium (DMEM), Minimum Essential Medium Eagle alpha (αMEM)), medium from Roswell Park Memorial Institute (RPMI) and several other well-established media, which have been subject of improvement over the years[64].

Culture medium formulations usually require the addition of a protein-rich supplement, containing growth and adhesion factors. The most commonly used culture supplement is animal serum, especially fetal bovine serum (FBS). Serum is a source of amino acids, proteins, vitamins, carbohydrates, lipids, hormones, growth factors and inorganic salts[64]. Moreover, it enhances cell adhesion, improves the pH-buffering capacity of the medium and helps reduce shear stress during cell manipulation. However, it presents significant disadvantages such as being ill-defined, wide batch-to-batch variability, risk of contamination with virus and prions and ability to transmit xenogeneic-antigens, leading to increased immunogenicity of cultured cells, thus limiting FBS application in the clinical setting[65,66]. Besides the cell biological perspective, ethical concerns and animal welfare issues arise from the use of animal serum, as serum collection causes animal suffering[65]. Furthermore, the global supply of FBS is declining over the years, and this tendency is expected to continue[65]. This will eventually result in a FBS supply that will not be able to meet the increasing demand. Therefore, given its disadvantages, using FBS for cell culture of clinically applied cell products is discouraged and should be avoided. By complying with current international guidelines and regulatory frameworks[67–69], there is need for developing alternative culture supplements.

In the last decade, the development of serum-/xeno(geneic)-free (S/XF) culture formulations (i.e. without serum or animal origin components) has been a priority for the field of cell therapies. Although these media represent a valuable alternative to FBS, as they are more consistent and standardized, they still contain a cocktail of growth factors, proteins and hormones derived from human serum or even plant hydrolysates, classified as chemically undefined[70]. Chemically defined, animal component-free media, on the other hand, consist exclusively of well-defined and characterized components and entirely free of animal (including human) derived products. These include purified recombinant proteins and synthetic bioactive molecules[70].

One of the well-established supplements used in S/XF media, proposed as an alternative to FBS, is human platelet lysate (hPL). As early as the 1980s, hPL-supplemented medium was found to support proliferation of established cell lines and primary fibroblasts[71,72]. hPL is usually prepared from fresh blood or platelet concentrates, containing bioactive molecules

such as growth factors, adhesion molecules and chemokines, which originate primarily in the α-granules of platelets[73]. Preparation of hPL from platelet concentrates can be achieved either by repeated freeze/thaw cycles, sonication, induced platelet activation by addition of thrombin or $CaCl_2$ or by solvent/detergent treatment[73].

Blood banks routinely prepare pooled allogeneic platelets from human blood donations. When these are not used for transfusion, they are used for further manufacturing into hPL, thus allowing a steady supply for manufacturing an allogeneic 'off-the-shelf' hPL product for cell culture[73,74].

Multiple studies have demonstrated hPL-supplemented media to be efficient for the isolation and expansion of MSC from various origins[75–77], cultured both in static and dynamic systems[78,79], already with several ongoing and completed clinical trials (clinicaltrials.gov). Moreover, it has been shown that both allogeneic and autologous hPL-supplemented media allow improved cell proliferation when compared to FBS-containing media[75,77,80,81]. The main differences in hPL protein content compared to FBS are the higher content of immunoglobulins and the possible presence of fibrinogen and other coagulation factors, when hPL is produced without thrombin activation[73].

In addition to its application for MSC expansion, hPL has been evidenced as an efficient growth medium supplement for *ex vivo* expansion of other cell types such as human gingival fibroblasts[82], chondrocytes[83], osteocytes, myocytes and tenocytes[84], as well as endothelial cells[85], indicating its potential applicability in multiple areas of cell therapies and regenerative medicine. Although hPL is considered safer than FBS by the scientific community and regulatory agencies, it still poses some constraints, such as the risk of transmission of human diseases by known or unknown viruses, ill-definition and the possibility of triggering immune responses[86]. Nonetheless, hPL products derived from pooled units and produced in large-scale are already commercially available[74] and seem to be the most promising alternative to FBS supplementation in cell culture medium in the near future. Moreover, novel gamma irradiated hPL products have been developed towards pathogen reduction. Results showed that gamma radiation allowed 4 $\log_{10}$ reduction of viral titer with low impacts on the potency for cell expansion[87].

There are other commercially available S/XF media that have been successfully applied for cell culture. StemPro® MSC SFM (Life Technologies) and MesenCult™-XF (STEMCELL™ Technologies) are two chemically undefined S/XF media that have been used to successfully expand MSC from different sources[88–91]. Although being chemically undefined, containing human-derived components, these media formulations represent an improvement for cell culture, due to better definition and lower batch-to-batch variability when compared to FBS- and hPL-supplemented media.

The ideal candidate for production of clinical-grade cell-based therapies would be a chemically defined, animal component-free media (including human), composed exclusively of well-defined factors that could replace serum and serum-derived products. These include synthetic bioactive molecules and purified recombinant proteins[70]. There are multiple factors that can be combined in order to replace serum, such as growth factors (e.g. EGF, FGF, TGF), hormones (e.g. growth hormone, insulin), carrier proteins (e.g. albumin, transferrin), lipids (e.g. cholesterol, fatty acids), transition metals (e.g. Se, Fe, Cu, Zn), vitamins, adhesion factors (e.g. fibronectin, laminin), polyamines and reductants (e.g. 2-mercaptoethanol)[64]. The number of possibilities that result from the combination of these components is enormous, making the selection of the most appropriate ones and their respective concentration in a medium formulation an extremely difficult task. For that purpose, design of experiments is possibly the best strategy to find the optimal concentration of each component in a culture medium, especially considering likely interactions between the components[64]. Consequently, S/XF media, especially chemically defined culture media are often cell type specific.

The chemically defined medium TheraPeak™ MSCGM-CD™ (Lonza) has been used for the expansion of MSC[92]. Successful expansion of T cells was also achieved using chemically defined S/XF media, relying for instance on the CTS™ Immune Cell Serum Replacement supplement[93,94].

In order to disseminate the development and application of serum-free media for cell culture, “FCS-free Database”, a freely accessible serum-free media database is available online (https://fcs-free.org/), providing an overview of FBS-free media for cell culture.

1.1.5.2. Physicochemical parameters

Besides biochemical factors such as nutrient/metabolite concentration and growth factors, physicochemical parameters such as pH, temperature, osmolality and oxygen tension are equally important for the maintenance of animal cell cultures. The optimal values for each of these physicochemical parameters will differ depending on the cell product, which poses an additional challenge in cell manufacturing.

Most cell lines grow successfully at pH 7.2 to 7.4. However, the optimum culture pH depends on the intended application. For example, differentiation of human MSC into osteoblasts can be improved by changing the pH of culture medium from normal to alkaline medium[95]. Usually the pH is controlled in cell culture by using the CO_2/HCO_3^- buffer system. Cells are typically cultured in humidified incubators with gas phase CO_2 at 5% and sodium bicarbonate as a medium additive. The CO_2 dissolved in the aqueous phase stays in equilibrium with HCO_3^-, adjusting the pH[64].

The optimal temperature to cultivate human and warm-blooded animal cells is 37ºC. However, cell culture at different temperatures may be advantageous for certain purposes.

For example, culturing MSC at 32ºC decreased the accumulation of oxidative damage and improved their osteogenic differentiation ability, when compared to 37ºC[96].

Although different cells have different optimal osmolality values, most cells grow well in the range between 290 mOsm and 310 mOsm[97,98]. As previously mentioned (section 1.1.5.1), the osmolality is mainly defined by the sodium chloride content in the medium.

Most animal cell cultures are performed at an atmospheric oxygen level (21% O_2). However, the oxygen concentration in most tissues is lower than the atmospheric one, due to gas transfer phenomena. Therefore, mimicking the *in vivo* oxygen concentration might have a positive impact in cell culture as well as on the therapeutic potential of the cultured cells. One canonical example would be the BM, which is characterized by a hypoxic environment, with oxygen concentration ranging in the interval between 1% and 6%[99,100].

In light of this observation, several studies were performed by exposing MSC to hypoxic conditions (compared to atmospheric (21%) O_2 levels). Hypoxic conditions were found to have an advantage for MSC expansion as well as in terms of differentiation[101–103]. A study performed by Oliveira and colleagues revealed that both BM MSC and AT MSC cultured in hypoxic conditions (2% O_2) experienced an immediate and concerted down-regulation of genes involved in DNA repair and damage response pathways[104]. Moreover, it revealed that AT MSC reacted to hypoxic environment more slowly than BM MSC, as different characteristics of each cell niche (e.g. degree of vascularization, oxygen tension, cell-cell interactions) determine distinct sensitivities to hypoxia *ex vivo*[104].

Besides the need to establish the most appropriate physicochemical conditions for a certain cell-therapy manufacturing process, maintaining these parameters at the correct values throughout culture is equally important. In traditional culture systems, these parameters are often observed, but rarely controlled, thus decreasing the robustness of the manufacturing process. The implementation of culture monitoring and control systems allows to overcome this limitation.

1.1.5.3. Scalable culture systems

Whether isolated cell populations need to undergo differentiation or expansion, appropriate cell culture vessels and systems are necessary.

In terms of complexity, at the rear-end of cell culture technology are simple plasticware containers. Different geometries make up a broad collection of vessels in order to cover any cell type and their projected application. Petri dishes, T-flasks, roller bottles and multiwell plates all incorporate cell culture plasticware and are typically made of polystyrene that is previously treated either chemically or physically in order to gain hydrophilic functional groups (e.g. ketones, aldehydes, hydroxyl and carboxyl groups)[105]. Indeed, surface treatment has a dramatic impact on adherent cell culture, with proper cell adhesion being a main concern.

Unfortunately, when using S/XF culture media, cell adhesion can be compromised due to deficiency in serum-derived adhesion factors[106]. Commercial enhanced plasma treatment plasticware (e.g. CellBIND® by Corning Life Sciences) and xeno-free surface coatings (e.g. CELLstart™ by ThermoFisher Scientific and Synthemax® by Corning Life Sciences) have been developed to address this issue[107,108].

Besides allowing gas exchange through the cap region and having excellent optical clarity, commonly used vessels are seriously limited regarding any type of monitoring and control. Conventional plasticware as culture flasks also lack an agitation mechanism, not being able to assure fully homogenized cell cultures. Since their design was directed mainly towards research purposes, manufacturers quickly identified scalability issues for large-scale production. Advanced and scalable culture systems based on plasticware were created to avoid laborious and unsustainable scale-out.

Although very simplistic, plastic malleable bags have a consolidated place in cell culture. Being integrated in basic plasticware, they offer a simple closed system solution which is critical for manufacturing under cGMP. However, limited culture control and poor agitation severely limit their application in optimized processes. Nevertheless, therapies based on hematopoietic cells (e.g. Tumor-infiltrating lymphocytes, CAR-T and HSPC) have relied on these platforms for cell culture, reaching human use in clinical trials [109–111].

Multi-layered flasks (e.g. Nunc™ Cell Factory™ System by ThermoFisher Scientific) were designed to increase culture area while reducing volumetric footprint of using multiple individual flasks. Additionally, closed versions with perfusion mechanisms of these flasks were also developed to overcome the open nature of conventional flasks. Large-scale expansion of MSC in serum-free conditions was achieved using HYPERStack system (Corning Life Sciences), yielding an average cell density of $2x10^4$ cell/cm^2, corresponding to a 4-fold increase in total cell number after 4 days[112]. Proprietary gas permeable films improve gas diffusion, which do not compromise cell viability in high density adherent cultures of tightly packed multi-layered flasks. Flask potential has been pushed further with the commercialization of the CellCube® by Corning Life Sciences, a closed system comprising of densely packed thin individual surfaces with continuous medium supply in laminar flow, reaching 85 000 cm^2 (39 cm x 25 cm) for adherent cell culture[113]. The Xpansion® multiplate system designed by Pall Corporation takes advantage of the same concept, aside from assuming a cylindrical geometry with capacity for up to 122 400 cm^2 of culture surface. Xpansion®-50 was used for large scale expansion of human periosteum derived stem cells for the treatment of bone defects, achieving a final cell density of $1.75x10^4$ cell/cm^2, corresponding to a 3.9-fold change in total cell number after 7 days, and presenting a final recovery efficiency of 45%[114].

Roller bottles have also been optimized for large scale manufacturing of cells. Improvement of this technology led to the design of RollerCell™ by Cellon, a system capable of simultaneously holding 40 roller bottles with automated robotic processors for cell handling. RollerCell™ comparison with CellCube® for cell line production yielded similar results[115].

Although planar systems have evolved to closed and scalable systems with possibility for dynamic regimen through continuous fluid flow (e.g. CellCube® and Xpansion®), bioreactors have been the ultimate objective for cell therapy manufacturing, seeing that they incorporate monitoring and control, reduce process footprint and minimize cell handling.

Incorporating highlighted challenges of a cell-centered process requires platforms capable of dealing with parameter complexity to deliver a safe and reproducible cell-based product. Table 1.2 enumerates current cell-based therapies in clinical trials that involve bioreactors in their cell production process. Innovative bioreactor designs have come forward to challenge more classical versions.

Table 1.2 - List of clinical trials using bioreactors for cell based-therapies. Clinical trials were obtained from "clinicaltrials.gov", on 21st March 2019, using the term "bioreactor" and selected for cell therapy applications.

Study name	Type of bioreactor	Cells	Condition	Phase
Extracorporeal Immune Support System (EISS) for the Treatment of Septic Patients (EISS-1)[A]	EISS-Immune-cell bioreactor device	Human donor granulocytes	Severe Sepsis and Septic Shock	Phase 1 and phase 2
Safety of Intramuscular Injection of Allogeneic PLX-PAD Cells for the Treatment of Critical Limb Ischemia[A]	PluriX™ 3D Bioreactor System	Placental Adherent Stromal Cells	Critical Limb Ischemia	Phase 1
Expansion of Invariant NKT Cells for a Cell Immunotherapeutic Approach Allowing the Control of GvHD and Preserving the Graft Versus Leukemia Effect After Allogeneic HSC Transplantation[B]	Bioreactor	NKT Cells	Allogeneic Hematopoietic Stem Cell (HSC) Transplantation	(not available)
Laryngo-Tracheal Tissue-Engineered Clinical Transplantation[C]	Stem-cell seeded bioartificial tracheal scaffold	Autologous stem cells	Tracheal Diseases	Not Applicable

Clinical trial status: A-Completed; B-not yet recruiting; C-Unknown

Stirred tank bioreactors (Figure 1.3 A) maintain widespread use, with their simpler and more standardized geometry. With extensive experience in what concerns the production of traditional biopharmaceuticals, much knowledge regarding these bioreactors has been transposed to cell-based therapies. These systems have mechanical impellers that are responsible for appropriate mixing and assuring dynamic flow. High compatibility with monitoring probes and respective modules has made culture control an intrinsic part of this bioreactor. Internal sparging mechanisms allow for efficient gas transfer, although shear stress associated with bubbling can be an issue to sensitive cells[116]. Exhaustive knowledge on fluid

profiles based on computational fluid dynamics (CFD) models have given significant predictive control on culture estimates.

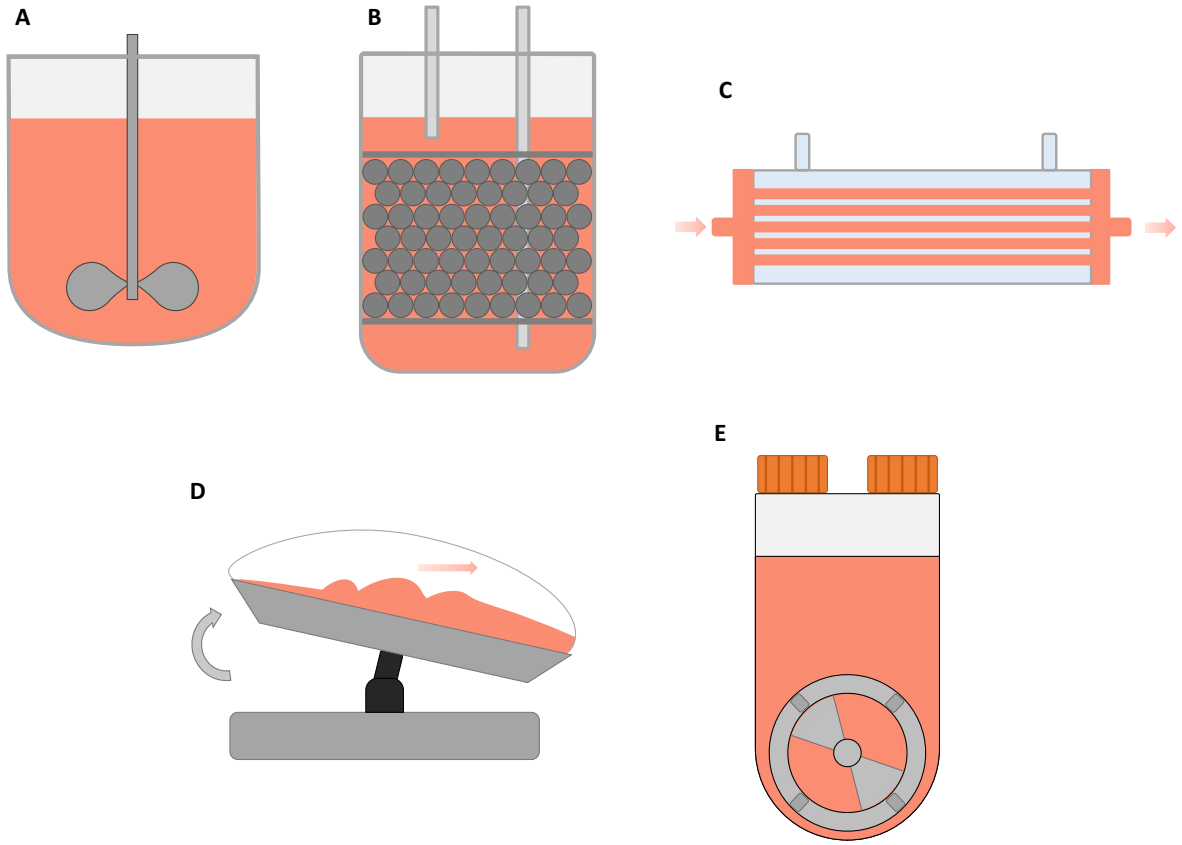

Figure 1.3 - Schematic representations of bioreactor configurations that can be potentially used in the manufacturing of cell-based therapies: (A) stirred tank bioreactor, (B) packed bed bioreactor, (C) hollow fiber bioreactor, (D) wave bioreactor and (E) Vertical-Wheel™ bioreactor.

While being naturally prone for suspension cultures[117], adherent cell culture has been adapted through microcarrier development. These spherical particles provide the surface area for cell adhesion to occur. A broad variety of materials, porosity levels and surface coatings have been developed to fulfil specific cell needs. The high variety of microcarriers has been extensively reviewed[118,119].

Of notice, our research group has performed pioneering work in the development of clinical-grade expansion of MSC of different human sources (i.e. BM and AT) in scalable microcarrier-based bioreactors using S/XF culture components, achieving the production of $1.1x10^8$ and $4.5x10^7$ cells for BM MSC and AT MSC, respectively, after 7 days of culture (working volume of 800 mL)[120]. Building on this platform, efforts were concentrated in maximizing cell productivity by changing different culture parameters. Feeding and agitation regimes were optimized and microcarrier screening was performed[89]. Furthermore, we have successfully incorporated an alternative MSC tissue source (i.e. UCM)[121] and have implemented a different bioreactor configuration with a vertical agitation design (Vertical-Wheel™) (section 1.1.5.4)[79].

The scalability potential of stirred tank bioreactors for cell-based therapies has been embodied by development of MSC expansion processes. While initial studies restricted their culture scale to spinner flasks, Rafiq and colleagues managed to scale-up MSC expansion to a 5 L stirred tank bioreactor, achieving a cell concentration of $1.7x10^5$ cell/mL, corresponding to over a 6-fold expansion in total number of cells[122]. Subsequently, Lawson and colleagues pushed the scalability of stirred tank MSC culture forward by successfully expanding human MSC in a 50 L bioreactor, being able to produce 177 clinical doses (70 million cells/patient assuming a 70 kg patient) in a single run[123]. In contrast to the above-mentioned scale-up, with contributions of multiple groups to ever increasing culture dimensions, Schirmaier and colleagues were able to perform an entire stepwise scale-up of AT MSC expansion from spinner flasks to 35 L cultures, yielding $1x10^{10}$ cells at the end (35 L scale)[124].Consequently, both adherent and suspension cultures are firmly established for cell culture in stirred tank bioreactors. Commercial versions of stirred tank bioreactors include the Celligene® series by Eppendorf and the Finesse series by ThermoFisher Scientific.

Mammalian cells are known to be more shear sensitive which stimulated efforts to develop non-abrasive environments during cell culture. Packed bed bioreactors (Figure 1.3 B) provide a fixed chamber where microcarriers or scaffolds are located[125]. Adhered cells that populate the chamber have translational movements restricted, thus being able to better mimic solid tissue presence. Their constrained movement also promotes structured organization and cell-cell interaction, leading to high density cultures. Low velocity fluid flow guarantees dynamic culture without causing shear damage to cells. Culture medium has access to the chamber providing necessary nutrients and removing metabolites. Diffusion limitations or nutrient deficiency can occur due to 3D culture organization. Furthermore, significant cellular organization can result in beneficial biological outcomes, but will normally complicate cell extraction and subsequent downstream processes. Expansion of MSC in a 2.5 L CelliGen® bioreactor (New Brunswick Scientific) with Fibra-Cel® (Eppendorf) disks demonstrated large-scale manufacturing potential for packed bed bioreactors, achieving $9.2x10^7$ cells after 9 days of culture, corresponding to a 9.2-fold increase in total cell number[126].

Increasing available area for cell culture while protecting cells from harsh conditions has inspired innovative bioreactor designs. Hollow fiber bioreactors (Figure 1.3 C) fulfill those requirements by joining thousands of hollow fibers. These fibers are made of thin and porous material that provide a selective passage of nutrients. Culture medium recirculates through the fibers producing interesting tangential flow, mimicking vasculature to some extent[125]. However, significant quantity of fibers originates successive diffusion barriers that cause concentration gradients for nutrients, signaling factors or gases. Similar to packed bed bioreactors, cell extraction processes are challenging to perform due to high cell interaction and difficulty in reaching cells uniformly inside the bioreactor.

With unprecedented tight regulatory measures, the field of bioreactors has moved towards disposable and single-use versions. In order to avoid clean-in-place (CIP) and steam-in-place (SIP) procedures and assure contamination-free product quality, conventional stainless steel or other reusable bioreactors are being substituted by plastic single-use bioreactors (SUB). They reduce cross-contamination and can be combined with limited monitoring probes. Disposable technology has been able to successfully adapt existing geometries, such as the Mobius series by EMD Millipore for stirred tank bioreactors and the Quantum® bioreactor by Terumo BCT for hollow fiber bioreactors. The latter bioreactor has been validated with adherent AT MSC, BM MSC, periosteum-derived MSC and neural stem cells[127–131]. However, novel designs, such as the wave bioreactor (Figure 1.3 D) and the Vertical-Wheel™ bioreactor (Figure 1.3 E), have also shown that there is space for bioreactor innovation that integrate single-use technology. Recently, an overview of SUB and their applicability towards cell therapy have been investigated[132]. It was observed that SUB designs have evolved, currently integrating well known principles of mass transfer and mixing. Their versatility and single-use nature align with cost reduction and demanding regulatory guidelines associated with cell therapies. However, culture monitoring remains a challenge and long-term bag stability must be assured.

Numerous bioreactor designs exist for performing cell culture, nevertheless selecting the correct culture vessel with an appropriate scalability strategy is the actual challenge for the manufacture of cell therapies. Achieving parallelization of individual units (scale-out) tends to be more associated with autologous therapies, while increasing bioreactor size and maintaining culture conditions (scale-up) is more adequate for an allogeneic production. A compromise between scalability and optimal culture conditions is deemed necessary.

1.1.5.4. Agitation

One of the crucial factors for successful cell expansion is culture medium homogenization. Bioreactors require sustained agitation of the culture system, in order to allow an appropriate mass transfer of nutrients and oxygen to the cells, as well as a removal of waste products derived from cell metabolism. For that purpose, cells must be maintained in suspension homogeneously, independently of whether the cells are cultured freely in suspension, as cellular aggregates or adherent to microcarriers/scaffolds.

However, agitation may have an impact on cellular physiology, due to increased shear stress. In this context, shear stress can be defined as the force component acting tangentially to a material, due to fluid motion[133]. Therefore, in bioreactor processing, cells are exposed to shear stress originating from fluid agitation. Shear stress has been described to have a significant impact on cell phenotype, which can be either negative or beneficial depending on the final application. In fact, it has been long established that animal cells in general are

sensitive to shear stress, which compromises their viability above certain levels[134–136]. Additionally, shear stress has been demonstrated to induce osteogenic differentiation of BM MSC through increased expression of osteogenic factors such as bone morphogenetic protein-2 (BMP-2), bone sialoprotein (BSP) and osteopontin (OP)[137] and also resulted in increased intracellular Ca^{2+} levels[138]. Shear stress also improved the angiogenic potential of human AT MSC through stimulation of vascular endothelial growth factor (VEGF) secretion[139].

The importance of agitation and the impact it has on culture outcome has led to the development of new technologies and bioreactor configurations that specifically target this issue. Wave bioreactors (Figure 1.3 D) are suitable for the manufacturing of shear sensitive cells. Their agitation through rocking motion prevents the use of an impeller exerting high shear forces directly in the cells. Very low level of shear stress was found in wave bioreactors compared to classical stirred tank reactors[140]. Wave bioreactor implementation for culture of suspension cells, with emphasis to hematopoietic lineages, is well-known[141,142].

In the same line, Vertical-Wheel™ bioreactors (Figure 1.3 E), developed by PBS Biotech, incorporate a vertically rotating wheel, allowing a more efficient mixing than the traditional horizontal stirring solutions. By allowing lower agitation rates, they are able to minimize shear stress effects. The vertical mixing allows a higher mass transfer rate and more homogenous and gentle particle suspension, favorable for anchorage dependent cells on microcarriers[143]. Moreover, this technology is fully scalable, being available at working volumes that range from 60 mL up to 500 L. Vertical-Wheel™ bioreactors have been successfully applied in microcarrier-based cell culture systems for the expansion of MSC from multiple sources[79,144], as well as for human induced pluripotent stem cells (iPSC)[145].

In summary, agitation can modulate culture conditions and have a significant impact on the characteristics of expanded cells. Different agitation rates and configurations can be used to influence the cell culture outcome. An appropriate balance needs to be found at an agitation rate that allows adequate mass transfer for cell growth, without compromising cell integrity or stem cell fate due to excessive shear stress. Different bioreactor technologies and configurations are available to fine-tune cell culture agitation for each specific application.

1.2. Extracellular vesicles

1.2.1. EV biology

All cells share the ability to secrete extracellular vesicles (EVs), phospholipid bilayer membrane structures enclosing a portion of their own cytoplasm[146] (Figure 1.4). The identification of EVs can be traced back to as early as 1946, when they were described as pro-coagulant particles in plasma[147] and later in the 1960s described as “platelet-dust” and as cartilage matrix vesicles associated with bone calcification[148,149]. A major breakthrough

occurred in 1983, when it was described a mechanism for the release of transferrin receptors from maturing red blood cells through vesicles[150,151]. These vesicles were later named "exosomes" in 1987[152].

For some time, EVs were only considered to be a means to remove unwanted material from the cell. However, the field of EVs was revolutionized in 1996 when exosomes were shown to play a role in antigen presentation, opening an entirely new discussion that EVs might play a role in the transfer of biological information between cells[153]. This was latter consolidated in 2006 and 2007, when EVs were shown to contain RNA (miRNA and mRNA) that could be delivered to recipient cells and changed their behaviour[154,155]. Since then, EVs have emerged as relevant players in intercellular communication, mainly through their ability to transfer their cargo of biomolecules, including proteins, lipids and nucleic acids, which trigger alterations on recipient cells.

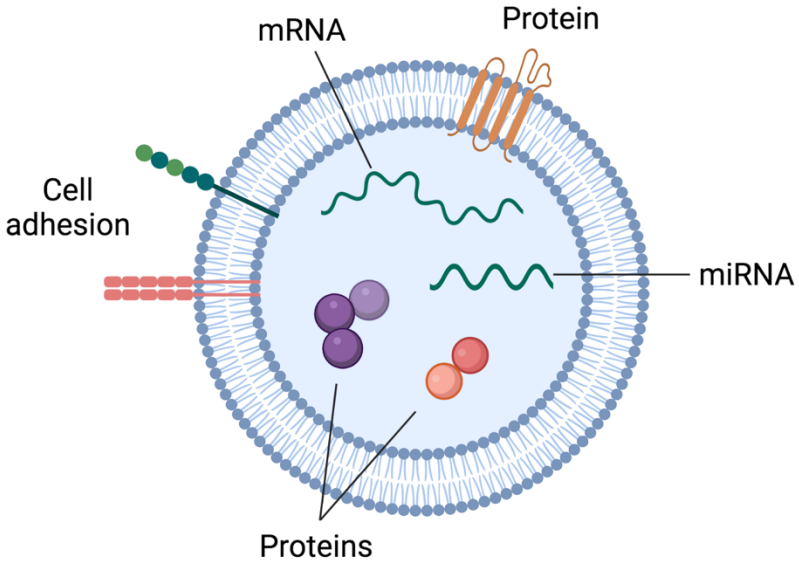

Figure 1.4 - Schematic representation of an EV and its biological composition. EVs are composed by a phospholipid bilayer membrane enclosing intraluminal fluid with cytoplasmic origin. They contain biomolecules from their cell of origin, which include, other than lipids, several types of proteins (e.g. involved in cell adhesion, as well as other transmembrane and intraluminal proteins with various functions) and nucleic acids (e.g. mRNA and miRNA). Figure created with BioRender.com.

The term EVs was proposed in 2011 to define all the different types of extracellular membrane structures[146]. However, EVs actually comprise a highly heterogeneous group. Depending on their biogenesis, EVs are broadly categorized either as exosomes, or microvesicles[156]. Exosomes are generated through the endosomal pathway[156,157]. Endocytosis at the cell membrane leads to the formation of early endosomes. During endosome maturation into late endosomes there is inward budding of endosomes resulting in the accumulation of intraluminal vesicles (ILV), which leads to the formation of multivesicular bodies (MVB), also named multivesicular endosomes (MVE). Upon fusion of MVE with the cell membrane, ILV are released to the extracellular space originating exosomes, which generally display 50-150

nm in diameter. Microvesicles are formed by outward budding of the plasma membrane, ranging in size from 50 nm to 1 μm in diameter or even higher[156]. Exosomes and microvesicles show overlapping properties, such as size, density and molecular composition, making it challenging to distinguish different co-isolated EV subpopulations[158]. Additionally, the composition of EVs may differ among different secreting cells.

The complexity of EVs is further increased when we consider other structures, such as apoptotic bodies released from cells undergoing apoptosis, which can span over a large size range (from 100 nm to 5 μm in diameter)[158] or the recently identified mitovesicles from mitochondrial origin[159]. Moreover, EVs display physical characteristics (i.e. size and density) similar to other secreted non-vesicular nanoparticles such as lipoproteins of various densities[160] and the recently identified exomeres[161].

1.2.1.1. EV biogenesis

Cargo incorporated in exosomes originate from endocytosis at the plasma membrane or are directly targeted to early endosomes via the biosynthetic pathway, from the *trans*-Golgi network[156]. These sorting processes are regulated by various Rab GTPases. Formation of ILV can be regulated by the endosomal sorting complex required for transport (ESCRT), a family of proteins that associate in a stepwise manner at the membrane of MVE[156,158]. Firstly, ESCRT-0 and ESCRT-I subunits cluster membrane-associated cargo in microdomains of the limiting membrane of MVE. The tumor susceptibility gene 101 protein (TSG101) is one of the main ESCRT-I components, being used as an EV protein marker. This is followed by ESCRT-II-mediated recruitment of ESCRT-III that performs budding and fission of this microdomain into the MVE lumen.

Although ESCRT-III is required for fission of ILVs, cargo clustering and membrane budding can be ESCRT-dependent or ESCRT-independent[156]. The latter can rely on syntenin and the ESCRT accessory protein ALG-2 interacting protein X (ALIX), which links cargo to ESCRT-III[156,162]. ESCRT-independent biogenesis is aided by lipids such as ceramide, which allows the generation of membrane subdomains imposing a spontaneous curvature on the membranes[163,164]. Additionally, proteins of the tetraspanin family (e.g. CD63, CD81 and CD9) have been shown to regulate ESCRT-independent cargo sorting to exosomes[156,165,166]. Some tetraspanins also show the potential to form microdomains and induce budding.

Mature MVE can follow a degradative route by fusion with lysosomes or autophagosomes. Alternatively, MVE are transported along microtubules to the plasma membrane. At this stage, MVE fuse with the plasma membrane leading to exosome release in a process mediated by Rab GTPases (e.g. Rab27A/B, Rab35), actin and SNARE (soluble *N*-ethylmaleimide-sensitive fusion attachment protein receptor) proteins[156,158,167–169].

Microvesicle biogenesis shares several mechanisms common to exosome biogenesis. This includes the formation of microdomains (in this case in the plasma membrane) where specific lipids and cargo are clustered as well as a similar role of ESCRT machinery and ceramide in vesicle formation[156]. However, microdomain formation is followed by the translocation of lipids between leaflets of the plasma membrane, a process unique to microvesicle formation. This process is mediated by Ca^{2+}-dependent enzymes (e.g. translocases, scramblases and calpain), rearranging the asymmetry of membrane phospholipids in a way that causes physical bending of the membrane, favoring membrane budding[158,170]. The most significant examples are the exposition of phosphatidylserine (PS) and phosphatidylethanolamine (PE) from the inner leaflet to the cell surface.

1.2.1.2. EV interaction with recipient cells

After being released into the extracellular space, EVs are able to interact with cells either close-by or far away, triggering phenotypic changes in these cells. EV binding to recipient cells can be mediated by tetraspanins, integrins, proteoglycans, lectins, lipids (e.g. PS) and ECM components (e.g. fibronectin and laminin)[156]. After binding to a recipient cell, EVs can follow multiple routes to deliver their message. EVs can elicit changes in recipient cells by simply binding to specific surface receptors, triggering signaling pathways (e.g. antigen presentation), but without delivering any EV cargo[156].

EVs can also be internalized through multiple EV uptake pathways[171] (Figure 1.5). EVs can undergo clathrin-mediated endocytosis, through the formation of a clathrin coat in a portion of cell membrane surrounding the EV to be internalized[172]. This clathrin coat promotes membrane deformation, which results in membrane invagination and formation of a bud that surrounds the EV that then pinches off, separating itself from the membrane[173]. Once in the cytosol, this internalized vesicle undergoes clathrin un-coating. EVs can also be internalized by clathrin-independent endocytosis, such as caveolin-mediated endocytosis involving the formation of cave-like invaginations in the plasma membrane named caveolae, which become internalized into the cell (similarly to clathrin-mediated endocytosis)[171,174]. Caveolin-1 is required for the formation of caveolae, which are also rich in cholesterol and sphingolipids. Clathrin-independent endocytosis may also occur via lipid rafts[175]. These plasma membrane microdomains have altered phospholipid composition, being more tightly packed and consequently less fluid, but float freely in the plasma membrane. Lipid rafts can be found in invaginations formed by caveolin-1 or in planar regions of the plasma membrane associated with flotillins[171]. However, lipid raft-mediated endocytosis of EVs seems to be caveolae-independent[172,175].

Alternatively, EV uptake can happen through non-specific processes such as phagocytosis and macropinocytosis[171,176,177]. Phagocytosis involves the formation of invaginations

surrounding material to be internalized, with or without the formation of enveloping membrane extensions[178]. Although this process is generally used to internalize larger particles, it has been observed to be used to take up EVs. Phosphatidylinositol-3-kinase (PI3K) plays an important role in this process[179]. In macropinocytosis, membrane extensions are formed surrounding a portion of extracellular fluid and fuse back with the plasma membrane internalizing that portion of extracellular content[171,178]. This requires Na^+/H^+ exchanger activity and is dependent on actin, cholesterol and the rac 1 GTPase. Both of these uptake mechanisms seem to be triggered (at least partially) by PS present on the outer leaflet of EV membranes.

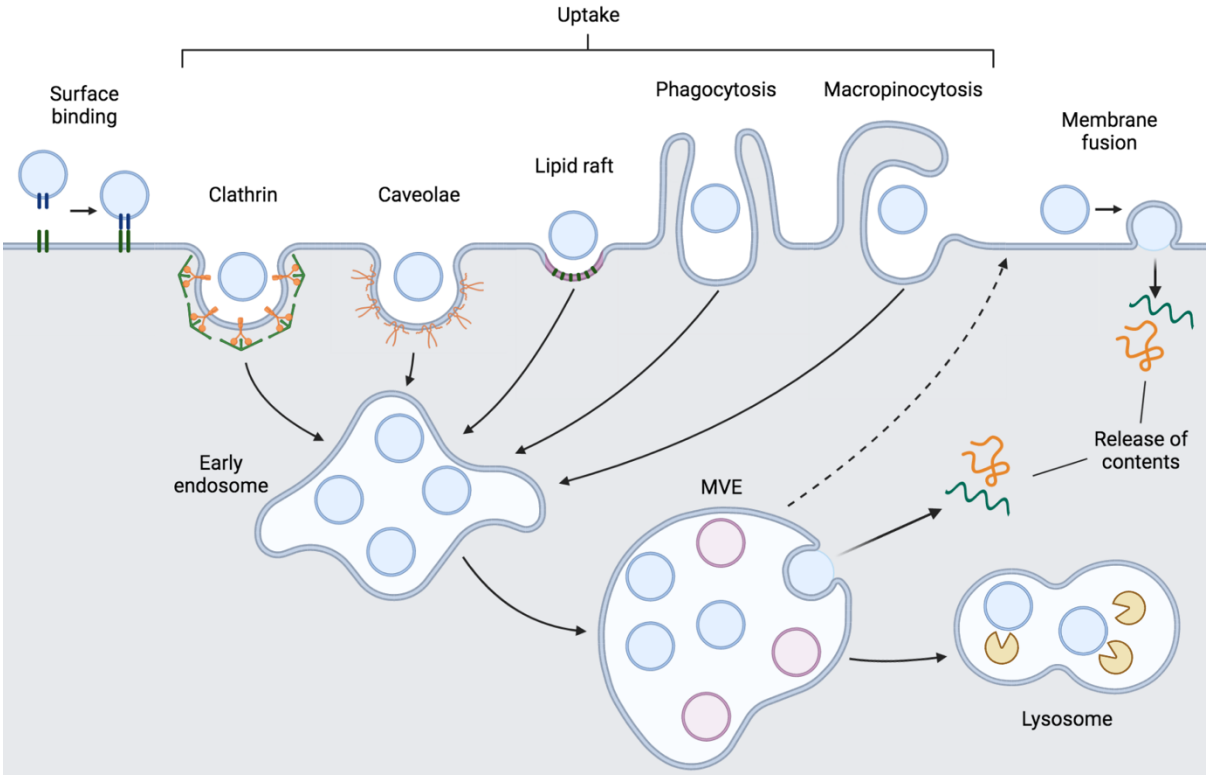

Figure 1.5 - Interaction of EVs with recipient cells. EVs bind to the surface of recipient cells in a process that can be mediated by several molecules, being able to elicit functional changes without entering the cell. EVs may also be internalized by recipient cells through different uptake routes, which include clathrin- or caveolin-mediated endocytosis, endocytosis mediated by lipid rafts, phagocytosis or macropinocytosis. Internalized vesicles follow the endosomal pathway, being sorted into early endosomes and proceeding to MVE. Then, EVs can follow different routes: they can be recycled back to the plasma membrane and released; EVs can fuse with the limiting membrane of MVE releasing their contents to the cytoplasm of the recipient cell; or MVE may fuse with lysosomes leading to EV degradation. In alternative to EV uptake, EVs may also fuse directly with the plasma membrane of the recipient cell, releasing their cargo directly into the cytosol. MVE - multivesicular endosomes. Figure created with BioRender.com.

Internalized EVs follow the endosomal pathway, eventually reaching MVE. At this stage, EVs can follow different fates[156,158]. They can be recycled back to the plasma membrane and released to the extracellular space. MVE can fuse with the lysosome leading to the degradation of the contents of internalized EVs, which can still be a relevant source of metabolites for the host cell. Alternatively, EVs may undergo endosomal escape, through back fusion with the limiting membrane of MVE, releasing their contents to the cytoplasm of the

recipient cell. EVs may also fuse directly with the plasma membrane, releasing their cargo directly into the cytosol of the recipient cell. Intraluminal material released by internalized EVs includes nucleic acids (miRNA, mRNA), proteins and lipids which are able to trigger alterations in the recipient cell. However, little is known about how EV cargo is unpackaged and delivered to the designated site of action, be it the cytoplasm or the nucleus. Intracellular delivery routes are being investigated and may include direct transfer into the endoplasmic reticulum[180] or the nucleus[181,182].

1.2.1.3. EVs in intercellular communication

1.2.1.3.1. Physiological roles of EVs

Given their ability to elicit changes in recipient cells, EVs have been implicated in numerous physiological processes[183,184]. In fertilization, EVs secreted from the egg promote sperm-egg fusion in a tetraspanin CD9-dependent process that was observed in mice[185]. Later on, microvesicles released by early embryo cells promote trophoblast migration and implantation in the uterus through JNK and FAK pathways, which are activated by microvesicle cargo proteins laminin and fibronectin[186]. EVs have been implicated in development by carrying key morphogen molecules such as Wnt proteins (e.g. Wingless) and Sonic Hedgehog[187–189]. Mating behavior can also be altered by EVs, since exosomes secreted by the reproductive glands of male *Drosophila melanogaster* interact with female reproductive tract epithelium and inhibit re-mating of females[190].

EVs are important in the nervous system, being secreted by neurons and glial cells alike to mediate intercellular communication[191]. Neuron-derived EVs have multiple relevant roles at synapses, such as promoting synaptic growth at the neuromuscular junction and regulating postsynaptic retrograde signaling[192–194]. Oligodendrocyte-derived EVs are able to promote neuronal viability and increase neuron firing rate[195]. EVs also play a role in the peripheral nervous system, where Schwann cells are able to secrete EVs to promote axon regeneration[196].

EVs play a relevant part in regulation of immune responses through exchange among multiple types of immune cells. EVs play a crucial role in major histocompatibility complex (MHC) class II antigen presentation, since dendritic cells (DC) secrete exosomes carrying peptide-containing MHCII that stimulate naïve $CD4^+$ T cells[197,198]. DC-derived exosomes were also able to differentiate T helper cells toward a T helper type 1 (Th1) phenotype and enhance immunogenicity *in vivo*[199]. In the opposite direction, T cell-derived exosomes are able to transport miRNA to antigen-presenting cells, modulating their mRNA expression levels[200]. Exosomes were also found to transfer miRNA between DC *in vivo*, modulating gene expression in the recipient cell[201]. Another study revealed that exosome-mediated miRNA

transfer from T regulatory (Treg) cells to Th1 cells was able to reduce inflammatory responses of recipient Th1 cells[202].

Physiological tissue regeneration processes are also supported by EVs. Endothelial cell-derived EVs were able to reduce atherosclerotic lesion formation when delivered to smooth muscle cells[203]. The authors of this study observed that alterations in endothelial cells previously described to be triggered by blood flow-induced shear stress led to enrichment of endothelial cell-derived EVs in specific miRNA molecules that had atheroprotective effects after delivery to smooth muscle cells. In a kidney injury model, injured epithelial cells secreted exosomes that activated fibroblasts to initiate tissue regenerative responses and fibrosis mediated by exosomal transforming growth factor (TGF)-β1 mRNA[204].

1.2.1.3.2. EVs in pathological processes

In addition to their relevant role under normal physiological conditions, EVs have been associated with multiple pathological processes[183,184,205]. Numerous studies reveal tumor-derived EVs as relevant mediators of intercellular communication within the tumor microenvironment (TME), which is composed of multiple non-tumorigenic cells able to collectively support tumor growth and progression such as endothelial cells, fibroblasts, immune cells, among others[206].

Under hypoxic conditions (1% O_2), glioblastoma multiforme (GBM)-derived exosomes amplified the activation of ERK1/2 MAPK, PI3K/Akt and FAK pathways in endothelial cells, compared to normoxic conditions, resulting in increased endothelial cell sprouting[207]. GBM-derived EVs were also found to skew monocyte-to-macrophage differentiation to a tumor-supportive M2-type macrophage phenotype[208]. Conversely, lymph node macrophages were able to suppress tumor growth by absorbing tumor-derived EVs and preventing their interaction with pro-tumorigenic B cells[209]. Tumor-derived EVs are able to suppress anti-tumor adaptive immunity as well. Tumor-derived EVs induced apoptosis of $CD8^+$ T cells and were also able to alter the differentiation of $CD4^+$ T cells into a state that suppresses cytotoxic T cell activity, contributing to tumor escape from the immune system[210].

Tumor-derived EVs also promote tumor invasion and metastasis. They help establishing pre-metastatic niches, by interacting with normal cells at the metastatic sites. Melanoma-derived exosomes recruited BM progenitor cells to future sites of metastasis and re-educated them toward a vasculogenesis supporting phenotype, enhancing tumor invasion and metastasis *in vivo*[211]. This re-education effect was mediated by a tyrosine kinase receptor differentially expressed in exosomes from highly metastatic melanoma cells compared to less aggressive ones.

In another study, exosomes from pancreatic cancer cells induced the formation of pre-metastatic niche in the liver of mice. These exosomes transferred migration inhibitory factor (MIF) to Kupffer cells in the liver that secreted TGF-β, which subsequently increased

fibronectin production by hepatic stellate cells. Fibronectin enhanced the recruitment and retention of BM-derived macrophages, establishing an environment favorable for metastasis[212].

Remarkably, the formation of pre-metastatic niches was found to be promoted by exosomes from different tumor types that targeted specific organs, depending on integrins displayed on their membrane[213]. Exosomes expressing integrins $\alpha_6\beta_4$ and $\alpha_6\beta_1$ were able to bind specifically to fibroblasts and epithelial cells in the lung, mediating lung tropism, while exosomes containing integrin $\alpha_v\beta_5$ bound to Kupffer cells, leading to liver tropism.

EVs derived from non-tumorigenic cells can also support tumor growth under specific circumstances. For instance, exosomes from astrocytes were found to support tumor growth in brain metastatic breast cancer *in vivo*. Astrocyte-derived exosomes mediated miRNA transfer to metastatic tumor cells, reducing the levels of a target mRNA encoding for the tumor suppressor PTEN[214]. Decreased PTEN levels triggered and increased secretion of CCL2 chemokine by metastatic tumor cells, resulting in recruitment of IBA1-expressing myeloid cells that enhanced proliferation and reduced apoptosis of metastatic tumor cells.

In addition to their roles as mediators in tumor progression, tumor-derived EVs also provide a way to eliminate chemotherapeutic agents from cancer cells, enabling chemotherapy resistance. Microvesicle-mediated release of gemcitabine was identified as a key factor for resistance to this drug in human pancreatic cancer cells, both *in vitro* and *in vivo*[215]. Moreover, just as tumor-stromal interactions mediated by EVs play a relevant role in tumor progression, stromal cell-derived EVs can also mediate resistance to therapy. Exosomes derived from stromal cells were able to mediate miRNA transfer to ovarian cancer cells increasing their chemoresistance to paclitaxel[216].

EVs are also involved in cell-cell transport of pathogenic proteins associated with neurodegenerative diseases such as the prion protein (PrP) abnormal isoform PrP^{SC} in prion disease, β-amyloid in Alzheimer's disease and α-synuclein in Parkinson's disease[217,218]. However, the relevance of EV-mediated versus EV-independent spread and propagation of these proteins in disease progression is still unclear. Contrastingly, some studies have described natural beneficial effects of EVs in these pathologies, namely in the clearance of β-amyloid peptides[219,220].

In cardiovascular diseases, EVs have also been found to mediate the cross-talk between different cell types in the heart with implications in disease progression. Secretion of cardiac fibroblast-derived exosomes triggered gene expression alterations in cardiomyocytes, leading to increased pathological cardiac hypertrophy, which contributes to heart failure[221]. In another study, macrophage-derived exosomes transferred miRNA to cardiac fibroblasts, suppressing fibroblast proliferation and promoting fibroblast inflammation during cardiac injury in mice[222].

In multiple infectious diseases, viruses are able to take advantage of EVs to transfer their genetic material between infected and non-infected cells in substitution of direct interaction between viruses and target cells[223]. For example, exosomes derived from human hepatoma cells infected with hepatitis C virus were able to transmit the infection to naïve hepatoma cells[224]. Moreover, this exosome-mediated transmission was partially resistant to antibody neutralization.

Considering the numerous roles of EVs in disease progression, EVs have been extensively studied as novel biomarkers for disease[225–227], as well as targets for new therapeutic strategies[228,229].

1.2.2. EVs as reconfigurable natural therapeutic systems

1.2.2.1. EVs as intrinsically therapeutic agents

Given their ability to participate in intercellular communication, conveying messages from their cells of origin to target recipient cells, EVs have innate therapeutic potential, particularly interesting for tissue regeneration. EVs are able to mediate some of the therapeutic effects from their cells of origin by carrying lipids, proteins and genetic material (mRNA and miRNA) and transferring this cargo to target cells, or by triggering signaling pathways through cell surface interactions.

EVs derived from stem and progenitor cells have gained particular interest due to numerous therapeutic properties attributed to them, which include immunomodulatory capacity (mainly by reducing inflammation)[230–233], suppressing apoptosis and stimulating cell proliferation[234,235], promoting angiogenesis[236,237], stimulating wound repair[238,239] and recruiting and reprograming cells for tissue regeneration[154]. Among the most studied EV-secreting cells with therapeutic properties we can find MSC, embryonic stem cells, iPSC, cardiac progenitor cells and DC[240].

In particular, a growing body of evidence indicates that many of the therapeutic features of MSC are exerted in a paracrine manner and mediated by EVs. The paracrine activity of MSC was initially observed in mice and pig models of myocardial infarction, where conditioned medium from MSC cultures limited infarct size and improved heart function[241–244]. This was followed by similar evidence supporting the paracrine activity of MSC in other organs[245]. In subsequent studies, EVs secreted by MSC were described as the mediators of these paracrine trophic activities, reducing myocardial ischemia/reperfusion injury[246] and also allowing improved recovery from acute kidney injury[247,248] in mice.

Numerous studies reporting different therapeutic activities of EVs derived from MSC and other cells were followed. MSC-derived EVs (MSC-EVs) allowed improved recovery from stroke in mice, by promoting neuronal survival and angioneurogenesis[249]. Human BM MSC-EVs allowed a better recovery from traumatic brain injury in mice[250] and improved the recovery

from acute spinal cord injury in rat[231]. Attenuated inflammation upon EV treatment supported a better recovery in both studies.

MSC-EVs obtained from different tissue sources showed therapeutic potential against hepatic indications. Human UCM MSC-EVs ameliorated liver fibrosis in mice by inactivating the TGF-β1/Smad signaling pathway and inhibiting epithelial-to-mesenchymal transition (EMT) in hepatocytes[251]. BM MSC-EVs reduced hepatic injury in mice, improving their survival[252]. Reduction in hepatocyte apoptosis was proposed to be mediated by the lncRNA Y-RNA-1 carried by EVs. Human UCM MSC-EVs also inhibited pulmonary infiltration of macrophages and suppressed the production of pro-inflammatory and pro-proliferative factors in a murine model of pulmonary hypertension[230].

The large number of preclinical studies using EVs has already been translated into a few clinical trials. The safety and efficacy of MSC-EVs have been evaluated in clinical trials for the treatment of type 1 diabetes (NCT02138331), macular holes (NCT03437759) and chronic kidney disease, with positive safety and efficacy results in the latter[253].

More recently, MSC-EVs have been proposed for the treatment of coronavirus disease-19 (COVID-19), aiming to reduce dysregulated immune responses and the cytokine storm associated with respiratory pathological states of this disease[254]. The rationale for using MSC-EVs is based on previously mentioned observations of inflammatory attenuation in several pathological conditions and supported by studies in relevant lung disease models including lung injury[255,256]. However, the mechanisms behind the beneficial effects of EVs are not fully elucidated yet. Some phase I/II clinical trials were already registered in different countries for the use of EVs for treatment of COVID-19, most of them using EVs derived from MSC either administered intravenously (e.g. NCT04798716) or by inhalation (e.g. NCT04602442) (clinicaltrials.gov, accessed on 24th May 2021, using the search term “(extracellular vesicles OR exosomes) AND COVID-19”).

1.2.2.2. EVs as drug delivery systems

In addition to their use as innate therapeutic products mainly in the context of regenerative medicine, EVs are also promising vehicles for drug delivery to treat numerous conditions. Given their small size and the ability to shuttle messages to other cells in virtually any site in the organism eliciting a functional response, EVs can be regarded as nature’s nanocarriers. In fact, EVs comprise numerous traits that make them appealing for the development of novel drug delivery systems (DDS), even outperforming synthetic nanocarriers in certain aspects.

By using EVs, we can take advantage of endogenous cellular machinery to produce the desired therapeutic cargo and sorting it inside EVs. Additionally, EVs have the ability to overcome biological barriers, namely tissue barriers (e.g. blood-brain barrier (BBB)), cellular barriers (by different EV uptake mechanisms) and intracellular barriers, exerting functional

effects on target cells[257–259]. Due to their biological origin, EVs are generally low immunogenic and are not toxic, opposite to some synthetic nanocarriers[260–262]. On the other hand, EVs are non-replicative and non-mutagenic, relieving some of the safety concerns associated with cell therapies. Therefore, EVs lie in a sweet spot between synthetic nanocarriers and cell-therapies, presenting exciting opportunities for developing next-generation DDS with increased efficacy and lower side-effects.

EVs are able to carry different cargos, including small molecules such as the natural compound curcumin or chemotherapeutic drugs (e.g. doxorubicin and paclitaxel), as well as delivering proteins and different RNA molecules (e.g. siRNA, miRNA and mRNA)[257,263–267]. In this way, EVs can deliver therapeutic molecules in a more efficient and selective manner to target diseased cells and tissues, while minimizing their side effects, as well as protecting cargo from degradation (particularly relevant for RNA molecules). For example, doxorubicin-loaded EVs showed similar cytotoxicity to the free drug in both *in vitro* and *in vivo* models of breast cancer, but with reduced cardiotoxicity[264].

Therapeutic cargo can be loaded into EVs by two different strategies, either exogenously, by inserting cargo directly into EVs after EV production and isolation, or endogenously, where therapeutic cargo is loaded into EVs at the moment of EV biogenesis[259,268]. Several techniques have been applied in order to accomplish exogenous loading of EVs such as direct incubation, electroporation, sonication, saponin, freeze/thaw cycles or extrusion[268]. For example, curcumin was loaded into EVs through direct incubation (e.g. mixing at 22ºC for 5 min) in several studies, yielding diverse positive therapeutic outcomes such as improved bioavailability and anti-inflammatory effect of this drug in a mouse model of inflammation[263], as well as enhanced tumor growth inhibition both *in vitro* and *in vivo*, compared to free curcumin[269]. Electroporation has been applied in numerous studies, for example to load EVs with therapeutic siRNA with positive outcomes in mouse models of Alzheimer's disease[257] and pancreatic ductal adenocarcinoma (PDAC)[270], or for loading small molecules such as doxorubicin, with improved outcomes in different *in vivo* cancer models[264,271,272].

A few studies compared the efficiency of exogenous loading of EVs using different techniques. The hydrophobicity of small molecules can influence their loading into EVs, since hydrophobic porphyrins were loaded in EVs from different cells simply by direct incubation, while hydrophilic porphyrins benefited significantly from active loading techniques such as electroporation, extrusion and especially saponin treatment[273]. In another study, exosomes were loaded with catalase and used to treat *in vitro* and *in vivo* models of Parkinson's disease[274]. Different loading techniques were tested (incubation, saponin treatment, freeze/thaw cycles, sonication and extrusion), revealing improved loading efficiency, sustained release and catalase preservation upon active loading, especially using sonication, extrusion or saponin treatment. Sonication also improved exosome loading with paclitaxel and

yielded positive therapeutic outcome in multidrug resistant (MDR) cancer cells[265]. However, active loading techniques induce temporary disruption of the EV membrane that can lead to loss of EV content or altered morphology and may also induce aggregation of EVs or their cargo as previously reported[275,276].

Additionally, EVs can be fused with liposomes previously synthesized to carry therapeutic cargo, thereby creating EV-liposome hybrids carrying this cargo[277]. MSC-EVs fused with liposomes loaded with a chemotherapeutic compound increased the drug delivery efficiency when compared with the free drug or the drug-loaded liposome in cancer *in vitro* models[278].

Endogenous loading of EVs can be achieved by taking advantage of the natural sorting machinery of cells for the production and/or loading of cargo into EVs. Cells can be loaded with a cargo by direct incubation, which is then sorted and released inside EVs. MSC incubated with paclitaxel incorporated this chemotherapeutic agent and released it inside EVs[279]. These paclitaxel-loaded MSC-EVs were able to inhibit tumor cell proliferation *in vitro*.

Alternatively, endogenous loading of EVs can be achieved by genetic modification of parental cells to express desired RNA molecules or proteins, which will then be loaded into EVs. For example, AT MSC were genetically modified to express miR-122, previously reported to reduce drug resistance in hepatocellular carcinoma[280]. Modified MSC secreted EVs packaging miR-122, which increased antitumor efficacy of chemotherapy on hepatocellular carcinoma *in vivo*.

A new system was developed to achieve protein loading into EVs using an optically reversible protein-protein interaction module[281]. The authors used a photoreceptor cryptochrome 2 (CRY2) and the CRY-interacting protein (CIBN), which bind under blue light illumination. CRY2 was fused with a cargo protein and CIBN was conjugated with the EV transmembrane protein CD9. As a result, the transient docking of CRY2-conjugated cargo proteins with CD9-conjugated CIBN was observed in the generated exosomes in the presence of blue light. When the blue light was removed, the proteins detached and the cargos were released into the intraluminal space of exosomes, allowing cargo proteins to be delivered to recipient cells both *in vitro* and *in vivo*. This strategy was used for the delivery of super-repressor IκBα to relieve sepsis-associated organ damage and reducing mortality in mice[282].

In addition to their unique drug loading abilities, EVs also exhibit intrinsic targeting properties that can be valuable for drug delivery, since protein and lipid composition of EVs can influence cell/organ tropism[283]. As previously mentioned, depending on integrins displayed on their membrane, EVs can show tropism towards lung or liver in pre-metastatic niche formation[213]. Another example is the involvement of PS in EV recognition and uptake by macrophages[284].

Still, EVs can be engineered in order to improve specificity to target cells. Akin to the techniques used for endogenous drug loading, parental cells can be genetically modified to

express a targeting moiety fused to an EV transmembrane protein. The first example relied on the fusion of lysosome-associated membrane protein 2 (Lamp2b) abundant on the surface of EVs with the rabies viral glycoprotein (RVG) peptide that binds to the acetylcholine receptor[257,285]. This strategy allowed EVs to target neurons, oligodendrocytes and microglia and functionally deliver electroporated siRNA for treatment of Alzheimer's disease to the brain in mice. Fusion of targeting moieties with Lamp2b has been used to endow EVs with targeting capacity in several studies, including an α_v integrin-targeting iRGD peptide to target tumor cells and tumor-associated vascular endothelium for doxorubicin delivery[286] and a fragment of interleukin 3 (IL3) to target IL3 receptors on chronic myeloid leukemia (CML) cells for delivery of a chemotherapeutic agent or siRNA[287].

Different types of targeting moieties and transmembrane proteins have been used (Table 1.3). For example, EV-producing cells have been modified to express recombinant anti-epidermal growth factor receptor (EGFR) nanobodies fused to glycosylphosphatidylinositol (GPI)-anchoring peptides[288]. Since EVs are enriched in GPI, EVs were enriched in GPI linked nanobodies displayed on their surface. This allowed EVs to target specifically EGFR-expressing tumor cells.

Table 1.3 - Overview of strategies to engineer EV targeting through genetic modification of producing cells to express a targeting moiety fused to an EV transmembrane protein.

EV transmembrane protein	Targeting moiety	Target	Purpose	Refs.
Lamp2b	RVG peptide	Acetylcholine receptor in neurons	Deliver BACE1 siRNA for Alzheimer's disease treatment	257,285
	RVG peptide	Acetylcholine receptor in neurons	Deliver miR-124 to promote neurogenesis after stroke	289
	iRGD peptide	α_v integrin-positive breast cancer cells	Deliver doxorubicin	271
	IL3 fragment	IL3 receptor in CML cells	Deliver Imatinib or BCR-ABL siRNA	287
	Cardiomyocyte specific peptide	Cardiomyocytes	Target cardiomyocytes	290
PDGFR	GE11 peptide	EGFR-expressing cancer cells	Deliver let-7a miRNA	291
GPI-anchoring peptide	Anti-EGFR nanobody	EGFR-expressing cancer cells	Target cancer cells	288

Lamp2b - lysosome-associated membrane protein 2; RVG - rabies viral glycoprotein; BACE1 - beta secretase 1; IL3 - interleukin 3; CML - chronic myeloid leukemia; PDGFR - platelet-derived growth factor receptor; EGFR - epidermal growth factor receptor; GPI - glycosylphosphatidylinositol.

Alternatively, targeting ligands can be exposed on the surface of EVs after EV isolation, avoiding challenging genetic engineering of producer cells. Several different strategies have been applied in this context (Table 1.4). A recombinant protein was developed, consisting of an anti-EGFR nanobody fused to the C1C2 domain of lactadherin, which binds to PS present on the surface of EVs, directing these modified EVs to EGFR-positive cancer cells[292]. In

another study, EVs were modified in order to target neuropilin-1 (NRP-1), which is a transmembrane glycoprotein overexpressed in glioma cells and the tumor vascular endothelium[293]. For this purpose, an NRP-1-targeting peptide was conjugated with the surface of EVs by click chemistry.

Table 1.4 - Overview of strategies to engineer EV targeting by anchoring a targeting moiety to EVs after EV production and isolation.

Linkage method	Targeting moiety	Target	Purpose	Refs.
Post-insertion of phospholipid (DMPE)-PEG fusion molecules in EV membranes	Anti-EGFR nanobody (conj. with DMPE-PEG)	EGFR-expressing cancer cells	Target cancer cells	294
Membrane anchoring cholesterol	AS1411 DNA aptamer (conj. with cholesterol)	Nucleolin on breast cancer cells	Deliver let-7 miRNA or VEGF siRNA	295
Electrostatic interaction between cationized pullulan and EVs	Cationized pullulan (a polysaccharide polymer)	Hepatocyte asialoglycoprotein receptors	Target injured liver	296
C1C2 domain of lactadherin binding to PS present on EV membrane	Anti-EGFR nanobody (conj. with C1C2)	EGFR-expressing cancer cells	Target cancer cells	292
Membrane anchoring cholesterol	RNA aptamers or folate (conj. with cholesterol)	PSMA, EGFR or folate receptor on prostate, breast or colorectal cancers, respectively	Deliver survivin-targeting siRNA	297
Click chemistry reaction	c(RGDyK) peptide	Integrin $\alpha_v\beta_3$ in reactive cerebral vascular endothelial cells after ischemia	Deliver curcumin to stroke lesions	298
ApoA-I mimetic peptide interaction with phospholipids on EV membrane	LDL peptide	LDL receptor on GBM cells	Delivery of KLA peptide and methotrexate	299
CP05 peptide binding to CD63 present on EV membrane	Muscle targeting peptide M12 (conj. with CP05)	Muscle	Deliver PMO to muscle for Duchenne muscular dystrophy treatment	300
Click chemistry reaction	NRP-1 targeting peptide (RGE)	NRP-1 in glioma cells and tumor vascular endothelium	Deliver SPIONs and curcumin for imaging and therapy of glioma	293
Covalent bond by protein ligating enzymes Sortase A or OaAEP1 ligase	EGFR-targeting peptide or nanobodies targeting EGFR or HER2	Cancer cells expressing EGFR or HER2	Deliver paclitaxel or mRNA	301

DMPE - 1,2-Dimyristoyl-sn-glycero-3-phosphoethanolamine; PEG - polyethylene glycol; EGFR - epidermal growth factor receptor; VEGF - vascular endothelial growth factor; PS - phosphatidylserine; PSMA - Prostate-specific membrane antigen; LDL - low-density lipoprotein; GBM - glioblastoma multiforme; PMO - phosphorodiamidate morpholino oligomer; NRP-1 - neuropilin-1; SPION - superparamagnetic iron oxide nanoparticles; HER2 - human epidermal growth factor receptor 2.

The promising results obtained in preclinical studies using EV-based DDS for numerous clinical indications prompted their use in pioneering clinical trials over the past few years[240]. Plant-derived EVs loaded with curcumin have been used for treatment of colon cancer (NCT01294072). Tumor-derived EVs loaded with chemotherapeutic agents (NCT01854866) and EVs derived from malignant pleural effusion loaded with methotrexate (NCT02657460) are being studied for treatment of malignant ascites and pleural effusion. Other clinical trials

are testing the use of allogeneic MSC-EVs enriched in miR-124 for treatment of acute ischemic stroke (NCT03384433) or loaded with $KRAS^{G12D}$ siRNA for treatment of metastatic pancreatic cancer (NCT03608631).

1.3. Azurin and p28 as anticancer tools

Azurin is a small (14 kDa) and water soluble bacterial protein secreted by *Pseudomonas aeruginosa*[302,303]. It is a member of the cupredoxin family, copper-binding proteins involved in the electron transport chain of prokaryotes. Azurin is composed of 128 amino acids and exhibits a Greek key β-barrel structure comprised of eight parallel and antiparallel strands and an α-helix region situated outside the barrel (Figure 1.6). Like other proteins of the cupredoxin family, this structure confers azurin the nature of a scaffold protein, with the ability to establish affinity interactions with multiple unrelated proteins. In fact, this seems to endow azurin with anticancer activity by interfering in multiple events associated with carcinogenesis and has sparked the interest in applying this protein for cancer therapy[304,305].

Azurin has the ability to preferentially enter cancer cells, compared with normal cells[306]. This internalization occurs substantially through lipid rafts, cholesterol-rich microdomains over-represented in cancer cells, namely through azurin interaction with lipid raft markers caveolin-1 and ganglioside GM-1[307]. After internalization, azurin forms a complex with the tumor suppressor protein p53, stabilizes it and increases its intracellular concentration, increasing apoptosis[304,305,308,309]. Azurin also targets an EphB2 tyrosine kinase-mediated cell proliferation pathway that is upregulated in many tumors[310]. Moreover, simultaneous treatment with azurin was observed to enhance the activity of chemotherapeutic anticancer agents such as doxorubicin and paclitaxel[307] as well as of the tyrosine kinase inhibitors gefitinib and erlotinib[311].

In addition, a particular peptide sequence from azurin, called p28 has been the main focus for clinical application in cancer therapy, due to its ability to act both as a cell-penetrating peptide (CPP) and an effective inhibitor of cancer cell proliferation in several cancer types, both *in vitro* and *in vivo*[312]. This 28 amino acid sequence of azurin (Leu^{50}-Asp^{77}) contains its α-helical domain (Figure 1.6) and is an amphipathic peptide with a negative net charge.

The peptide p28 was identified as the domain responsible for the penetration of azurin into cancer cells[313] (i.e. the protein transduction domain, PTD) and similarly to azurin, it preferentially enters and accumulates in a variety of solid tumor cells, compared to equivalent non-cancerous cells[306]. Cancer cell penetration of p28 occurs via endocytotic, caveosome-directed, and caveosome-independent pathways, unlike cationic CPP that essentially bind to cell membrane glycosaminoglycans (GAGs)[306]. Further studies revealed a shorter sequence of 18 amino acids containing the α-helical domain of p28, named p18 (Leu^{50}-Gly^{67}) as the minimal motif for the PTD (Figure 1.6), relevant for the preferential internalization of azurin

into tumor cells[306]. However, the whole p28 sequence seems to be required to exert an anti-proliferative activity.

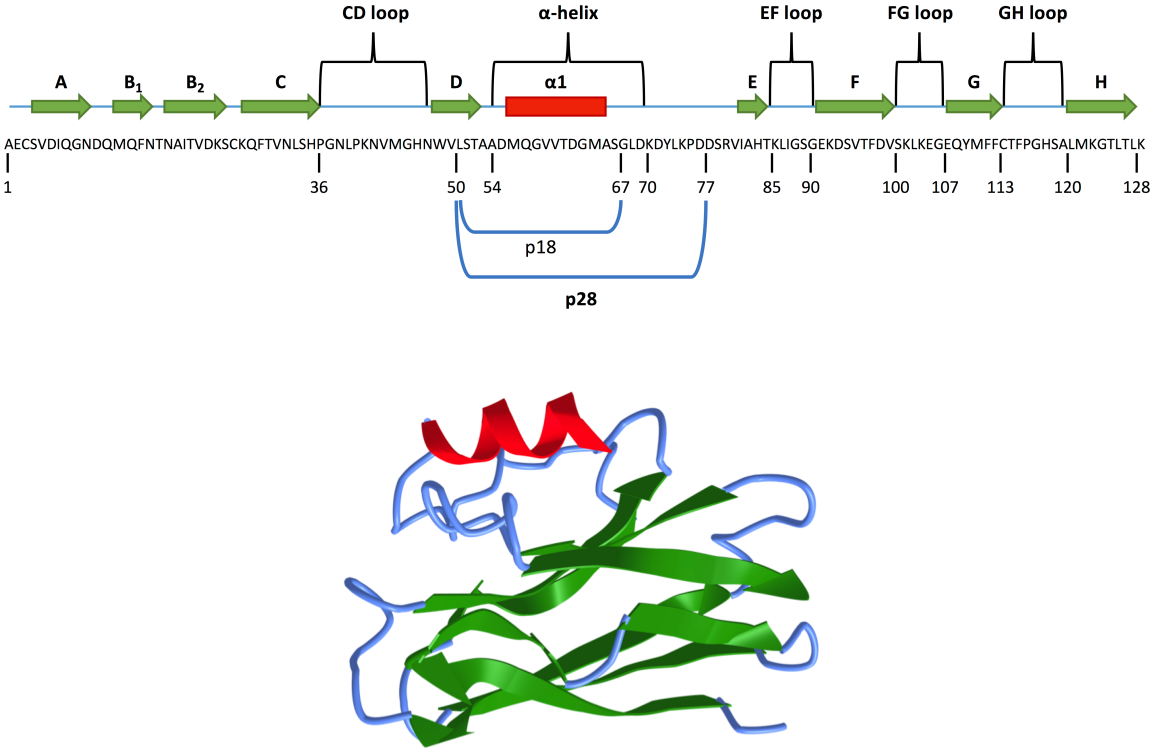

Figure 1.6 - Structure of azurin from P. aeruginosa. Primary structure of azurin (128 aa) and its derived peptides p28 (28 aa) and p18 (18 aa), with secondary elements illustrated as arrows for β-sheets and rectangles for α-helix. Ribbon drawing of azurin (1jzg) generated using iCn3D[314], based on the structure obtained from the Protein Data Bank (PDB)[315,316].

After entering cancer cells, p28 also binds to both wild-type and mutant p53, blocking the binding of E3 ligase Cop1, subsequently inhibiting Cop1-mediated ubiquitination and proteasomal degradation of p53, thus stabilizing p53[317,318]. This results in increased p53 levels that upregulate p21 and p27 cell-cycle inhibitors, downregulating FoxM1 or alternatively inhibiting CDK2 and cyclin A expression, thus leading to G_2–M cell-cycle arrest, ultimately resulting in apoptosis of cancer cells. Given its p53 stabilizing role, p28 also enhances the efficacy of multiple chemotherapy drugs, either DNA damaging agents (e.g. doxorubicin, dacarbazine and temozolamide) or antimitotic agents (e.g. paclitaxel and docetaxel)[319].

In addition, p28 (as well as azurin) preferentially enters endothelial cells, co-localized with caveolin-1 and VEGFR-2 and inhibits angiogenesis. The phosphorylation of VEGFR-2, focal adhesion kinase-1 (FAK) and protein kinase B (Akt) is decreased by p28. This inhibits endothelial cell motility and migration, thereby inhibiting angiogenesis within the TME[320].

Notably, two phase I clinical trials have been completed using azurin-p28 in adult patients with various tumors[321] and in children with brain tumors[322]. Results revealed no significant toxicity or adverse events and presented favorable tumor regression in several patients.

Subsequently, in December 2015, the FDA granted approval to azurin-p28 as an orphan drug for the treatment of brain tumor glioma.

1.4. Motivation and thesis outline

Cancer is one of the leading causes of death worldwide with over 19 million new cases and nearly 10 million people dying from cancer in 2020[323]. In fact, some estimations indicate that 2 out of 5 people may develop cancer in their lifetimes[324]. Conventional cancer therapies present several limitations such as low success rates and lack of selectivity that result in considerable loss of healthy tissue and major side-effects sometimes with limited beneficial results. In spite of considerable progress recently made in early detection and in the development of improved therapeutic solutions, new therapies are required in order to cope with the increasing prevalence of cancer.

DDS are one of the strategies that have been used to improve the efficacy of cancer therapies, relying on incorporation of highly concentrated drugs protected inside nanocarriers that are able to reach tumors and deliver drugs more efficiently[325]. However, most DDS are based on synthetic nanocarriers, which do not fully capture the complexity of the cellular membrane, presenting some limitations regarding toxicity and rapid clearance[260]. EVs are a promising alternative for drug delivery due to their natural role in intercellular communication. Moreover, they can be engineered in numerous ways to incorporate therapeutic payload and to improve their targeting to diseased sites.

In addition to their potential for drug delivery, EVs present innate therapeutic properties promising for regenerative medicine due to their ability to mediate some of the therapeutic effects from their cells of origin. MSC have been particularly regarded as a promising source for the production of EVs for therapeutic application, considering their intrinsic trophic properties[14,15], a favorable safety profile[326] and good expansion capacity when cultured *ex vivo*[89,120–124]. Despite the promising potential of EVs for therapeutic applications, robust and scalable manufacturing processes for EV production are still lacking.

In order to overcome current limitations in EV manufacturing and aiming to achieve a product closely translatable to a clinical setting, we strived for the establishment of a scalable platform for the production of MSC-EVs. The main aim of the thesis was to establish novel DDS for cancer therapy by combining MSC-EVs with the anticancer p28 peptide from the bacterial protein azurin.

Chapter 1 introduces relevant concepts for this thesis and presents a detailed review of the relevant progresses in the fields of MSC and EVs, as well as the potential of using azurin and its lead peptide p28 as anticancer tools.

Chapter 2 features a scalable microcarrier-based bioreactor culture system to produce MSC-EVs under S/XF conditions in a Vertical-Wheel™ bioreactor using MSC from three

different human tissue sources (BM, AT and UCM). MSC-EVs were produced in a bioreactor system, characterized in what concerns relevant biochemical and biophysical parameters and compared with the same EVs obtained in static culture platforms in order to evaluate the impact of bioreactor culture.

Chapter 3 addresses the comparison of the functional activity of MSC-EVs obtained from two different human tissue sources (BM and UCM) in conditions closely translatable to a clinical setting. MSC were cultured under S/XF conditions in planar culture systems, and a scalable and selective EV isolation method that combined tangential flow filtration (TFF) with size exclusion chromatography (SEC) was applied. One of the most studied functional activities of MSC-EVs is their pro-angiogenic capacity and subsequent beneficial impact on tissue regeneration[236,237,327,328]. Therefore, the functional activity of MSC-EVs was studied by investigating their impact on angiogenesis using *in vitro* models employing endothelial cells, namely a scratch wound assay, a 3D spheroid sprouting assay and an assay to examine the activation of ERK1/2 and Akt pathways.

Chapter 4 comprises the application of MSC-EVs decorated with the p28 peptide on their surface to develop anti-cancer DDS. Since p28 was described to preferentially enter a variety of cancer cells compared with normal cells[306], EV decoration with p28 may improve EV targeting to cancer cells. Thus, a novel p28-conjugated peptide able to anchor to the surface of EVs after they were isolated was designed by fusing p28 with a previously described EV-anchoring peptide[300]. The impact of surface decoration of MSC-EVs with p28 on their uptake by breast cancer cells was studied. MSC-EVs were manufactured in conditions closely translatable to a clinical setting as in Chapter 3.

Chapter 5 summarizes the main achievements of this thesis and its contribution to the state-of-the-art, presenting general considerations about the outputs of this thesis that could lead to future work and speculates about the future of EV therapeutics.

2. Scalable production of human mesenchymal stromal cell-derived extracellular vesicles under serum-/xeno-free conditions in a microcarrier-based bioreactor culture system

This chapter was adapted from the original research paper: de Almeida Fuzeta, M., Bernardes, N., Oliveira, F.D., Costa, A.C., Fernandes-Platzgummer, A., Farinha, J.P., Rodrigues, C.A.V., Jung, S., Tseng, R.-J., Milligan, W., Lee, B., Castanho, M.A.R.B., Gaspar, D., Cabral, J.M.S., da Silva, C.L. (2020) Scalable Production of Human Mesenchymal Stromal Cell-Derived Extracellular Vesicles Under Serum-/Xeno-Free Conditions in a Microcarrier-Based Bioreactor Culture System. Front Cell Dev Biol 8:553444.

2.1. Summary

MSC hold great promise for tissue engineering and cell-based therapies due to their multilineage differentiation potential and intrinsic immunomodulatory and trophic activities. Over the past years, increasing evidence has proposed EVs as mediators of many of the MSC-associated therapeutic features. EVs have emerged as mediators of intercellular communication, being associated with multiple physiological processes, but also in the pathogenesis of several diseases. EVs are derived from cell membranes, allowing high biocompatibility to target cells, while their small size makes them ideal candidates to cross biological barriers. Despite the promising potential of EVs for therapeutic applications, robust manufacturing processes that would increase the consistency and scalability of EV production are still lacking.

In this work, EVs were produced by MSC isolated from different human tissue sources (BM, AT and UCM). A serum-/xeno-free (S/XF) microcarrier-based culture system was implemented in a Vertical-Wheel™ bioreactor (VWBR), employing a hPL culture supplement (UltraGRO™-PURE), towards the scalable production of MSC-EVs.

The morphology and structure of the manufactured EVs were assessed by atomic force microscopy, while EV protein markers were successfully identified in EVs by Western blot, and EV surface charge was maintained relatively constant (between -15.5 ± 1.6 mV and -19.4 ± 1.4 mV), as determined by zeta potential measurements. When compared to traditional culture systems under static conditions (T-flasks), the VWBR system allowed the production of EVs at higher concentration (i.e. EV concentration in the conditioned medium) (5.7-fold increase overall) and productivity (i.e. amount of EVs generated per cell) (3-fold increase overall). BM, AT and UCM MSC cultured in the VWBR system yielded an average of 2.8 ± 0.1 x 10^{11}, 3.1 ± 1.3 x 10^{11} and 4.1 ± 1.7 x 10^{11} EV particles (n=3), respectively, in a 60 mL final volume. This bioreactor system also allowed to obtain a more robust MSC-EV production, regarding their purity, compared to static culture.

Overall, we demonstrate that this scalable culture system can robustly manufacture EVs from MSC derived from different tissue sources, towards the development of novel therapeutic products.

2.2. Background

MSC exhibit multilineage differentiation ability, as well as intrinsic immunomodulatory and trophic activities , standing as promising candidates for tissue engineering and cell-based therapies[14,15]. MSC are able to inhibit apoptosis and scarring (fibrosis), promote angiogenesis and support growth and differentiation of progenitor cells into functional regenerative units[14,15]. The array of beneficial effects attributed to MSC has made them one of the most studied cells

in clinical trials[16]. The trophic activity of MSC relies greatly on the secretion of bioactive factors that assist in repair and regeneration processes through paracrine signaling[14,15].

Recently, increasing evidence suggests that several MSC-associated paracrine therapeutic features are mediated by EVs[246,247,329,330]. EVs, such as exosomes and microvesicles, are lipid membrane enclosed structures actively secreted by cells. These vesicles have emerged as relevant mediators of intercellular communication, through the transfer of a cargo of proteins and RNA (i.e. microRNA and mRNA), which trigger alterations on host cells[153–155]. Their small size (generally 50 - 1000 nm) and resemblance to the cell membrane makes EVs ideal candidates to cross biological barriers, thus providing high biocompatibility to target cells[156,257,331].

EVs can be used in therapeutic settings through two different approaches. On one hand, EVs are able to mediate some of the therapeutic effects from their cells of origin[246,248]. Therefore, EVs could be potentially used in substitution of their cell of origin, as a cell-free therapy triggering equivalent therapeutic effect. On the other hand, EVs can be used as drug delivery vehicles, by loading EVs with therapeutic cargo, as an alternative to synthetic DDS[260].

MSC are particularly interesting for EV production for a number of reasons. MSC are considered immune evasive cells and the safety of their administration has already been confirmed in a number of clinical trials[326]. Therefore, it is reasonable to assume that MSC-EVs are not prone to immune reaction from the host immune system[332,333], and promising for the development of allogeneic (i.e. off-the-shelf) therapeutic products. MSC are intrinsically therapeutic, with promising applications for multiple diseases and MSC-EVs convey similar benefits as well[329,334]. Finally, MSC show great ability for expansion when cultured *ex vivo* and robust expansion platforms have already been established[89,120–124].

Despite the promising potential of EVs for therapeutic applications, robust manufacturing processes that would increase the consistency and scalability of EV production are still lacking. Similarly to the cell therapy context, where large cell numbers per dose are required[335–337], very large numbers of EVs are expected to be required for clinical use (e.g. each patient may require 0.5 - 1.4 x 10^{11} EVs[338]). In order to achieve such large production capacities, robust and scalable manufacturing processes need to be developed.

The development of cell-based therapies faces multiple challenges (recently reviewed[339]) and these also apply to manufacturing of EV products. One of these challenges is the use of appropriate cell culture medium. The most commonly used culture medium supplement in *ex vivo* expansion platforms of MSC is FBS, which presents several disadvantages when considering the production of cell-based therapies for human use due to their animal origin. As an alternative to animal derived products, S/XF culture supplements have been developed, such as hPL.

Another major challenge is determining the appropriate cell culture platform for scalable manufacturing of cell-based therapies[339]. In order to achieve large product batches for clinical use, culture platforms require scalability as well as the ability to monitor and control culture parameters, which cannot be accomplished in traditional static culture systems. Multiple bioreactor configurations operating in dynamic culture conditions have been developed for this purpose[339,340]. Expansion of MSC immobilized on microcarriers has been explored in stirred tank bioreactor configurations[339,340]. These bioreactors use an agitation system to maintain microcarriers in suspension and allow medium homogenization. However, agitation impacts cellular physiology due to increased shear stress.

In order to improve agitation patterns in cell culture, PBS Biotech has developed scalable VWBR that can provide gentle and uniform mixing with minimal shear stress. A vertically rotating wheel promotes radial and axial fluid flow and creates a more homogeneous hydrodynamic environment compared with traditional stirred tank bioreactors. In addition, the Vertical-Wheel™ impeller can fully suspend microcarriers with minimal power input and thus minimize shear stress effects[143]. Moreover, this technology is scalable, being available at working volumes that range from 100 mL up to 500 L. Recently, VWBR have been successfully applied in microcarrier-based cell culture processes for the expansion of MSC from multiple sources[79,144], as well as for human induced pluripotent stem cells[145,341].

In this work, EVs were produced by MSC isolated from different human tissue sources, namely BM, AT and UCM. A S/XF microcarrier-based culture system was implemented in a single-use VWBR, employing a hPL culture supplement (UltraGRO™-PURE), towards the production of MSC-EVs.

When compared with traditional static culture systems (i.e. T-flasks), the bioreactor-based culture system allowed a substantial improvement in EV production. This culture system is expected to contribute to robustly manufacture human MSC-EVs in a scalable manner, which can be applied as intrinsic medicines or as delivery vehicles in different therapeutic settings.

2.3. Materials and methods

2.3.1. MSC isolation from human samples

Human MSC used in this study are part of the cell bank available at the Stem Cell Engineering Research Group (SCERG), iBB-Institute for Bioengineering and Biosciences at Instituto Superior Técnico (IST). MSC were previously isolated/expanded according to protocols previously established at iBB-IST. UCM MSC were isolated in hPL-supplemented medium according to the protocol described by de Soure *et al*[78]. BM MSC were isolated in hPL-supplemented medium by adapting the protocol for cell isolation using FBS-supplemented medium described by dos Santos *et al*[102]. AT MSC were originally isolated in

FBS-supplemented medium according to Oliveira *et al*[104], cryopreserved and later adapted for 1 or 2 passages to hPL-supplemented medium. Originally, human tissue samples were obtained from local hospitals under collaboration agreements with iBB-IST (bone marrow: Instituto Português de Oncologia Francisco Gentil, Lisboa; adipose tissue: Clínica de Todos-os-Santos, Lisboa; umbilical cord: Hospital São Francisco Xavier, Lisboa, Centro Hospitalar Lisboa Ocidental, Lisboa). All human samples were obtained from healthy donors after written informed consent according to the Directive 2004/23/EC of the European Parliament and of the Council of 31 March 2004 on setting standards of quality and safety for the donation, procurement, testing, processing, preservation, storage and distribution of human tissues and cells (Portuguese Law 22/2007, June 29), with the approval of the Ethics Committee of the respective clinical institution. Human MSC from the different sources (BM, AT and UCM) were cryopreserved in a liquid/vapor-phase nitrogen container.

2.3.2. MSC expansion in static conditions

In general, MSC expansion in static conditions was performed as previously described[79]. In summary, previously isolated BM, AT and UCM MSC were thawed and plated on T-flasks (Falcon), at a cell density between 3000-6000 cell/cm^2. MSC were cultured in low glucose (1 g/L) DMEM (Gibco, Life Technologies), supplemented with 5% v/v of the hPL UltraGRO^{TM}-PURE (AventaCell Biomedical) and Antibiotic-Antimycotic (1x) (Gibco, Life Technologies).

Cells were maintained at 37°C and 5% CO_2 in a humidified atmosphere and culture medium was changed every 3-4 days. At 70-80% cell confluence, MSC were detached from the flasks using the xeno-free cell detachment solution TrypLE™ Select (1x) (Gibco, Life Technologies) for 7 min at 37°C. Cell number and viability were determined using the Trypan Blue (Gibco, Life Technologies) exclusion method.

After thawing, MSC were passaged at least once before either final inoculation into T-flasks for EV production under static conditions or inoculation in VWBR. MSC were always plated at 3000 cell/cm^2. For each cell source, MSC from three independent donors (n=3) in passages (P) from P4 to P5 were used to inoculate either the final T-flasks for EV production or the VWBR (specifically, BM1 (P4); BM2 (P5); BM3 (P4); AT1 (P4); AT2 (P4); AT3 (P5); UCM1 (P4); UCM2 (P4); UCM3 (P5)) (Figure 2.1).

2.3.3. MSC-EV production under static conditions

For the production of MSC-EVs under static conditions, previously cultured MSC were passaged to T-175 flasks, at 3000 cells/cm^2. Cells were cultured in the same conditions described before for MSC expansion under static conditions. When maximum cell confluency in the flasks was achieved (90-100%), cells were washed once with basal DMEM low glucose (i.e. supplemented only with Antibiotic-Antimycotic) and subsequently cultured for 48 h in basal DMEM low glucose (20 mL per T-175), for medium conditioning. At the end of the 48 h

period, the conditioned medium was recovered, centrifuged (360 x *g*, 10 min) to remove cell debris and stored at 4ºC for less than 1 week until processing for EV isolation.

After recovery of the conditioned medium, MSC were detached from the flasks and cell number was determined as previously described. Cells were re-suspended in phosphate buffered saline (PBS) for pelleting and stored at -80ºC until further analysis (i.e. Western blots).

2.3.4. MSC expansion and MSC-EV production in the bioreactor culture system

Expansion of human MSC in VWBR was generally performed as previously described[79]. In summary, previously isolated and expanded human MSC were inoculated in a PBS 0.1 MAG bioreactor (PBS Biotech Inc.) with a working volume of 100 mL. Animal product-free SoloHill plastic microcarriers (PALL) were used in order to provide a surface for MSC to adhere and proliferate. Inoculation in the VWBR was performed in 60 mL of the same culture medium used for static conditions (i.e. DMEM low glucose, 5% v/v UltraGRO^{TM}-PURE, Antibiotic-Antimycotic 1x), with an initial MSC number of $5x10^6$ and 2 g of microcarriers. The VWBR was placed at 37°C and 5% CO_2 in a humidified atmosphere.

After an initial intermittent agitation regime, a continuous agitation mode was set at 25 rpm, as previously described[79]. This agitation rate was always maintained, except for AT MSC culture, which required an increment in the agitation rate to 30 rpm at day 2 or 3 of culture and to 35 rpm at day 4 or 5, due to increased medium viscosity and the subsequent formation of cell aggregates.

After 2 days of culture, 40 mL of fresh culture medium with a glucose pulse (3 g/L) was added to the VWBR, achieving a final working volume of 100 mL. From this day onward, 25% v/v of culture medium was exchanged every 24 h, with the addition of fresh culture medium supplemented with a glucose pulse (3 g/L). Cell growth and viability were assessed every day, as previously described[78]. Growth rate was determined by performing an exponential fitting to experimental data corresponding to the exponential growth phase. Cell visualization on microcarriers was performed by staining the cells with 4′,6-diamidino-2-phenylindole (DAPI, Sigma, 1.5 µg/mL in PBS), as previously described[78].

When MSC cultures reached stationary growth and the maximum cell concentration was achieved, the MSC expansion stage of the process was concluded and the EV production stage started. The culture medium was removed from the VWBR, after a 10 min sedimentation of cells attached to microcarriers inside the vessel. The VWBR was washed with 60 mL basal DMEM low glucose medium, at 30 rpm agitation, in order to remove hPL components. The cells on microcarriers were sedimented once again for 10 min and the washing medium was removed. MSC were kept in culture in the VWBR for 48 h in 60 mL basal DMEM low glucose

medium, under the same conditions (i.e. agitation speed, temperature, O_2 and CO_2 concentrations) used for MSC expansion.

At the end of the 48 h period, the whole culture volume was recovered from the VWBR and transferred to 50 mL tubes (Falcon), where cells on microcarriers were sedimented for 10 min. The MSC conditioned medium was recovered and centrifuged at 360 x *g* for 10 min, to remove remaining microcarriers, cells and cell debris. Conditioned medium was stored at 4ºC for less than 1 week until processing for EV isolation. After recovery of the conditioned medium, cells attached to microcarriers were re-suspended in PBS and stored at -80ºC for further analysis (i.e. Western blots).

2.3.5. Isolation of EVs from MSC cultures

EVs were isolated using the Total Exosome Isolation reagent (Invitrogen, Life Technologies), according to the manufacturer instructions. Briefly, MSC conditioned medium was centrifuged for 30 min at 2000 x *g*, to remove cell debris and incubated overnight at 4ºC with the isolation reagent. This mixture was then centrifuged for 1 h at 10000 x *g* and 4ºC. The supernatant was discarded and the EV fraction was recovered by thoroughly washing the walls of the centrifuge tube with PBS 1x (Invitrogen, Life Technologies) in UltraPure™ DNase/RNase-Free Distilled Water (Invitrogen, Life Technologies). EV samples were re-suspended in a PBS volume corresponding to a concentration factor of 20x to 70x relatively to the processed conditioned medium volume. EV samples were frozen at -80ºC in aliquots (50-100 µL), in order to minimize freeze-thawing cycles.

2.3.6. Comprehensive characterization of manufactured EVs

2.3.6.1. Protein quantification

Total protein was quantified in EV samples using the Pierce™ BCA Protein Assay Kit (Thermo Scientific), according to manufacturer instructions for the microplate procedure. Samples were quantified either undiluted or after a 2x dilution. Three replicates were quantified for each sample. Sample concentration was determined by applying a linear fit to the bovine serum albumin (BSA) standards and using the resulting equation to determine each sample concentration from its absorbance measurement.

2.3.6.2. Nanoparticle tracking analysis

EV size distribution profiles and concentration measurements were obtained by nanoparticle tracking analysis (NTA), using a NanoSight LM14c instrument equipped with a 405 nm laser (Malvern) and NTA software version 3.1 (Malvern). Silica 100 nm microspheres (Polysciences, Inc.) were routinely analyzed to check instrument performance[342]. NTA acquisition and post-acquisition settings were optimized and kept constant for all samples.

These settings were established using silica 100 nm microspheres[342] and subsequently adjusted for optimal detection of MSC-EVs.

EV samples were diluted in 2 mL of PBS 1x in UltraPure™ DNase/RNase-Free Distilled Water, to obtain a final concentration in the range of $5x10^8$ to $3x10^9$ particles/mL. Samples were measured using a camera level of 13. Acquisition temperature was controlled and maintained at 20ºC. Each sample was recorded 10 times for 30 s, using fresh sample for each acquisition (by pushing the sample syringe). The detection chamber was thoroughly washed with PBS between each sample measurement. A threshold level of 7 was applied for video processing. Each video recording was analyzed to obtain the size and concentration of EVs.

2.3.6.3. Western blot

Cells were lysed with Catenin lysis buffer (1% Triton X-100, Sigma, 1% Nonidet P-40, Sigma, in PBS) supplemented with protease inhibitor (Sigma) and phosphatase inhibitor (Sigma) for 10 min on ice and then centrifuged at 14000 x *g* for 10 min at 4ºC to remove insoluble material. Supernatants were recovered and used as whole cell lysates (WCL). For CD63 and CD81 detection, cells and EV samples were lysed with RIPA lysis buffer (150 mM NaCl, 25 mM Tris pH 7.4, 1% Nonidet P-40, 0.5% sodium deoxycholate, 0.1% sodium dodecyl sulfate (SDS)) and sonicated (three rounds of 5 s, at 50% intensity). Total protein content in WCL and EV samples was quantified using the BCA kit as previously described.

Both WCL and EV samples were mixed with sample buffer in reducing conditions and heated to 100ºC for 10 min. For CD63 and CD81 detection, urea containing sample buffer was used. All samples were loaded (6-30 µg of total protein) in 4-12% Bis–Tris polyacrylamide gels (Invitrogen, Life Technologies), in equal protein content for each gel, and subjected to electrophoresis.

Proteins were transferred into nitrocellulose membranes using a Power Blotter System (Invitrogen, Life Technologies). Membranes were blocked with 5% w/v non-fat dry milk solution in tris-buffered saline (TBS) Tween 20 buffer 1x (Thermo Fisher Scientific), for 1 h with mild orbital agitation at room temperature and incubated with primary antibodies overnight at 4ºC. For CD63 and CD81 detection, membranes were blocked with 5% BSA solution in TBS Tween 20 buffer 1x. Finally, membranes were incubated with HRP conjugated secondary antibodies for 1 h at room temperature and Pierce™ ECL Western Blotting Substrate (Thermo Fisher Scientific) was applied for membrane revelation.

Primary antibodies included anti-Calnexin (1:1000, BD), anti-Syntenin (1:1000, Abcam), anti-CD63 (1:1000, Genetex), anti-CD81 (1:500, Abcam) and anti-GAPDH (1:1000, Santa Cruz). Secondary antibodies included Goat anti-Mouse IgG (H+L) Cross-Adsorbed Secondary Antibody, HRP (1:5000, Invitrogen, Life Technologies) and Goat anti-Rabbit IgG HRP-

conjugated (1:1000, R&D Systems). Image acquisition was performed on iBright™ CL1500 Imaging System (Invitrogen, Life Technologies).

2.3.6.4. Atomic force microscopy imaging

EV samples were prepared for atomic force microscopy (AFM) imaging in freshly cleaved mica without any previous dilution. A volume ranging between 30-70 µL was used and samples were allowed to deposit during 30 min to 2 h. After this period, the samples were washed with filtered MilliQ water and air dried. AFM imaging was performed with a JPK Nano Wizard IV mounted on a Zeiss Axiovert 200 inverted microscope (Carl Zeiss). The AFM head is equipped with a 15 µm z-range linearized piezoelectric scanner and an infrared laser. Uncoated silicon ACL cantilevers from AppNano were used, with resonance frequencies and spring constants ranging between 160-225 kHz and 36-90 N/m, respectively. Scan speeds were between 0.1-0.3 Hz. Total areas with 10 x 10 µm were scanned with a 512 x 512 pixel resolution, in AC mode. Height and error images were recorded, and line fitted. Image processing was performed on JPK SPM data processing software version spm-6.0.55.

2.3.6.5. Zeta potential

EV samples were diluted to a final protein concentration of 25 µg/mL, in PBS. Samples were loaded into disposable zeta cells with gold electrodes and allowed to equilibrate for 15 min at 37°C. Zeta potential measurements consisted in a set of 15 runs, each one resulting from an automatically defined number of subruns (ranging from 10 to 100) performed on the Zetasizer Nano ZS (Malvern), at a constant voltage of 40 V.

2.3.7. Lactate dehydrogenase activity measurements

Cell culture medium samples from VWBR cultures were recovered daily and centrifuged at 360 x *g* for 10 min, to remove remaining microcarriers, cells and cell debris. Lactate dehydrogenase (LDH) activity was quantified in cell culture supernatants using the Pierce LDH Cytotoxicity Assay Kit (Thermo Scientific) by adapting the manufacturer instructions for the microplate procedure. The same procedure was applied to a positive control (1 µL LDH Positive Control in 10 mL of 10% BSA in PBS). Three replicates were quantified for each sample. The LDH activity was reported as the quotient between the LDH activity of each sample and the LDH activity of the positive control, according with the following equation.

$$LDH\ activity\ (\%) = \frac{LDH_{sample}}{LDH_{pos.control}} \times 100$$

2.3.8. Statistical analysis

Statistical analysis was performed using GraphPad Prism 8 Software. Results are presented as mean ± standard error of the mean (SEM) of the values obtained from different MSC donors (i.e. biological replicates) or as mean ± standard deviation (SD) of the values from technical replicates. Paired t test was applied to evaluate the statistical significance of

the differences in EV concentration and specific EV concentration in the conditioned medium from MSC cultures in static and VWBR systems. These data sets passed normality tests. P-values result from two-tailed tests with a 95% confidence interval. Differences were considered significant at $P < 0.05$ and statistical output was represented as **<0.01.

2.4. Results

2.4.1. MSC expansion and medium conditioning for MSC-EV production from 3 different human sources (BM, AT and UCM) was achieved in the bioreactor culture system

Bioreactors have been implemented as scalable platforms for MSC manufacturing. Building on previous work from our group[79], a S/XF microcarrier-based culture system implemented in a VWBR originally targeting MSC expansion was adapted to the production of cell-derived products such as MSC-EVs and compared with traditional static culture systems (i.e. T-flasks) (Figure 2.1).

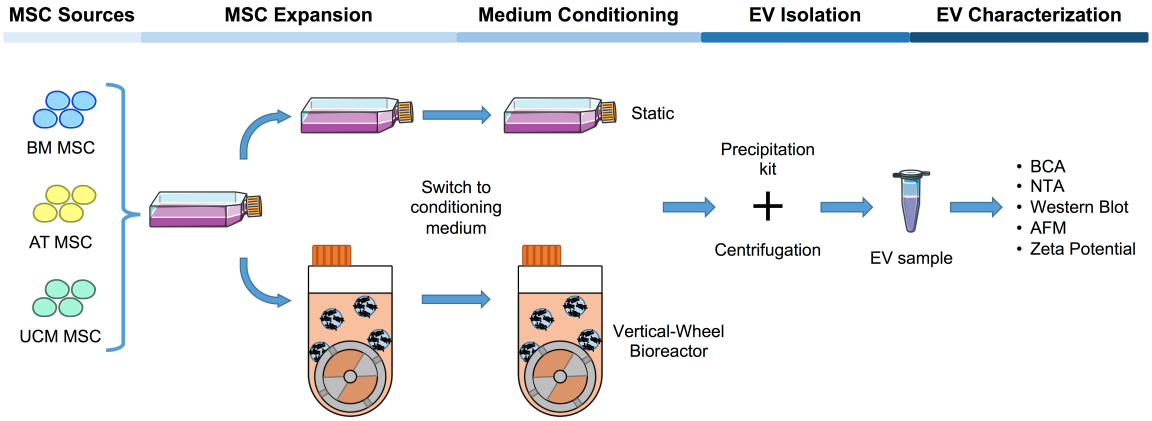

Figure 2.1 - Workflow of the production and characterization of MSC-EVs in bioreactors and static systems. MSC were isolated from 3 different human tissue sources: BM, AT and UCM. Firstly, MSC were expanded in static conditions (i.e. T-flasks) in hPL supplemented DMEM. These cells were subsequently used to inoculate a VWBR (5M cells; 100 mL final working volume), as well as to maintain a static culture in T-175 flasks. For each cell source, MSC from three independent donors (n=3; BM1, 2, 3; AT1, 2, 3; UCM1, 2, 3) were used to inoculate either the final T-flasks for EV production or the VWBR, in passages from P4 to P5 (specifically, BM1 (P4); BM2 (P5); BM3 (P4); AT1 (P4); AT2 (P4); AT3 (P5); UCM1 (P4); UCM2 (P4); UCM3 (P5)). Upon reaching stationary growth phase in VWBR or maximum confluency in static, the culture medium was changed for supplement-free culture medium and culture was maintained for 48 h. Over this period, culture medium was enriched in EVs secreted by cultured MSC. This conditioned culture medium was recovered and EVs were isolated by precipitation using a commercially available kit. Finally, EV production was quantified in both static and dynamic systems and samples were characterized using multiple techniques. MSC - mesenchymal stromal cells. EV - extracellular vesicles. VWBR - Vertical-Wheel™ bioreactor. hPL - human platelet lysate. BM - bone marrow. AT - adipose tissue. UCM - umbilical cord matrix. NTA - nanoparticle tracking analysis. AFM - atomic force microscopy. The cells, T-flask and Eppendorf cartoons were obtained from Smart Servier Medical Art (https://smart.servier.com).

BM, AT and UCM MSC were successfully expanded in the VWBR system (Figure 2.2 A, upper panel). The expansion of BM MSC was the most heterogeneous among donors (n=3), with final post-expansion cell numbers ranging between $12.0 \pm 3.6 \times 10^6$ and $53.4 \pm 5.5 \times 10^6$, depending on BM donor. The expansion culture period also ranged from 7 to 11 days in BM MSC cultures. AT and UCM MSC expansion curves were more homogeneous, reaching an

average of 29.2 ± 1.7 x 10^6 and 19.9 ± 2.4 x 10^6 cells, respectively, at the end of the expansion period. This expansion period was 7 days for AT MSC and 9-10 days for UCM MSC.

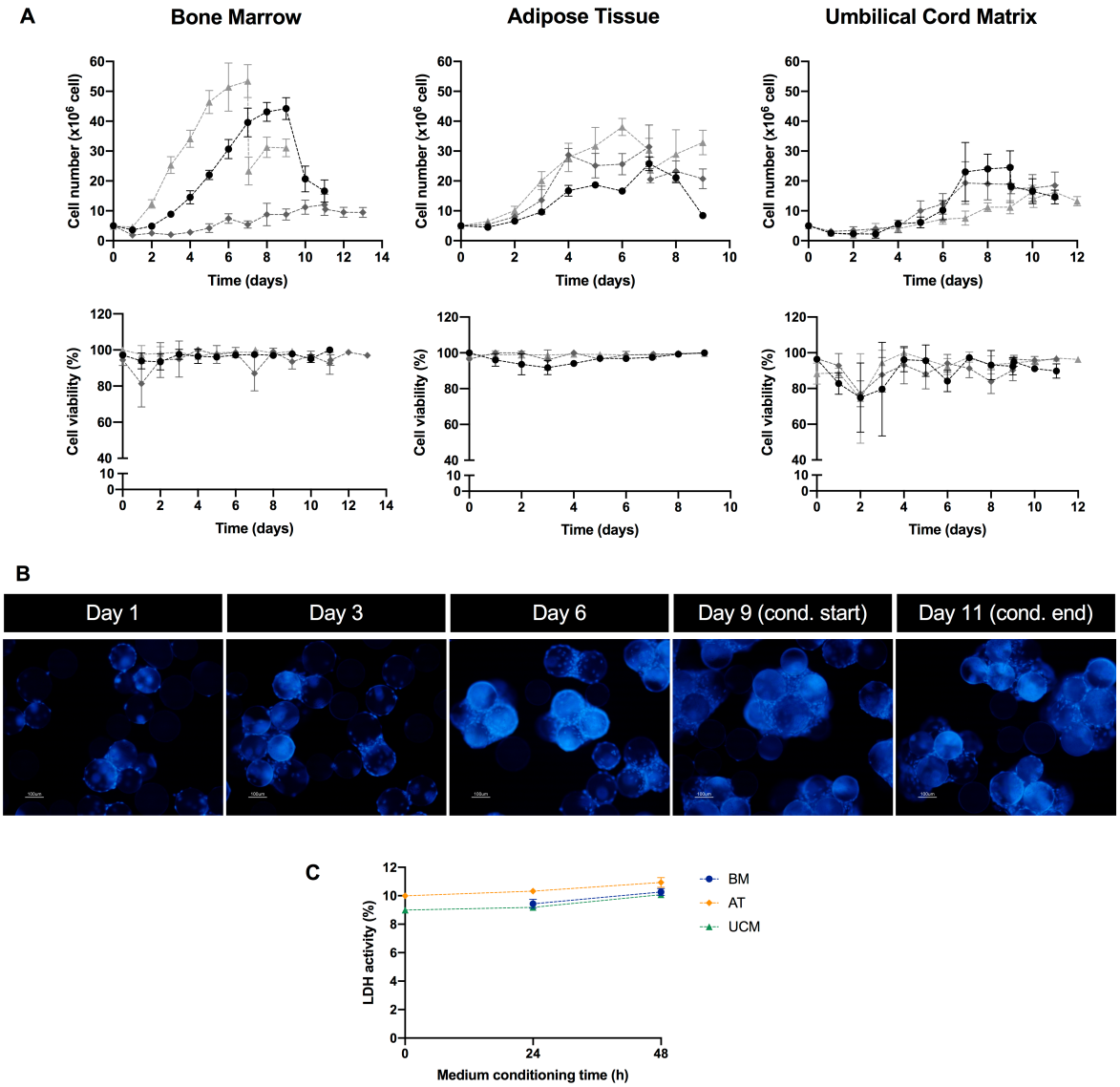

Figure 2.2 - MSC culture in the microcarrier-based bioreactor system. A) Evolution of cell number (upper panel) and cell viability (lower panel) over culture period time, for MSC from 3 different human tissue sources (bone marrow, adipose tissue and umbilical cord matrix). MSC from 3 different donors (i.e. 3 biological replicates) were used per tissue source, which are represented in 3 different shades of grey. Two data points are presented for the same day when the medium conditioning stage (i.e. EV production) started. Results are presented as mean ± SD of cell count for each time point. **B)** Representative images of microcarrier occupation by MSC throughout culture. Cell nuclei were stained with DAPI and images were acquired using a fluorescence microscope. In this case, EV production started on day 9 of culture and finished on day 11. Scale bar = 100 µm. **C)** LDH activity profile during the medium conditioning (i.e. EV production) stage in the VWBR system. Culture medium samples were taken at 0, 24 and 48 h after medium conditioning started. Results from one experiment for each MSC source (BM, AT and UCM). Results are presented as mean ± SD (n=3). LDH - lactate dehydrogenase. VWBR - Vertical-Wheel™ bioreactor. BM - bone marrow. AT - adipose tissue. UCM - umbilical cord matrix.

Estimated adhesion efficiency of MSC to microcarriers after VWBR inoculation was higher for AT MSC (110 ± 12 %), followed by BM MSC (68 ± 17%) and UCM MSC (55 ± 4%) (Table 2.1). AT MSC adhered and started proliferating in less than 24 h, which resulted in estimated adhesion efficiencies higher than 100%. BM MSC showed the highest average growth rate

(0.47 ± 0.05 day^{-1}), which was very similar to AT MSC (0.45 ± 0.06 day^{-1}), while UCM MSC showed the lowest growth rate (0.35 ± 0.09 day^{-1}), as a consequence of the lower initial adhesion efficiency observed.

Table 2.1 - Parameters from cultures of MSC from 3 different human sources (BM, AT and UCM) in bioreactors. Average initial cell adhesion efficiency, growth rate and duplication time for each MSC source. Adhesion efficiency was estimated by dividing the total cell number 24 h after inoculation (day 1) by the cell number used in bioreactor inoculation (day 0). Three biological replicates (i.e. MSC from 3 different human donors) were used for each MSC source (n=3). Results are presented as mean ± SEM.

	Adhesion efficiency	Growth rate (day^{-1})	Duplication time (day)
BM	68 ± 17%	0.47 ± 0.05	1.49 ± 0.13
AT	110 ± 12%	0.45 ± 0.06	1.60 ± 0.19
UCM	55 ± 4%	0.35 ± 0.09	2.30 ± 0.61

In general, BM and AT MSC maintained cell viability close to 100% throughout culture (Figure 2.2 A, lower panel). Cell viability suffered more oscillations in UCM MSC cultures, especially in the first days of culture.

Throughout the culture period, microcarrier colonization by cells increased progressively as MSC expanded (Figure 2.2 B). The increasing microcarrier occupancy was followed by microcarrier aggregation, as MSC expansion reached higher cell numbers. We observed that cell expansion stopped when large microcarrier aggregates were formed, likely due to lack of surface available to attach and proliferate (Figure 2.2 A and B).

In some cultures, a significant decrease in cell number was observed at the start of the medium conditioning stage, immediately after the culture medium was changed from hPL-supplemented medium to supplement-free culture medium. This can be explained, at least partially, by a possible removal of microcarriers during medium change operation, resulting in a loss of cells from the vessel. Additionally, it should be noticed that microcarrier aggregation might affect our estimation of cell numbers at this stage. In the medium conditioning stage, MSC were cultured for 48 h in a supplement-free medium, which could be a stress factor for cell culture. Although a decrease in the cell number was occasionally observed during the 48 h medium conditioning period, this was an exception rather than the rule (Figure 2.2 A). High cell viabilities were maintained (Figure 2.2 A) and there were no visible differences in microcarrier occupancy during this stage (Figure 2.2 B). Still, in order to thoroughly assess if MSC were experiencing induced cell stress, the levels of LDH activity in culture were monitored during the 48 h conditioning period. LDH activity can be used as a readout of cell stress, as this toxic compound is released to cell culture medium upon plasma membrane damage[343]. LDH activity did not change significantly over this period for any of the MSC

sources (Figure 2.2 C). Therefore, there were no indications that MSC were experiencing significant stress in stirred culture due to the absence of hPL in the 48 h conditioning period.

2.4.2. Characterization of MSC-EVs reveals improved properties upon bioreactor manufacturing

EVs were successfully isolated from the conditioned medium of MSC cultures. We were able to identify the presence of EVs from static and bioreactor cultures of MSC, from the 3 different sources (i.e. BM, AT and UCM) through AFM (Figure 2.3 A and Supplementary Figure 2.1). Individual vesicles of different sizes were observed, as well as vesicle aggregates. The formation of aggregates and collapsed vesicles may be caused by sample processing techniques, which involve sample dehydration. Larger vesicles were observed for AT MSC (Figure 2.3 A). These vesicles may have a higher tendency to aggregate or even fuse together due to the higher medium viscosity observed in AT MSC cultures.

The production of EVs was also confirmed by Western blot analysis (Figure 2.3 B and Supplementary Figure 2.2). The EV protein markers syntenin, CD63 and CD81 were successfully detected in EV samples, while the negative EV protein marker calnexin (a protein from the endoplasmic reticulum) was present in cells, but absent in EV samples, as expected (Figure 2.3 B i). In general, syntenin and CD63 presence were verified for MSC-EVs obtained from both static and bioreactor systems, using MSC from the 3 different tissue sources (Figure 2.3 B ii). Interestingly, both syntenin and CD63 presence were increased when EVs were obtained from bioreactors. Contrarily to EVs, cells showed higher syntenin expression under static conditions compared to the bioreactor. CD81 was detected in EVs obtained from BM and AT MSC obtained from both static and bioreactor systems, but not from UCM MSC. CD81 was detected in higher quantity in EVs obtained from AT MSC cultured in bioreactors, compared with static conditions.

The surface charge of MSC-EVs was also quantified. MSC-EVs presented a negative surface charge, as determined through zeta potential measurements (Figure 2.3 C). Overall, no significant differences were observed in the zeta potential between samples obtained from static or bioreactor platforms, neither between different MSC tissue sources. The zeta potentials ranged between -15.5 ± 1.6 mV and -19.4 ± 1.4 mV.

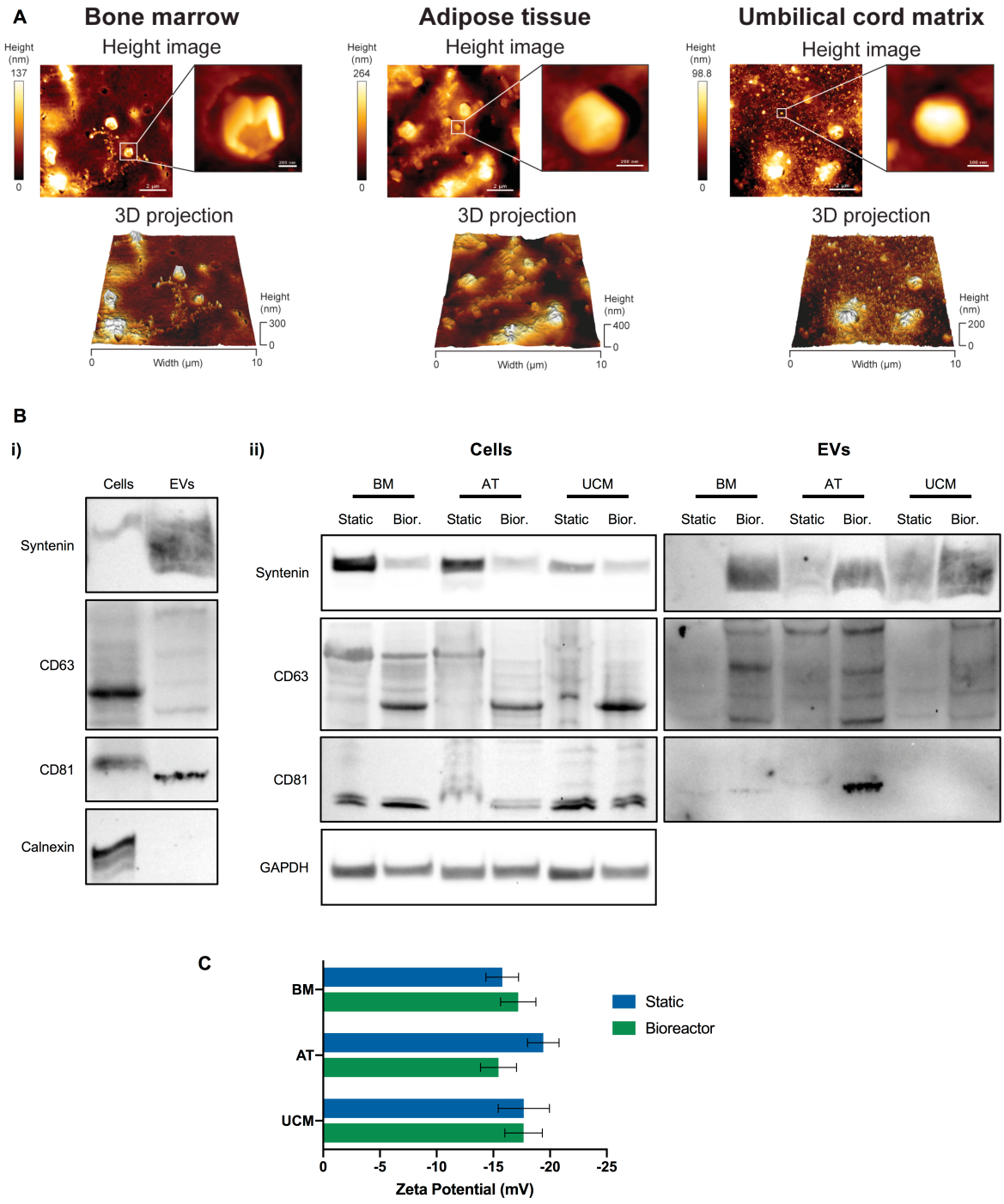

Figure 2.3 - Characterization of MSC-EVs. A) Representative AFM images of MSC-EVs obtained in the VWBR system, using MSC from 3 different human tissue sources (bone marrow, adipose tissue and umbilical cord matrix). AFM height images (top) and respective 3D projections (bottom), capturing a total area of 10 x 10 µm. A close-up image focusing on a single EV is presented for each AFM height image. **B)** Western blots of MSC lysates and MSC-EV samples. i) Representative Western blot images of syntenin, CD63, CD81 and calnexin detection in MSC-EVs and corresponding WCL (i.e. cells) obtained from VWBR cultures. ii) Western blot detection of syntenin, CD63 and CD81 in MSC-EV samples and corresponding WCL (i.e. cells), obtained from BM, AT and UCM MSC after EV production in static and VWBR systems. Detection of the housekeeping protein GAPDH in the same WCL preparations. **C)** Zeta potential measurements of the surface charge of MSC-EVs (mV), obtained in either static or VWBR systems, using MSC from 3 different human sources (BM, AT and UCM). Results correspond to one representative experiment for each condition. Results are presented as mean ± SD. AFM - atomic force microscopy. WCL - whole cell lysates. BM - bone marrow. AT - adipose tissue. UCM - umbilical cord matrix. VWBR - Vertical-Wheel^{TM} bioreactor.

The size distribution of MSC-EVs was determined by NTA. In general, MSC-EV samples showed a size distribution profile mostly enriched in small EVs (<200 nm) (Figure 2.4 A and Figure 2.4 B). Although EVs derived from AT MSC showed a more homogeneous size distribution when obtained from the bioreactor compared to static cultures, no significant difference was observed for other MSC sources. The sizes of EVs produced from AT MSC in the static platform were significantly larger, possibly due to vesicle aggregation or fusion. Therefore, the bioreactor system reveals potential to produce EVs with lower size dispersity, as observed for AT MSC-EVs.

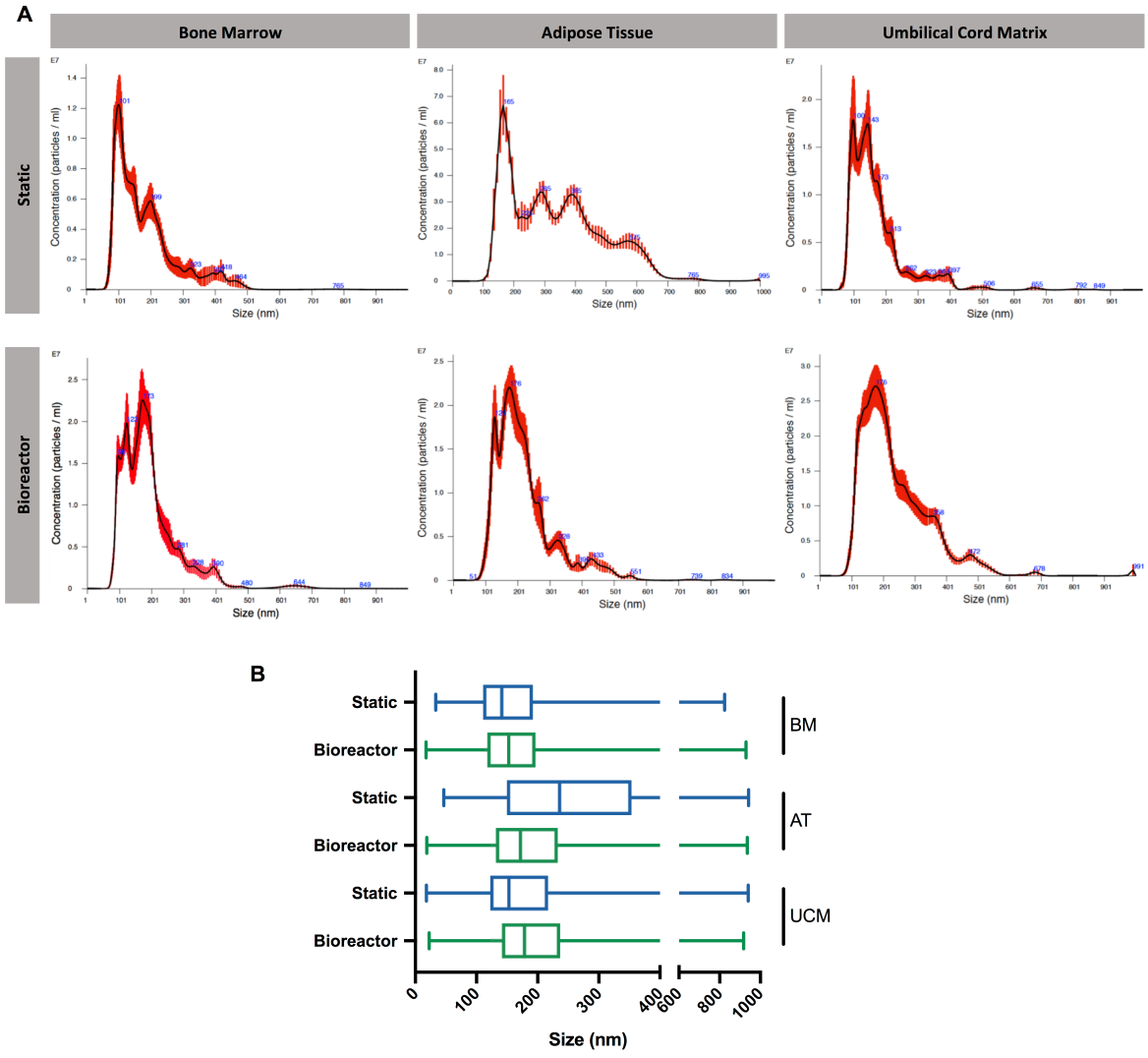

Figure 2.4 - Size distribution of MSC-EVs. A) Representative size distribution curves of EV samples obtained from BM, AT and UCM MSC, cultured in static or Vertical-Wheel^{TM} bioreactor systems. **B)** Box plots representing the size distribution profiles of EV samples obtained from BM, AT and UCM MSC, cultured in static or Vertical-Wheel^{TM} bioreactor systems. The minimum, 1st quartile, median, 3rd quartile and maximum values are represented for each condition. MSC from 3 different donors were used for each tissue source (i.e. n=3 biological replicates). BM - bone marrow. AT - adipose tissue. UCM - umbilical cord matrix.

2.4.3. Bioreactor culture improves the production of MSC-EVs

MSC-EVs produced in the bioreactor system were quantified by NTA after EV isolation and compared with MSC-EVs obtained from static cultures. When EVs were produced in the bioreactor system, their concentration was significantly increased (Figure 2.5 A), at an overall fold increase of 5.7 ± 0.9 (Table 2.2). When analyzed individually, we observed a fold increase of 4.0 ± 0.6 for BM MSC, 4.4 ± 1.2 for AT MSC and 8.8 ± 3.8 for UCM MSC, when EVs were produced in the bioreactor system (Table 2.2). Bioreactor cultured UCM MSC yielded the highest average EV concentration in the conditioned medium (6.9 ± 1.7 $x10^9$ particles/mL) (Figure 2.5 A). The average EV concentration in bioreactor cultures was similar for BM and AT MSC (4.6 ± 0.2 $x10^9$ and 5.1 ± 2.1 $x10^9$ particles/mL, respectively), although the latter presented higher heterogeneity between experiments.

In order to evaluate if the conditions in the bioreactor might modulate the intrinsic capacity of cultured MSC for the production of EVs compared to static conditions, we estimated the EV productivity (i.e. specific EV concentration, per cell) by dividing the concentration of EVs (from NTA) by the cell concentration at the beginning of the conditioning period. When EVs were produced in the bioreactor system, EV productivity increased compared with static culture (Figure 2.5 B) at an overall fold increase of 3.0 ± 0.5 (Table 2.2). Although this difference was not statistically significant (which is likely due to the heterogeneities between the different tissue sources and donors used), the bioreactor system allowed an improved productivity of MSC-EVs for most of the MSC donors used (i.e. in six out of eight MSC donors).

EV productivity increased in the bioreactor by a fold increase of 1.4 ± 0.3 for BM MSC, 3.7 ± 1.0 for AT MSC and 3.9 ± 1.4 for UCM MSC (Table 2.2), compared with static conditions. Bioreactor cultured UCM MSC yielded the highest average EV productivity (2.7 ± 0.6 $x10^4$ particles/cell) (Figure 2.5 B). The average EV productivity in bioreactor cultures was similar for BM and AT MSC (1.6 ± 0.5 $x10^4$ and 1.7 ± 0.6 $x10^4$ particles/cell, respectively).

A particle to protein ratio (PPR) was also determined by dividing the EV concentration (determined by NTA) by the total protein concentration in the same sample (determined through BCA protein assay). The PPR can be used to assess the purity of an EV sample, as the higher is this ratio, the lower is the amount of co-isolated protein contaminants, thus the higher is the sample purity[344]. EV samples from BM and UCM MSC cultures presented a more homogeneous PPR in the bioreactor system than in static conditions (Figure 2.5 C). EV samples from AT MSC cultures presented a homogeneous PPR for both culture platforms, but the average PPR was slightly higher in the bioreactor. Overall, the PPR was relatively constant in the bioreactor system, ranging between $1.63x10^8$ and $3.40x10^8$ particles/µg protein (Figure 2.5 C). PPR was much more heterogeneous in static conditions (i.e. T-flasks), ranging between $3.47x10^7$ and $9.88x10^8$ particles/µg protein. Additionally, the median PPR was higher for the EVs produced in the bioreactor system.

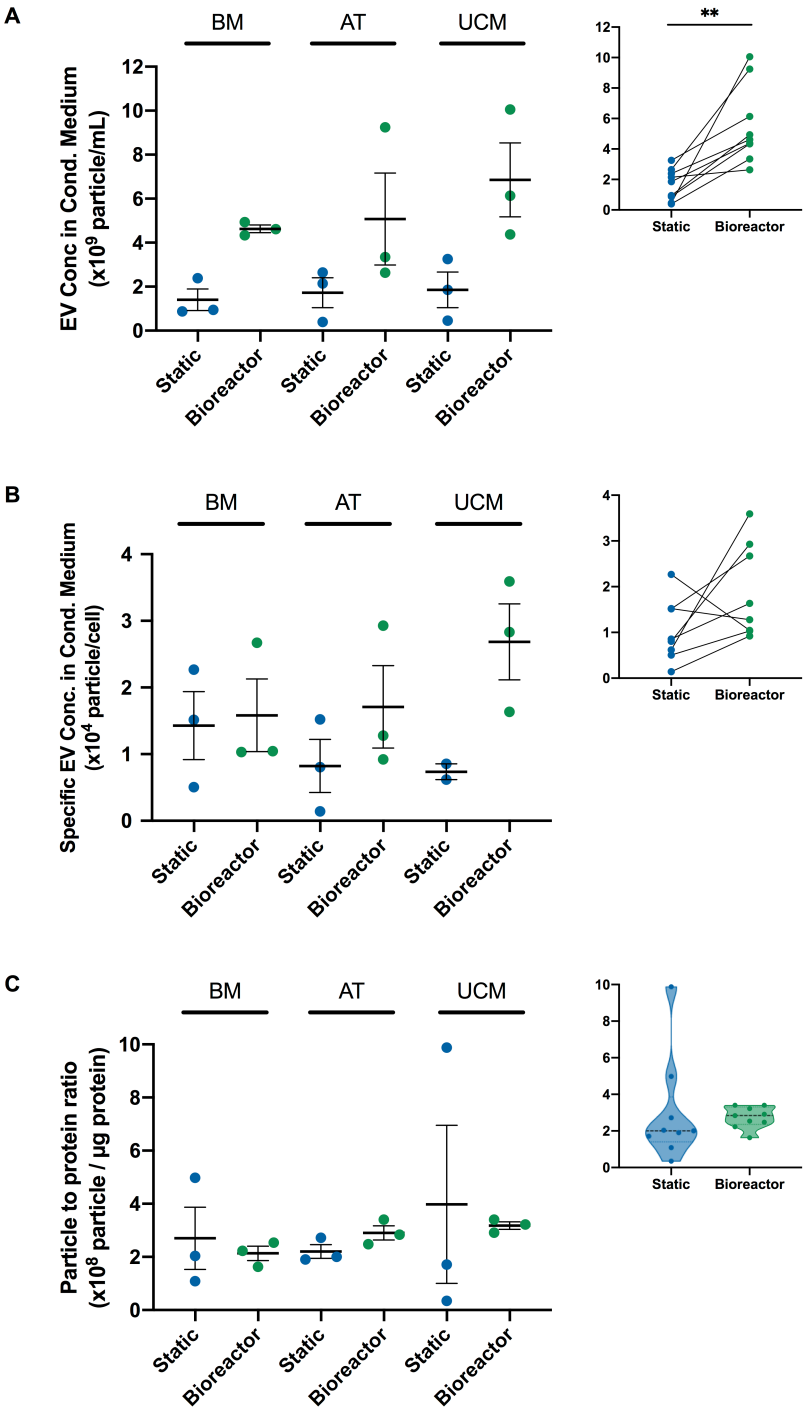

Figure 2.5 - Comparing MSC-EV production in bioreactor and static culture systems, using MSC from different sources. A) EV concentration (particles/mL) in the cell culture conditioned medium from BM, AT and UCM MSC cultures in static and Vertical-Wheel™ bioreactor systems. MSC from 3 different donors were used for each tissue source (i.e. n=3 biological replicates). Results are presented as mean ± SEM (n=3). Upper-right panel: Summarized paired analysis comparing EV concentration in static and Vertical-Wheel™ bioreactor systems, for each MSC donor. Paired statistical analysis (paired t test **P=0.0027) (n=9). **B)** Specific EV concentration (particles/cell) in the cell culture conditioned medium from BM, AT and UCM MSC cultures in static and Vertical-Wheel™ bioreactor systems. MSC from 3 different donors were used for each tissue source. In static cultures, each T-175 yielded 1.2 - 6.6 x 10^6 cells upon 4 - 9 days of expansion, regardless of the cell tissue source. Results are presented as mean ± SEM (n=3; n=2 for UCM-static). Upper-right panel: Summarized paired analysis comparing specific EV concentration in static and Vertical-Wheel™ bioreactor systems, for each MSC donor. **C)** Particle to protein ratios (PPR) (particle/µg protein) of EV samples obtained from BM, AT and UCM MSC, cultured in static and Vertical-Wheel™ bioreactor systems. MSC from 3 different donors were used for each tissue source. Results are presented as mean ± SEM (n=3). Upper-right panel: Violin plot of PPR of MSC-EV samples obtained in static and Vertical-Wheel™ bioreactor systems.

Table 2.2 - Fold changes in EV concentration and EV productivity (i.e. specific EV concentration, per cell) in the cell culture conditioned medium from the bioreactor system compared to static conditions. Results from each of the 3 MSC sources used (BM, AT and UCM), as well as global fold change averages from all the sources. Three biological replicates (i.e. MSC from 3 different human donors) were used for each MSC source (n=3). For each MSC source, results are presented as the average of fold changes for each donor, in order to account for biological diversity. Global fold changes are presented as the average of fold changes from each MSC source. Results are presented as mean ± SEM.

	EV concentration fold change (bioreactor/static)	**EV productivity fold change (bioreactor/static)**
BM	4.0 ± 0.6	1.4 ± 0.3
AT	4.4 ± 1.2	3.7 ± 1.0
UCM	8.8 ± 3.8	3.9 ± 1.4
Global	5.7 ± 0.9	3.0 ± 0.5

2.5. Discussion

MSC hold great promise for the development of cell-based therapies for a variety of disorders. MSC-derived products such as MSC-EVs offer the opportunity to develop new therapeutic products benefiting from MSC regenerative properties in cell-free formulations. These cell-free therapies are expected to present significant advantages, obviating the complexity and safety issues in utilizing cells themselves as therapeutic systems in a clinical context[260,345].

MSC-EVs can be used as intrinsically therapeutic products, by mediating some of the effects conveyed by MSC. MSC-EVs present therapeutic properties for neurological, cardiovascular, immunological, kidney and liver diseases, among others[332,334,346]. MSC-EVs have been described to reduce myocardial ischemia/reperfusion injury in mice[246] and also allowed improved recovery from acute kidney injury[248] and from stroke[249]. Indeed, there are multiple studies describing their pro-angiogenic[236,237] and wound healing capacity[238,239].

Alternatively, EVs can be engineered towards the development of novel DDS. Drug loaded EVs can be used to transport and deliver therapeutic cargo to target diseased cells and tissues[260,268]. These natural DDS could be an appealing alternative to the more established synthetic DDS, by avoiding toxicity and rapid clearance from the organism, as well as a better membrane matching capacity[260]. Dendritic cell-derived EVs were able to deliver siRNA to the brain in mice, demonstrating their potential use as targeted therapy for neurological diseases[257]. Macrophage-derived EVs loaded with catalase provided increased neuroprotective effects in *in vitro* and *in vivo* models of Parkinson's disease, compared to free catalase[274]. Recently, multiple studies have successfully developed EVs as DDS for cancer therapy[265,271,279,292–294,347,348]. Intravenously injected EVs from dendritic cells delivered

doxorubicin specifically to tumor tissues in mice, leading to the inhibition of tumor growth with lower toxcicity[271]. MSC incubated with a high paclitaxel concentration secreted EVs loaded with this drug, successfully inhibiting tumor growth *in vitro*[279]. Additionally, EVs can be further engineered to improve specificity and retention on target cells and tissues[292–294].

Despite the promising potential of EVs for therapeutic applications, large EV doses are expected to be required to achieve therapeutic effects in clinical settings. This requires the development of robust manufacturing processes that could increase the consistency and scalability of EV production, which are currently lacking.

The present work aimed to establish a scalable culture platform for the manufacturing of MSC-EVs in S/XF culture conditions. This was achieved by building on previous work from our group where a S/XF microcarrier-based culture system was implemented in single-use bioreactors (VWBR), employing a hPL culture supplement (UltraGRO™-PURE) for MSC expansion[79]. In the present study, EVs were produced by MSC isolated from 3 different human tissue sources (BM, AT and UCM) in a process that comprises a cell expansion stage and a culture medium conditioning stage.

S/XF culture conditions were implemented by exclusively applying products without any animal components, namely hPL as a culture supplement used in the cell expansion stage, instead of the more commonly used FBS, as well as animal product-free plastic microcarriers and TrypLE as a cell detaching solution. Multiple studies have revealed hPL-supplemented media to be efficient for the isolation and expansion of MSC from various origins[75–77], cultured both in static and dynamic systems[78,79], as well as for the expansion of other cell types[82–85]. However, the fact that hPL products originate from human donors presents some constraints, such as the risk of transmission of human diseases by viruses, ill-definition and the possibility of triggering immune responses[86]. The ideal option for production of clinical-grade cell based therapies would be a chemically defined, animal component-free medium (including human). However, there are very few of these options available, namely for MSC culture. Therefore, presently, hPL seems to be the most promising and cost-effective alternative to FBS supplementation in cell culture medium for now, being more readily translatable to a clinical setting, especially considering that gamma irradiated hPL products allowing significant viral reduction have already been developed[87].

Culture medium supplements such as FBS and hPL have a large amount of protein and vesicle contents, presenting an additional challenge for their use in EV manufacturing. These components are prone to be co-isolated with the EV fraction, thus contaminating the end product[349]. For this reason, we removed hPL at the end of the MSC expansion period and hPL-free medium was used for the medium conditioning period. MSC were cultured for 48 h in this supplement-free medium, which could be a stress factor for cell culture. However, we did not observe any significant reduction in cell number, cell viability or microcarrier occupancy

during this stage. Furthermore, LDH activity did not change significantly over this period for any of the MSC sources. Therefore, there were no indications that MSC were experiencing significant stress in culture, due to the absence of hPL in the 48 h conditioning period. Still, MSC might potentially undergo some alterations over this period. Minimal identity criteria commonly used to define multipotent MSC could suffer modifications, namely their *in vitro* multilineage differentiation capacity or their immunophenotype (i.e. expressing CD73, CD90 and CD105, lacking the expression of hematopoietic and endothelial markers CD11b, CD14, CD19, CD34, CD45, CD79a and HLA-DR)[350]. Of notice, MSC expanded in the VWBR system maintain the typical MSC immunophenotype, as previously reported by our group[79]. Further work could be performed by comparing the MSC features before and after the culture medium conditioning period.

Bioreactor systems such as VWBR present several advantages for the manufacturing of cell-based therapies. Cell culture on microcarriers in suspension inside a bioreactor allows an increase of available surface area per volume ratio, enabling higher cell concentrations in culture. Bioreactors also allow the implementation of culture monitoring and control systems, providing an additional advantage to optimize culture conditions, by adjusting feeding regimes and physicochemical parameters (e.g. O_2 concentration and pH) according to real-time culture measurements.

In this work, we established a bioreactor process in 100 mL VWBR vessels. This process can be scaled-up to VWBR with a working volume of 3 L or higher (up to 500 L), which include an integrated control system, allowing for a controlled manufacturing process. To the best of our knowledge, this study is the first to establish a S/XF microcarrier-based culture system in bioreactors for the manufacturing of MSC-EVs, using MSC from 3 different human tissue sources (BM, AT and UCM). It is also the first to implement the VWBR configuration for EV production. Cell expansion in this bioreactor culture system allowed an increase in EV concentration in the conditioned medium when compared to traditional static systems (5.7 ± 0.9 global fold increase), partly due to higher cell concentrations obtained in VWBR. However, in addition to that, the EV productivity (i.e. specific EV concentration) also increased in bioreactors (3.0 ± 0.5 global fold increase), meaning that each cell secreted more EVs when MSC were cultured in the VWBR, compared to static conditions. Although this difference was not found to be statistically significant, this was likely due to the heterogeneities between different tissue sources and donors. For example, if we had not considered the results from one of the BM MSC donors (for which EV productivity decreased in the bioreactor, contradicting the observed general tendency of our study), this difference would be statistically significant. This reinforces the relevance of testing MSC from multiple tissue donors in order to account for intrinsic biological variability. Of notice, this study was performed using MSC from 3 different donors for each tissue source, comprising a total 9 random human donors.

Still, further work may be performed with additional donors in order to more thoroughly account for donor variability and its impact. Altogether, the higher EV concentrations achieved in VWBR were due to higher cell densities, as well as to higher EV productivities by MSC.

Overall, in the conditions of our study, UCM MSC allowed the highest EV concentration and EV productivity in the bioreactor system. They also showed the highest fold increase in both parameters when compared to static systems. Therefore, UCM seems to be the MSC source that benefits the most from cultivation in the VWBR system, being the most promising of the three tissue sources studied for scalable MSC-EV production. This is in line with previous work where UCM MSC have been described to allow higher EV productivity than BM and AT MSC in static culture[351].

Nonetheless, the real applicability of these MSC-EVs depends on their biological function. Given their different tissue origins, we can expect that EVs obtained from cells derived from each MSC source will have different functional characteristics. Indeed, different intrinsic therapeutic features have been described for MSC derived from different tissues[40]. In order to develop therapeutic products, based on the MSC-EVs manufactured in this work, additional functional studies will be required. These could include, for example, (i) scratch assays or tube formation assays using endothelial cells to determine the ability of MSC-EVs to promote angiogenesis in the context of vascular repair[237] or (ii) cell uptake assays to determine EV uptake by target cancer cells, to assess their potential as drug delivery vehicles for cancer therapy[292].

The increase observed in EV productivity in VWBR can be explained by multiple reasons. EV secretion by MSC may have been stimulated by fluid flow, promoted by the VWBR mixing system. Fluid flow has already been described to stimulate EV secretion in osteocytes through a Ca^{2+}-mediated response[352]. Additionally, when MSC were cultured in the bioreactor system, cells attached to the surface of plastic microcarriers and proliferated. Later in culture, microcarrier aggregates were formed and, consequently, MSC formed aggregates as well, as previously observed[353,354]. MSC culture in spheroids has been described to lead to higher secretion of paracrine factors[355,356], as well as to an increased secretion of microvesicles[357]. Hence, aggregate formation could be leading to an increased EV secretion in the VWBR system. Finally, MSC cultured in the VWBR system are likely to be exposed to lower oxygen concentrations than in static platforms. The VWBR agitation system allows mixing of the cell culture medium, achieving a homogeneous oxygen concentration. However, there is no aeration system in the 100 mL VWBR, so oxygen exchange occurs only at the surface gas-liquid interface. Considering the differences between the geometries of the VWBR vessel and the T-flask, oxygen concentration would be expectedly lower in the VWBR system than in static. This could potentially be a contributing factor for the observed increase in EV secretion when cells were expanded in the bioreactor system. Previous studies have demonstrated an

increase in EV secretion when different cell types (including MSC) were cultured under hypoxic conditions (ranging from 0.1% to 3% O_2, compared to controls)[327,358,359]. Although all of these factors might lead to an increased EV productivity in the VWBR, additional studies would be needed to determine their actual contributions.

Zeta potential measurements revealed that the surface charge of obtained MSC-EVs were generally similar, regardless the production platform and MSC source used, ranging between -15.5 ± 1.6 mV and -19.4 ± 1.4 mV. These surface charges are moderately negative, as it was expected considering that EVs are cell-derived nanoparticles, therefore containing negatively charged phospholipids. The values of zeta potential obtained herein were in line with other studies reporting zeta potential measurements for EVs derived from cell culture[360–363].

Further EV characterization revealed that bioreactors improved not only EV quantity but also their purity, as assessed by Western blot and PPR. Western blot analysis revealed that syntenin, CD63 and CD81 (key proteins involved in EV biogenesis and commonly used as protein markers) were in general more abundant in EVs obtained from bioreactors than from their static counterparts (Figure 2.3 B ii). Therefore, EVs from bioreactors seem to have a higher purity than EVs obtained from static system, since a higher amount of syntenin, CD63 and CD81 were detected for the same amount of total protein. This observation corroborates the increased EV concentration in VWBR identified by NTA. The fact that bioreactor EV samples showed increased levels of EV protein markers validates the hypothesis that the increased concentration of particles detected by NTA corresponds to an increased concentration of EVs and not of protein aggregates.

EV purity was also assessed by estimating the PPR for each EV sample[344]. PPR was more homogeneous and reproducible in EV samples obtained from bioreactors compared to those produced under static conditions and the median PPR was higher in the bioreactor system (Figure 2.5 C). A more homogeneous environment in VWBR offers a more reproducible process for different sources and donors. Constant agitation provides the cells with a more homogeneous access to nutrients, thus allowing a more robust MSC-EV manufacturing process. Therefore, the bioreactor platform established in this work is expected to allow the robust production of MSC-EVs at higher purities, compared to static systems.

In our previous work focused on the establishment of a S/XF microcarrier-based culture system in single-use bioreactors (VWBR)[79], an economic evaluation revealed that the application of this culture system allowed a cost reduction for MSC manufacturing when compared to static cell culture using T-flasks. Therefore, it can be expected that the application of this bioreactor system will also allow a cost reduction for the production of MSC-EVs, compared to static platforms.

A few manufacturing processes for the production of EVs have been previously studied. The Integra CELLine culture system is a static platform that has been used to optimize EV

production[364]. This is a two-compartment culture flask with a semi-permeable membrane separating a cell-containing compartment from a larger medium compartment. When mesothelioma and NK cells were cultured in this system, a 12-fold and a 8-fold increase in EV (protein) concentration was observed, respectively, compared to traditional T-flasks[364]. This system also allowed a 13- to 16-fold increase in EV (protein) concentration from bladder carcinoma cells[365]. The CELLine system allows culture medium change while EVs are retained in the cell compartment, enabling higher EV concentrations. However, this static system has limited scalability, thus not being the most suitable option for large-scale EV production.

Watson and colleagues developed a hollow-fiber bioreactor platform for the production of HEK-derived EVs[366]. The authors reported a 10-fold increase in EV concentration compared with static culture, which was sustained by an increased purity (both increased PPR and protein marker expression). However, EV size distribution profiles were more dispersed in the bioreactors, which is the opposite from what we observed in our study with the VWBR system. Mendt and colleagues manufactured BM MSC-derived EVs in a closed system, hollow-fiber bioreactor, named Quantum[333]. They were able to achieve $1.04x10^{10}$ particles/mL on average, which was higher, but comparable with the EV concentrations we obtained in the VWBR system ($5.5 \pm 0.8 \times 10^{9}$ particles/mL) herein.

Hollow-fiber bioreactors (i.e. without mechanical agitation) provide surface immobilization of cells on the fibrous material and represent a suitable configuration to obtain an increased EV concentration in culture, since culture medium can be recirculated while EVs are retained by the hollow-fiber membranes. However, stirred bioreactors as the VWBR may allow a better fine-tuning of EV production by manipulating process parameters. For example, agitation may play an important role in EV secretion, since fluid flow seems to have impact on this process. Further studies may be developed in the VWBR, testing the impact of agitation on EV production. Other process parameters, such as oxygen concentration, temperature and pH, are also likely to play a role in EV secretion by cultured MSC and are more easily controlled in a VWBR, especially when integrated with a control system. Further studies addressing the impact of these parameters on EV production using the VWBR system would be relevant to fine-tune and optimize MSC-EV production.

In conclusion, we have successfully developed a scalable S/XF microcarrier-based bioreactor culture system for the robust production of MSC-EVs, using MSC from 3 different human tissue sources (BM, AT and UCM). This system allowed the production of MSC-EVs at higher concentration and productivity when compared to traditional static culture systems. It also allowed to obtain a more robust MSC-EV manufacturing process, regarding their purity. Further developments of this system will need to take into consideration a proper balance between EV production and function. Additional studies will be required to characterize the therapeutic potential of these MSC-EVs. The MSC-EVs obtained through this scalable

platform are promising for the development of multiple therapeutic products and DDS, targeting a variety of diseases.

2.6. Supplementary material

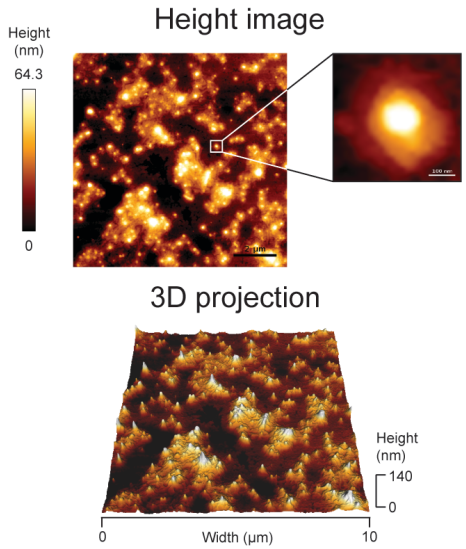

Supplementary Figure 2.1 - Representative AFM image of MSC-EVs obtained in static conditions (in this particular case EVs were obtained from AT MSC cultures). AFM height image (top) and respective 3D projection (bottom), capturing a total area of 10 x 10 µm. A close-up image focusing on a single EV is presented. AFM - atomic force microscopy.

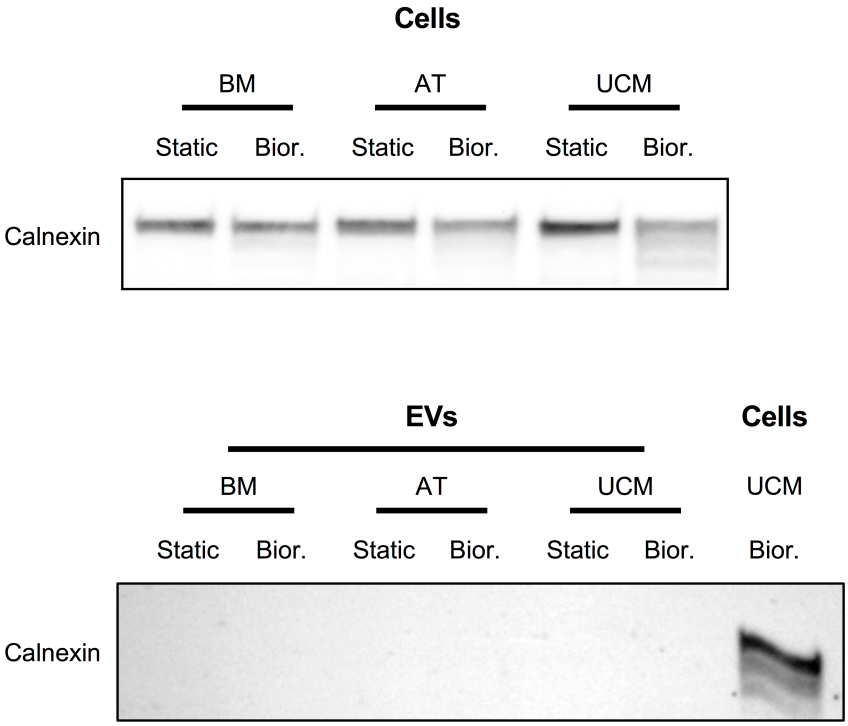

Supplementary Figure 2.2 - Western blot detection of calnexin in MSC lysates (i.e. cells) and MSC-EV samples obtained from BM, AT and UCM MSC after EV production in static and Vertical-Wheel™ bioreactor systems. BM - bone marrow. AT - adipose tissue. UCM - umbilical cord matrix.

3. Angiogenic activity of mesenchymal stromal cell-derived extracellular vesicles *in vitro*

3.1. Summary

EVs have been receiving interest for therapeutic application both as drug delivery vehicles and intrinsically therapeutic agents for regenerative medicine, due to the ability to mediate therapeutic effects from their parental cells. In particular, a growing body of evidence suggests that several therapeutic features of MSC are mediated by EVs, including cardiac regeneration and the ability to stimulate angiogenesis. MSC showed different therapeutic activity depending on the tissue source they were isolated from, thus EVs obtained from cells derived from each MSC source are likely to have different functional attributes as well.

In this work, we studied and compared the functional activity of MSC-EVs obtained from different human tissue sources, namely BM and UCM, by investigating their impact on angiogenesis. MSC-EVs were produced in conditions readily translatable to a clinical setting, by combining S/XF conditions and a scalable and selective EV isolation method that combined TFF with SEC. The potential to stimulate angiogenesis was assessed by studying the effect of MSC-EVs on endothelial cells in different *in vitro* assays, namely a scratch wound assay, a 3D spheroid sprouting assay and by investigating their ability to activate ERK1/2 and Akt pathways.

We observed a functional effect of MSC-EVs from both BM and UCM in the 3D sprouting assay, confirming the capacity of these EVs to promote angiogenesis. Results from scratch wound assay and ERK/Akt activation assay were inconclusive. Both BM and UCM MSC-EVs increased the total sprouting length per spheroid by 1.9-fold, revealing a similar pro-angiogenic potential. However, the number of new sprouts formed and their elongation was different between both types of EVs, suggesting that MSC-EVs obtained from different tissue sources might stimulate angiogenesis through different mechanisms.

Overall, we produced MSC-EVs derived from different human tissue sources in conditions closely translatable to a clinical setting that are promising for regenerative medicine applications.

3.2. Background

MSC hold great promise for cell-based therapies due to their inherent immunomodulatory and trophic activities[14,15]. Increasing evidence suggests that several MSC-associated therapeutic features are exerted in a paracrine manner and mediated by EVs[241,243,246–248]. These vesicles play a role in intercellular communication by transferring their cargo of biomolecules, including proteins, lipids and nucleic acids (e.g. miRNA and mRNA), which trigger alterations on recipient cells, or by initiating signaling pathways through cell surface interactions[153–155]. EVs are non-replicative and non-mutagenic, relieving some of the safety concerns associated with cell therapies. Thus, EV-based therapies are expected to present

advantages over cell therapies by conveying some of the therapeutic effects from their producing cells while obviating the complexity and safety issues in utilizing cells themselves as therapeutic systems in a clinical context.

MSC-EVs can be used as intrinsically therapeutic agents, by mediating some of the effects conveyed by MSC. MSC-EVs present therapeutic properties for cardiovascular, neurological, immunological, renal and hepatic diseases, among others[332,334,346]. MSC-EVs have been described to reduce myocardial ischemia/reperfusion injury in mice[246] and also allowed improved recovery from acute kidney injury[248] and from stroke[249]. Indeed, several studies have described their anti-inflammatory[230,231], pro-angiogenic[236,237] and wound healing capacity[238,239].

The therapeutic applicability of MSC-EVs may depend on the tissue source from which MSC are obtained. We have previously observed that the production yields and the biochemical and biophysical characteristics of MSC-EVs can vary between different MSC tissue sources (Chapter 2)[367]. Similarly, EVs obtained from cells derived from each MSC source are likely to have different functional characteristics. Indeed, different intrinsic therapeutic features have been described for MSC derived from different tissues[40,368].

In this work, we investigated the functional activity of MSC-EVs obtained from different human tissue sources, namely BM and UCM, produced under S/XF conditions by studying their impact on angiogenesis. We isolated EVs from MSC cell cultures through a SEC method, previously described to allow the production of EVs with higher functionality compared with more traditional EV isolation methods[369]. The potential to stimulate angiogenesis was assessed by studying the effect of MSC-EVs on endothelial cells in different *in vitro* assays. A scratch wound assay was used to study the impact of MSC-EVs on endothelial cell migration and wound-healing[237], while an endothelial spheroid sprouting assay was used to study the impact of these EVs on formation of vasculature in a 3D configuration[237,370]. The mitogen-activated protein kinase1/2 (MAPK1/2)–extracellular signal-regulated kinase1/2 (ERK1/2) pathway is known to play an important role in cell survival, migration and angiogenesis during wound healing[371,372]. Similarly, the protein kinase B (Akt), a key protein in the PI3K-Akt pathway, plays multiple relevant roles, including cell survival, growth, proliferation, angiogenesis, metabolism, and migration[373]. Thus, EV-induced ERK1/2 and Akt phosphorylation (i.e. the active forms of both kinases) were also used as a read-out to evaluate the possible functional effect of MSC-EVs[369,374].

We observed a functional effect of MSC-EVs from both BM and UCM, particularly in the 3D sprouting assay, confirming the capacity of this EVs to promote angiogenesis. However, additional experimental work will be required to fully elucidate the functional activity of MSC-EVs in the context of angiogenesis.

3.3. Materials and methods

3.3.1. Cell culture

Human microvascular endothelial cells (HMEC-1) (CDC, Atlanta, GA) were cultured on 0.1% gelatin coated flasks (Sigma) in MCDB-131 medium (Gibco) supplemented with 10% FBS (Gibco), 1x Penicillin-Streptomycin (Gibco), hydrocortisone (Sigma H6909-10), human endothelial growth factor (EGF, 10 ng/mL, Peprotech/Invitrogen 016100-15-A) and L-glutamine (5x, Gibco, 25030-024) as previously described[370,374]. Cells were incubated at 37°C and 5% CO_2 in a humidified atmosphere and passaged at 80–90% confluency using 0.25% trypsin digestion[374].

MSC were obtained and isolated from human samples as previously described (Chapter 2)[367]. MSC were cultured as previously described for cell expansion in static conditions as well as to obtain MSC conditioned medium for isolation of MSC-EVs (Chapter 2)[367].

3.3.2. EV isolation from MSC cultures

EVs were isolated using TFF combined with SEC. MSC cell culture conditioned medium (CM) was precleared from cell debris by centrifugation at 2000 x *g* for 15 min, followed by filtration using a 0.45 µm bottle top filter unit with PES membrane (Nalgene, ThermoFisher). Then, CM was concentrated by TFF using a Minimate 100 kDa MWCO Omega Membrane (PALL) to a volume of 5 mL. EVs present in the CM were isolated by SEC, using an HiPrep 16/60 S-400 Sephacryl column connected to an AKTA Start chromatography system (both GE Healthcare) as previously described[369]. EV-containing fractions were pooled after elution, sterilized by syringe filtration using a 0.45 µm SFCA membrane (Corning) and concentrated using a 100 kDa MWCO Amicon Ultra-15 centrifugal filter unit (Merck MilliPore). The entire isolation protocol was performed at 4ºC in order to preserve the integrity of EVs. EVs were stored at 4ºC for less than one week until further use, or stored at -20ºC until further analysis by Western blot.

3.3.3. Comprehensive characterization of MSC-EVs

3.3.3.1. Nanoparticle tracking analysis

EV size distribution profiles and concentration measurements were obtained by NTA, using a Nanosight NS500 instrument (Malvern) equipped with a 405 nm laser and NTA software version 3.4 (Malvern). Samples were diluted in PBS to obtain a final concentration in the range of $5x10^8$ to $2x10^9$ particles/mL. NTA acquisition and post-acquisition settings were kept constant for all samples. Using a scripted control function, each sample was recorded 3 times for 30 s. Fresh sample was measured for each acquisition, by pumping fresh sample into the detection chamber. Samples were measured using a camera level of 16 and acquisition temperature was controlled and maintained at 25ºC. For post-acquisition analysis, all post-

acquisition settings were set to “Auto”, with the exception of a fixed detection threshold of level 5. Each video recording was analyzed using the NTA software.

3.3.3.2. Protein quantification

Total protein was quantified in EV samples using the Micro BCA™ Protein Assay Kit (Thermo Scientific), according to manufacturer instructions for the microplate procedure. EVs were previously lysed in 1x RIPA buffer for 10 min at room temperature. Two replicates were quantified for each sample. Sample concentration was determined by applying a linear fit to the BSA standards and using the resulting equation to determine each sample concentration from its absorbance measurement. All samples and standards were prepared in the same final RIPA buffer concentration.

3.3.3.3. Western blot

Cells were lysed in 1x RIPA buffer (Merck Milipore) supplemented with protease and phosphatase inhibitors (Roche) and then centrifuged at 12 000 x *g* for 15 min at 4ºC to remove insoluble material. Supernatants were recovered and used as whole cell lysates (WCL). Total protein content in WCL and EV samples was quantified using the Micro BCA kit as previously described.

Both WCL and EV samples were mixed with sample buffer in reducing conditions (except for CD63 detection, where non-reducing conditions were used) and heated to 95ºC for 10 min. All samples were loaded in 4-12% Bis–Tris polyacrylamide gels (Invitrogen, Life Technologies), in equal protein content for each gel lane (1 µg of total protein), and subjected to electrophoresis.

Proteins were transferred into PVDF membranes using an iBlot 2 Dry Blotting System (Invitrogen, Life Technologies). Membranes were blocked with 5% BSA solution in tris-buffered saline (TBS) for 1 h at room temperature and incubated with primary antibodies diluted in a solution of 0.5% BSA in TBS with 0.1% Tween-20 (TBST) overnight at 4ºC. Finally, membranes were incubated with secondary antibodies diluted in 50% v/v Odyssey Blocking Buffer (LI-COR Biosciences) in TBS for 1 h at room temperature. Proteins were visualized using an Odyssey Infrared Imager (LI-COR Biosciences) at 700 and 800 nm.

Primary antibodies included ALIX 1:500 (Thermo Fisher Scientific, MA1-83977), Calnexin 1:1000 (GeneTex, GTX101676), CD9 1:500 (Abcam, ab92726), CD63 1:1000 (Abcam, ab8219), CD81 1:1000 (Santa Cruz Biotechnology, sc-166029), TSG101 1:1000 (Abcam, ab30871) and β-actin 1:2000 (Sigma-Aldrich, 014M4759). Secondary antibodies consisted of either anti-mouse IgG conjugated to AlexaFluor 680 (Thermo Fisher Scientific, A-21057) or anti-rabbit IgG conjugated to IRDye 800CW (LI-COR Biosciences, 926-32211) and were applied at a 1:10 000 dilution in staining buffer.

3.3.4. Functional assays with endothelial cells

3.3.4.1. Sprouting assay

Endothelial cells (HMEC-1) were used to make spheroids as described before[237,370]. For this, 1000 cells/well were seeded in low-binding 96-well round-bottom plates in 0.1% methylcellulose (Avantor) in MCDB-131 medium. After 24 h, the spheroids were embedded in non-supplemented MCDB-131 medium containing 1 mg/mL collagen (Advanced Biomatrix), in 48-well plates, with or without the addition of EVs. MCDB-131 medium supplemented with 20% FBS was used as positive control. Three wells from 48-well plates were prepared for each condition, each well containing c.a. 10-12 spheroids. Cells were incubated at 37°C and 5% CO_2 in a humidified atmosphere. Bright field microscopy images were acquired after 24 h. *In vitro* sprouting was quantified by measuring the length of the tubular outgrowth and the number of tubes (i.e. sprouts), using ImageJ software to perform a blinded analysis. Form these measurements, the total sprout length, sprout number and average sprout length were calculated for each spheroid.

3.3.4.2. Scratch assay

The effect of MSC-EVs on scratch wound closure was determined following previously described protocols[237]. Endothelial cells (HMEC-1) were seeded in 48-well plates and cultured in complete culture medium. When a confluent cell monolayer was achieved (24 - 48 h latter), a scratch was made using the tip of a 200 µL pipet tip. Floating cells were removed and the medium was replaced with non-supplemented MCDB-131 medium, with or without the addition of EVs. MCDB-131 medium supplemented with 20% FBS was used as a positive control. Triplicates were prepared for each condition. Cells were incubated at 37°C and 5% CO_2 in a humidified atmosphere. Bright field microscopy images (2 images per well) were acquired immediately after exposure (t=0 h) and 6 h latter. Image J was used to determine the scratch wound area and length. By dividing the scratch wound area by the length we obtained the average scratch width for each acquired image. Cell migration was determined by calculating the difference in the average scratch width between the initial and final time points, while the wound closure percentage was determined by dividing the average migration width (i.e. the previously described cell migration parameter) by the initial average scratch width.

3.3.4.3. ERK/Akt assay

The effect of EVs on ERK1/2 and Akt phosphorylation in endothelial cells was determined as described before[369,374]. Briefly, endothelial cells (HMEC-1) were seeded on 48-well plates and cultured in complete culture medium. When a confluent cell monolayer was achieved (24 - 48 h latter), cells were starved in basal MCDB-131 medium for 3 h. Then, EVs were added to the culture medium (PBS was added as control) and cells were cultured for 30 min. Duplicates were prepared for each condition. Cells were lysed using lysis buffer supplemented

with protease and phosphatase inhibitors (Roche) for 5 min on ice, followed by centrifugation at 14 000 x *g* for 10 min at 4ºC. Protein levels of phosphorylated ERK1/2 and Akt, as well as total ERK1/2 and Akt were assessed using Western blotting as previously described. Samples were normalized on total protein content and the maximum amount of total protein possible was used. Primary antibodies included pERK1/2 (1:1000, Cell Signaling, 9101), ERK1/2 (1:1000, Cell Signaling, 9102), pAkt (1:1000, Cell Signaling, 4060) and Akt (1:1000, Cell Signaling, 9272). Membranes were incubated in goat anti-rabbit Immunoglobulins/HRP secondary antibody (1:2000, Dako, P044801) diluted in a solution of 5% milk in TBST. To visualize proteins a chemiluminescent peroxidase substrate (BioLedgend, 426303) was used. Image acquisition was performed on ChemiDoc™ MP Imaging System (Bio-Rad). Signal intensity was quantified on ImageJ software using the "Gels" analysis tool.

3.3.5. Statistical analysis

Statistical analysis was performed using GraphPad Prism 8 Software. Results are presented as mean ± SEM. Ordinary one-way ANOVA test with Turkey's multiple comparisons test were applied to evaluate the statistical significance of the differences in relative values of each parameter from the endothelial sprouting assay (i.e. total sprout length, sprout number and average sprout length) between different conditions. Alternatively, Brown-Forsythe and Welch ANOVA tests with Dunnett's T3 multiple comparisons test were applied when significant differences in SD between data sets were observed. These data sets passed normality tests. P-values result from two-tailed tests with a 95% confidence interval. Differences were considered significant at $P<0.05$ and statistical output was represented as follows: $P\leq0.0001$ (****); $0.0001<P\leq0.001$ (***); $0.001<P\leq0.01$ (**); $0.01<P\leq0.05$ (*); $P>0.05$ (ns).

3.4. Results

3.4.1. EV isolation through size exclusion chromatography is appropriate for functional studies

EVs were isolated from BM and UCM MSC cultures in static conditions using SEC. According with MISEV guidelines[375], Western blot analysis was used to confirm the presence of EV protein markers (in BM MSC-EVs). CD81 and CD63 were successfully detected and enriched in EV samples (Figure 3.1 A). However, TSG101, ALIX and CD9 were not detected in EV samples. The organelle marker calnexin was present in cells but not in EVs, confirming the absence of cellular contamination in EV isolates.

BM and UCM MSC-EVs showed a size-distribution profile typical of small EVs (i.e. diameter generally bellow 200 nm), with average diameters of 103 ± 3 nm (n=4) and 101 nm (n=1), respectively (Figure 3.1 B and Table 3.1). Generally, UCM MSC allowed higher EV yields than BM MSC, showing a higher number of EVs per volume of conditioned medium as well as more

EVs secreted per cell (Table 3.1). Still, both MSC sources originated EV samples at similar purity assessed by their PPR.

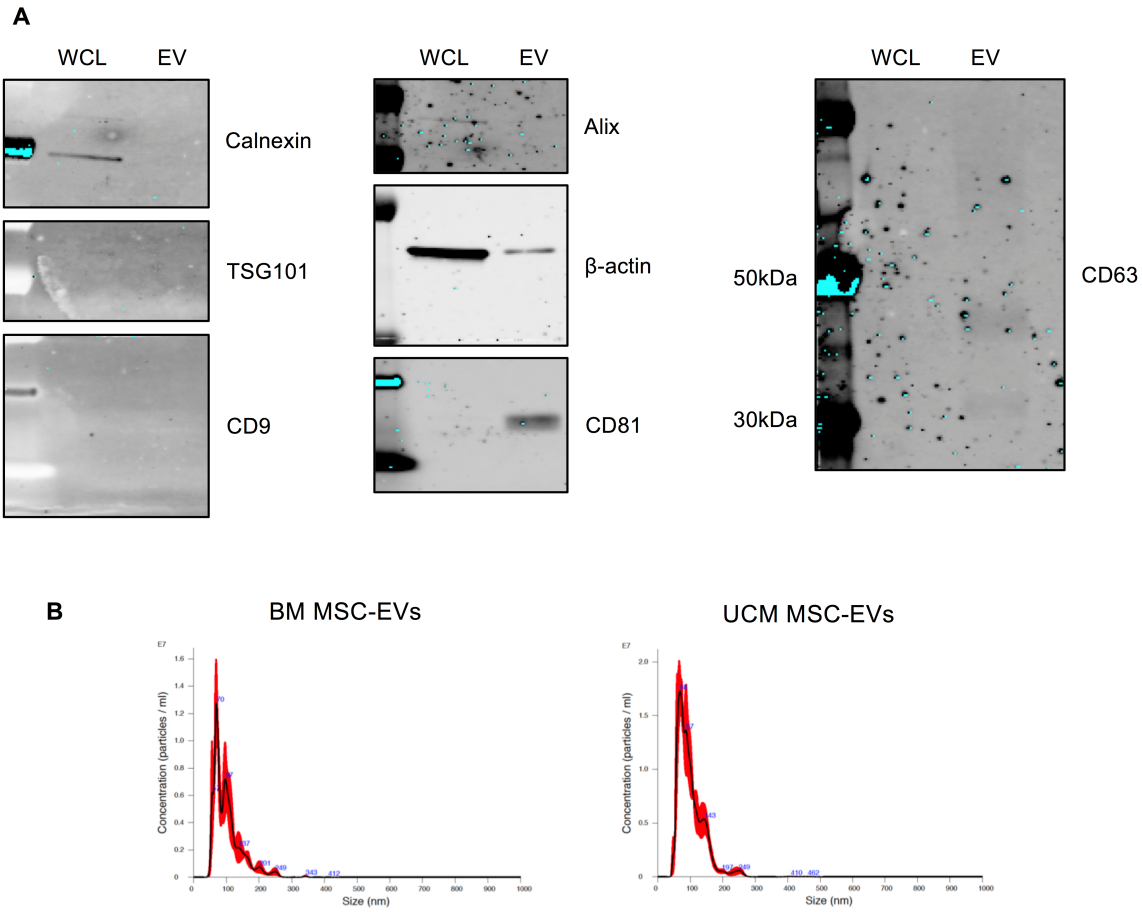

Figure 3.1 - Characterization of MSC-EVs isolated by SEC. A) Western blots of whole cell lysates (WCL) and EV samples, obtained from BM MSC. Detection of common EV markers (CD9, CD63, CD81 ALIX and TSG101), EV-negative marker calnexin and housekeeping protein β-actin. **B)** Representative NTA size distribution curves of EV samples obtained from BM and UCM MSC. SEC - size exclusion chromatography. NTA - nanoparticle tracking analysis. BM - bone marrow. UCM - umbilical cord matrix.

Table 3.1 - Comparison of MSC-EV isolations from different tissue sources (BM and UCM), using cells from only one donor for each source. Values of average and mode of EV sizes, EV concentration in conditioned medium, number of EVs generated per cell and per each T-flask and particle per protein ratio. Results are presented as mean ± SEM. BM - bone marrow. UCM - umbilical cord matrix. CM - conditioned medium. PPR - particle per protein ratio.

EV producing cells	BM MSC (n=4)	UCM MSC (n=1)
Avg. size (nm)	103.0 ± 3.4	100.6
Mode of size (nm)	71.5 ± 3.3	73.8
EV conc. in CM (part./mL)	$2.38 \pm 1.05 \times 10^{8}$	4.68×10^{8}
EV productivity (part./cell)	$2.01 \pm 0.89 \times 10^{3}$	7.57×10^{3}
EV number per T-175 (part./flask)	$4.77 \pm 2.11 \times 10^{9}$	9.37×10^{9}
PPR (part./µg protein)	$3.02 \pm 1.46 \times 10^{9}$	3.76×10^{9}

The performance of SEC for isolation of MSC-EVs was compared with previous data from MSC-EV isolation using a commercial precipitation kit (Chapter 2). EV yields (i.e. number of EVs per volume of conditioned medium) were 4-fold lower using SEC, while EV purities (i.e. PPR) were 15 to 22-fold higher using SEC (Table 3.2). EV isolation using SEC resulted in EV samples with lower EV sizes compared with previous isolations using the commercial precipitation kit, as observed through lower average and mode of EV sizes (Table 3.2). Moreover, a comparison between Western blot analysis reveals a more significant enrichment in EV protein markers CD81 and CD63 in EVs isolated through SEC, thus corroborating a higher EV purity obtained with this method (Figure 3.1 A and Figure 2.3 B). In spite of reduced EV yields, a much higher EV purity obtained through SEC isolation will be relevant to study the functional activity of MSC-EVs more rigorously.

Table 3.2 - Comparison of MSC-EV isolations using two different isolation methods (TEI kit and SEC). Comparisons using the same BM donor and the same UCM (i.e. only one donor per source). TEI - Total Exosome Isolation. SEC - size exclusion chromatography. NTA - nanoparticle tracking analysis. BM - bone marrow. UCM - umbilical cord matrix. CM - conditioned medium. PPR - particle per protein ratio.

MSC source	Isolation method	EV conc. in CM (part/mL)	PPR (part/µg protein)	Avg. size (nm)	Mode of size (nm)	No. isolations
BM	TEI kit	9.50×10^{8}	2.04×10^{8}	171	124	n=1
	SEC	2.38×10^{8}	3.02×10^{9}	103	72	n=4
UCM	TEI kit	1.86×10^{9}	1.71×10^{8}	144	121	n=1
	SEC	4.68×10^{8}	3.76×10^{9}	101	74	n=1

3.4.2. MSC-EVs improve the angiogenic capacity of endothelial cells *in vitro*

Increasing evidence has proposed EVs as mediators of many of the MSC-associated paracrine therapeutic features, including cardiac regeneration and the ability to stimulate angiogenesis[237,246]. The functional activity of MSC-EVs was investigated by studying their angiogenic effect on endothelial cells in different *in vitro* assays.

A 3D *in vitro* assay using endothelial spheroids was applied to study the angiogenic potential of BM and UCM MSC-EVs. Endothelial cell (HMEC-1) spheroids were treated with MSC-EVs previously isolated by SEC. Both BM and UCM MSC-EVs significantly enhanced sprouting in an endothelial spheroid assay, increasing the total sprouting length per spheroid by 1.9-fold compared to controls after 24 h of treatment (Figure 3.2). EVs from both cells enhanced the number of sprouts formed, but UCM MSC-EVs led to a significantly higher increase (2.0-fold) than BM MSC-EVs (1.4-fold). BM MSC-EVs improved the average sprout length (by 1.4-fold) but UCM MSC-EVs did not have a relevant impact in this parameter.

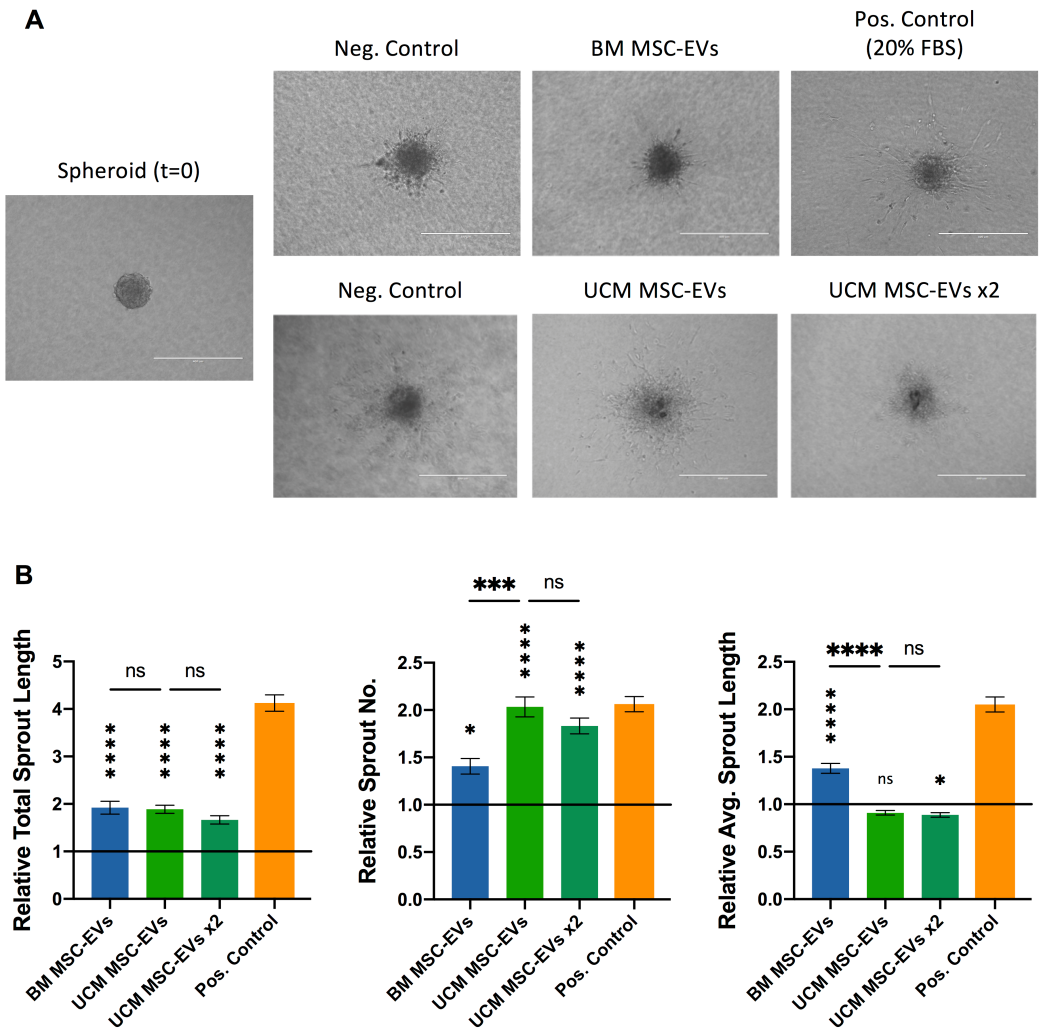

Figure 3.2 - Sprouting assay. A) Representative microscopy images of endothelial spheroids embedded in a collagen matrix at the beginning of the assay (t=0 h) or 24 h after treatment with different EV conditions. Either $2x10^{10}$ or $4x10^{10}$ (i.e. x2 dose) EV particles were added per well of a 48-well plate. PBS was used for negative controls and 20% FBS was used for positive controls. Scale bar = 400 µm. **B)** Total length of sprouts formed per spheroid relative to negative controls; Number of sprouts formed per spheroid relative to negative controls; Average sprout length per spheroid relative to negative controls. Results are presented as mean ± SEM. Between 2-3 wells with c.a. 10 spheroids each were used per condition; the cumulative n (total number of spheroids analyzed per condition) varied between 16 and 28. Ordinary one-way ANOVA test with Turkey's multiple comparisons test or Brown-Forsythe and Welch ANOVA test with Dunnett's T3 multiple comparisons test; P-value output represented in the following way: P≤0.0001 (****); 0.0001<P≤0.001 (***); 0.001<P≤0.01 (**); 0.01<P≤0.05 (*); P>0.05 (ns).

The effect of EV dosage was studied by exposing endothelial spheroids at twice the dose of UCM MSC-EVs (i.e. $2x10^{10}$ vs. $4x10^{10}$ particles/well). Increasing the EV dose did not show any significant impact on endothelial sprouting (Figure 3.2).

A scratch wound *in vitro* assay using the same endothelial cells (HMEC-1) was also applied to study the angiogenic potential MSC-EVs. Scratches were made on HMEC-1 monolayers followed by treatment with UCM MSC-EVs for 6 h at two doses ($2x10^{10}$ and $4x10^{10}$ particles/well). No differences were observed in scratch wound closure upon EV treatment (Figure 3.3). Moreover, no differences were observed in positive controls (20% FBS treatment), which was unexpected. Poorly defined scratch margins and floating cells

hampered image analysis. This may have led to an unreliable image analysis and may justify the lack of any observed effects.

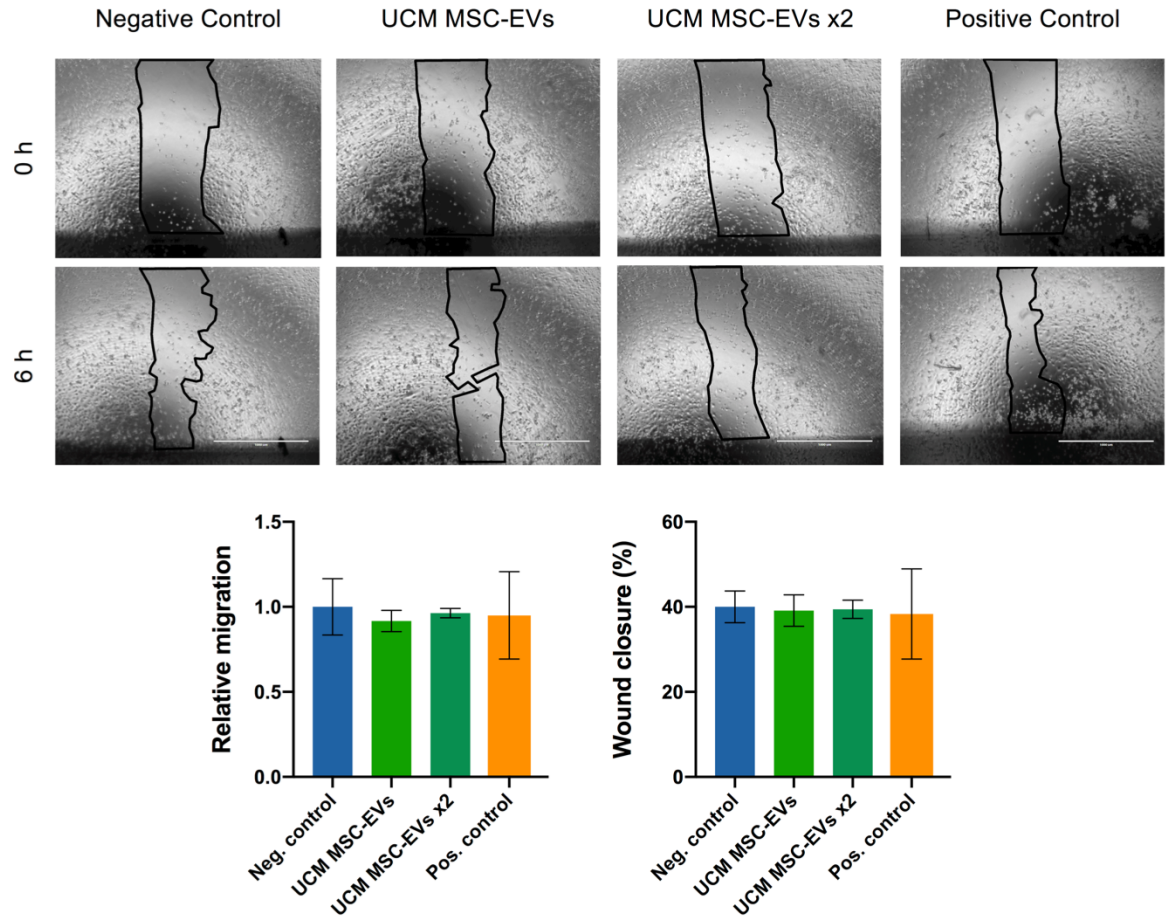

Figure 3.3 - Scratch assay. Representative microscopy images of scratch wounds on endothelial cell monolayers, at the beginning of the assay (t=0 h) or 6 h after treatment with UCM MSC-EV at different concentrations. Either $2x10^{10}$ or $4x10^{10}$ EV (i.e. x2) particles were added per well of a 48-well plate. PBS was used for negative controls and 20% FBS was used for positive controls. Scale bar = 1 mm. Relative endothelial cell migration and wound closure percentage over 6 h of treatment. Relative migration only considers the absolute distance migrated by cells to close the scratch wound, while wound closure is affected by the initial scratch area. Results are presented as mean ± SEM (n = 3 technical replicates).

Activation of ERK1/2 and Akt signaling in endothelial cells was also used as a readout to evaluate the functional effect of MSC-EVs. HMEC-1 cells were treated for 30 min with BM MSC-EVs previously isolated by SEC. Protein levels of phosphorylated ERK1/2 and Akt, as well as total ERK1/2 and Akt were determined using Western blotting. No clear increase in ERK1/2 or Akt phosphorylation was observed with BM MSC-EVs treatment (Figure 3.4). Upon EV treatment pERK/ERK ratio was similar, while pAkt/Akt ratio increased slightly.

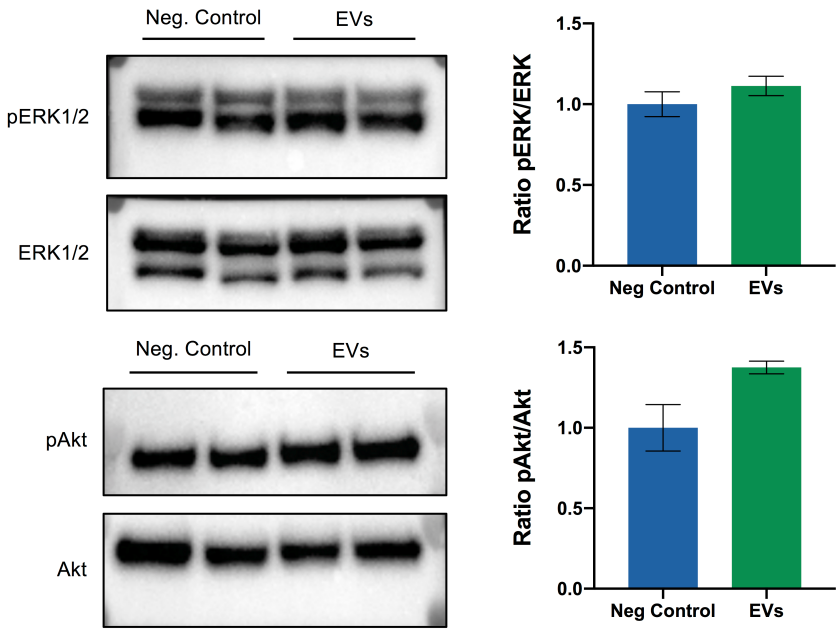

Figure 3.4 - ERK/Akt assay. Western blot analysis of ERK1/2 and Akt expression and their respective phosphorylated forms (pERK1/2 and pAkt) in endothelial cells cultured with or without the addition BM MSC-EVs ($1x10^{10}$ EV particles were added per well of a 48-well plate). Results are presented as mean ± SEM (n = 2 technical replicates).

3.5. Discussion

Following decades of research and investment aiming to apply MSC for numerous therapeutic purposes and with only a few MSC-based products already commercially available, MSC-EVs are rising as the new promise for several therapeutic applications. Intense research over the past decade has revealed EVs as the mediators of many MSC therapeutic features, with promising applications in regenerative medicine. Recently established clinical trials have been studying their application for the treatment of type 1 diabetes (NCT02138331), macular holes (NCT03437759) and chronic kidney disease[253] and very recently for COVID-19 treatment (e.g. NCT04798716, NCT04602442).

EVs can be isolated from cell culture conditioned medium of *in vitro* expanded cells through multiple techniques. In spite of extensive research in the field, no EV isolation method developed so far could be deemed as ideal[376]. Each isolation method presents a different recovery yield and different specificity (i.e. EV purity), which are typically inversely proportional, considering that the higher the specificity of a certain technique, the lower recovery can be expected[375]. High recovery, low specificity methods include commercially available precipitation kits that concentrate both vesicular and non-vesicular material.

Other techniques such as ultracentrifugation (e.g. differential centrifugation or density gradient centrifugation), affinity methods or SEC allow more specific isolation of EVs, which is particularly relevant for studying the functional activity of EVs. In particular, SEC allows a scalable EV isolation, unlike ultracentrifugation methods, as well as preventing aggregation

and EV collapse caused by high centrifugation speeds[377]. SEC allows to separate components from cell culture conditioned medium according to their size, resulting in the elution of EVs before free proteins, which typically have a lower size. This allows a more reliable study of EV function with less influence of co-isolated free-protein contaminants.

In this work, we investigated the functional activity of MSC-EVs obtained from two different and clinically relevant human tissue sources (BM and UCM) by studying their impact on angiogenesis. MSC-EVs were produced in S/XF conditions using hPL as a culture supplement (similarly to Chapter 2)[367] and isolated using a scalable and selective EV isolation method that combines TFF with SEC[378], as an alternative to the previously used precipitation-based method. By employing S/XF cell culture conditions we avoided traditional animal-based cell culture supplements like FBS that present significant limitations for application in a clinical setting (e.g. risk of contamination with virus and prions, ability to transmit xenogeneic-antigens, supply limitations and ethical concerns)[65,66].

Clinical application of EVs will require the production of very high numbers of EVs (e.g. each patient may require 0.5 - 1.4 x 10^{11} EVs[338]). Therefore, in order to manufacture EV-based products for therapeutic purposes, robust and scalable processes need to be implemented. Most of the studies in the EV field use ultracentrifugation-based methods for EV isolation[379], which have very limited scalability. SEC is a more scalable process, considering the possibility to increase manufacturing capacity, scaling-up the operation by changing the column dimension (i.e. increasing its width) as well as scaling-out by increasing the number of columns. Additionally, SEC is a more reproducible method since it is less dependent on the operator. Thus, by combining S/XF manufacturing conditions with scalable processes we aimed to study the functional activity of MSC-EVs in conditions that are more readily translatable to a clinical setting.

We were able to reproducibly obtain EV preparations from both MSC sources at a relatively high purity, estimated by their PPR (c.a. 3x10^9 particles/µg protein), as well as an enrichment of typical EV markers (CD81 and CD63) in EV samples, in line with previous results using a comparable SEC protocol for isolation of MSC-EVs[380]. EV preparations also presented a well-defined size distribution profile, with particle diameters generally bellow 200 nm. These observations confirm that the employed isolation process allowed a selective isolation of EVs, reproducibly obtaining samples suitable for functional studies.

Higher EV yields were obtained from UCM MSC than BM MSC, regarding both the number of EVs per volume of conditioned medium and the number of EVs secreted per cell. This is in line with previous results we have obtained using a commercial precipitation kit for EV isolation (Chapter 2)[367]. This result seems to corroborate our previous conclusion that UCM MSC were likely able to secrete more EVs than BM MSC. However, in order to make a rigorous comparison between the EV productivity of both MSC sources using this isolation protocol,

more EV isolations need to be performed, preferentially including MSC from additional tissue donors, since only one donor for each tissue source was studied in the present work.

One of the best-established therapeutic activities of MSC-EVs is their ability to regenerate damaged tissue, particularly in cardiovascular injury. The first report revealed that MSC-EVs were able to reduce myocardial ischemia/reperfusion injury in mice[246]. Since then, multiple studies reported the tissue regeneration potential of MSC-EVs in diverse contexts using *in vivo* models, including improved recovery from acute kidney injury[247,248], stroke[250], hepatic injury[252] and pulmonary hypertension[230].

We observed that both BM and UCM MSC-EVs stimulated angiogenesis in a 3D *in vitro* model, improving sprouting of endothelial spheroids. This pro-angiogenic capacity of MSC-EVs is in line with previous reports in the literature[236,237,327,328,381]. MSC-EVs were able to enhance VEGF expression in tumor cells by activating ERK1/2 pathway[381] and were able to promote angiogenesis in a rat myocardial infarction model[236]. Although several studies reported MSC-EVs to play a key role in angiogenesis, this role is still controversial since some contradictory results can be found in the literature describing also an anti-angiogenic effect by MSC in certain conditions[382,383]. A study reported that MSC-EVs were able to suppress angiogenesis both *in vitro* and *in vivo*, by downregulating VEGF expression in tumor cells, describing that miR-16 transfer by MSC-EVs was partially responsible for this effect[382]. Apparently different factors can be involved in the regulation of angiogenesis by MSC-EVs and their effect could depend on the specific context, such as the nature or environmental stimuli of cultured MSC (e.g. MSC tissue source or oxygen concentration) or the target cells studied (e.g. different types of endothelial cells or cancer cells). As a result, MSC-EVs are potentially able to support or suppress angiogenesis and contradictory roles of MSC-EVs in regulating angiogenesis have been attributed to heterogeneity between MSC and differences in the angiogenesis models used[382].

Interestingly, although MSC-EVs from both MSC tissue sources revealed a similar potential to induce angiogenesis overall (i.e. similar improvement of total sprout length per spheroid), this was achieved in different ways. While BM MSC-EVs improved the total sprout length by stimulating both the formation of new sprouts (i.e. increased sprout number) and their elongation (i.e. increased average sprout length), UCM MSC-EVs only stimulated the formation of new sprouts, but to a higher level than BM MSC-EVs. This suggests that MSC-EVs may induce angiogenesis through different mechanisms depending on the MSC tissue source. More studies would be required to elucidate the mechanisms involved in angiogenic stimulation by MSC-EVs and the differences between distinct MSC sources. Multiple mechanisms have been proposed for the modulation of angiogenesis by MSC-EVs obtained from different MSC tissue sources[384]. These include the transfer of miRNA (e.g. miR-125a[385] and miR-31[386]), proteins (e.g. VEGF[387], PDGF-D[388] and EMMPRIN[237]) and transcription

factors (e.g. STAT3[389]), as well as the activation of signaling pathways such as NF-κB[390] and Wnt4/β-catenin[391]. Therefore, a combination of some of these mechanisms, and possibly others not yet described, were responsible for stimulating angiogenesis in the 3D *in vitro* assay performed in this work.

In contrast with results from the endothelial sprouting assay, no indication of angiogenic stimulation from MSC-EVs was observed in the ERK/Akt assay, since no clear increase in ERK1/2 or Akt phosphorylation in endothelial cells was observed upon treatment with BM MSC-EVs. This was unexpected since both ERK1/2 and Akt are involved in several processes associated with tissue regeneration such as cell survival, growth, proliferation, angiogenesis, and migration[371–373], all of them previously reported to be stimulated by MSC-EVs in multiple models[230,237,249,252,381]. A possible explanation could be the fact that negative controls seemed to reveal unusually high signals of both phosphorylated forms. Considering this, it is likely that endothelial cells were accidentally stimulated for some reason during the experimental procedure. Therefore, this assay would need to be repeated, similarly to the scratch assay, in order to obtain conclusive results.

Further work using these angiogenesis *in vitro* assays would be relevant to better establish dose-response profiles of MSC-EV treatment, as well as to elucidate on anticipated differences between MSC-EVs from different MSC tissue sources. Here, no differences were observed when we duplicated the dose of UCM MSC-EVs (in either sprouting or scratch assays). This could mean that we were already observing the maximum functional effect in the sprouting assay at the standard dose used (i.e. $2x10^{10}$ EVs per well of a 48-well plate), or alternatively we would need to increase the EV dose even further to observe an improved functional outcome. A wider dose range would need to be applied with several different EV doses in order to understand the dose-response profile of MSC-EV treatments in these conditions.

It would also be relevant to compare the angiogenic potential of MSC-EVs with EVs obtained from other cells. Different cells secrete EVs capable of inducing angiogenesis with promising therapeutic application including endothelial cells[392,393], platelets[394,395] and cardiomyocyte progenitor cells (CPC)[237,396]. Interestingly, a similar pro-angiogenic effect was described between EVs obtained from CPC and MSC, isolated through differential centrifugation[237]. It would be interesting to see if this observation would be maintained using the present SEC isolation protocol. In fact, preliminary work developed in collaboration with colleagues at UMC Utrecht revealed that CPC-EVs and MSC-EVs isolated by SEC showed similar effect in the endothelial sprouting assay (data not shown). In addition to the therapeutic potential of their secreted EVs, each cell source has different relevant features such as the availability and easiness to isolate from human tissue sources, cell expansion ability and the

EV secretion capacity. Therefore, each factor should be considered when selecting a cell source to produce EVs for therapeutic application.

The use of EVs as therapeutic products faces several challenges. One of them is the need to produce a large number of EVs so as to obtain a significant functional effect upon administration. In this work, relatively high doses ($2x10^{10}$ EVs per well of a 48-well plate) were used to obtain functional effects *in vitro*, which required large numbers of cultured MSC (c.a. 10 million BM MSC or 2.6 million UCM MSC to obtain $2x10^{10}$ EVs). In a clinical context this type of therapy will likely require doses a few orders of magnitude higher and multiple administrations in order to achieve a significant efficacy. For this reason, the need to implement scalable EV production platforms becomes even more crucial. Scalable manufacturing processes such as the one developed by our group (Chapter 2)[367] using a microcarrier-based bioreactor culture system and by others using hollow-fiber bioreactor systems[333,366] offer promising options for scalable EV production from cell culture conditioned medium. These strategies will be particularly promising when combined with scalable EV isolation processes such as the one used in this work, combining TFF and SEC.

Efficient delivery of EVs into target tissues to elicit a functional response is another challenge in the field. Although EVs offer promising benefits for therapy compared with synthetic nanoparticle formulations, they still present similar limitations regarding off-target accumulation in tissues such as the liver and spleen[397]. Improving EV specificity and retention in target tissues may be a necessity for most clinical applications and multiple strategies have already been developed for this purpose, typically involving either genetic engineering of EV producing cells or anchoring targeting moieties to EVs after their isolation[257,283,294].

The therapeutic potential of EVs secreted by MSC or other cells may also be improved by modulation of EV secreting cells or their microenvironment. Different strategies have been implemented to improve the therapeutic capacity of MSC by preconditioning these cells with specific physicochemical or biochemical cues[89,139,356,398–400]. For example, our group has recently reported that *ex vivo* culture of UCM MSC in a dynamic microcarrier-based culture platform as well as under hypoxic conditions (2% O_2) improved the *in vitro* angiogenic potential of MSC conditioned culture medium[400]. In fact, shear stress had been previously observed to improve the angiogenic potential of human AT MSC through stimulation of VEGF secretion[139] and hypoxia preconditioning also increased the secretion of angiogenic factors by MSC[242,401]. Thus, similar preconditioning strategies might improve the angiogenic activity of MSC-EVs.

In this work, we studied and compared the angiogenic activity of MSC-EVs using MSC from two different human tissue sources (i.e. BM and UCM). MSC-EVs were manufactured through a process closely translatable to a clinical setting by employing S/XF conditions and using a scalable and selective EV isolation method that combines TFF with SEC. MSC-EVs originated from both MSC tissue sources revealed similar pro-angiogenic potency overall in a 3D *in vitro*

assay by stimulating sprouting in endothelial cell spheroids. Nevertheless, the number of new sprouts formed and their elongation was different between both types of EVs, suggesting that MSC-EVs obtained from different tissue sources may stimulate angiogenesis through different mechanisms. Further studies will be required in order to elucidate the mechanisms involved in angiogenic stimulation by MSC-EVs and possible differences between distinct MSC sources. MSC-EVs obtained through the clinically relevant manufacturing conditions used in this work are promising for regenerative medicine applications.

4. Surface modification of mesenchymal stromal cell-derived extracellular vesicles with the azurin-p28 peptide for cancer-targeted therapy

4.1. Summary

EVs have been increasingly recognized as promising drug delivery vehicles for the treatment of numerous diseases, due to their inherent ability to shuttle messages between cells, supporting their use to transport and deliver therapeutic molecules to diseased cells. Multiple strategies have been used to engineer EVs to deliver therapeutic cargo to diseased cells and tissues, including the display of targeting moieties on the surface of EVs.

In this work, we modified the surface of MSC-EVs by anchoring the p28 peptide derived from the bacterial protein azurin to their surface, aiming for a targeted anti-cancer drug delivery vehicle. This p28 peptide has been described to preferentially enter a variety of cancer cells compared with normal matched-tissue cells and to trigger apoptosis. Thus, we hypothesized that EV decoration with p28 would improve EV targeting to cancer cells.

Human BM MSC-EVs were produced in conditions readily translatable to a clinical setting, by combining S/XF conditions and a scalable and selective EV isolation method that combined TFF with SEC. We designed a novel conjugated peptide by fusing the cancer-targeting p28 peptide with the CP05 peptide, previously described to anchor to the transmembrane EV protein CD63. This CP05-p28 conjugated peptide was successfully anchored to previously isolated EVs, after incubation at different peptide to EV ratios and using different incubation protocols. Anchoring of p28 peptides to the surface of EVs led to a 2.4-fold increase in the EV uptake by breast cancer cells.

Therefore, we propose the use of p28-decorated MSC-EVs, manufactured in conditions closely translatable to a clinical setting, for the development of novel EV-based DDS applied to cancer therapy. Further work focusing on loading EVs with chemotherapy agents or anti-cancer RNA molecules may reveal enhanced functional drug delivery by p28-decorated EVs with subsequent improved anti-cancer activity.

4.2. Background

EVs are increasingly being considered as promising natural drug delivery vehicles for the treatment of multiple diseases. EVs are lipid membrane enclosed structures naturally secreted by cells, with sizes ranging from 50 to 1000 nm. These vesicles are able to transfer their cargo of biomolecules, including proteins, lipids and nucleic acids (e.g. miRNA and mRNA) triggering alterations in recipient cells[153–155].

Their small size and resemblance to the cell membrane makes EVs ideal candidates to cross biological barriers, while providing high biocompatibility to target cells[156,257,331]. Thus, EVs have emerged as promising DDS, presenting advantageous features that may allow them to outperform synthetic nanocarriers. Due to their biological origin, EVs present generally low immunogenicity and toxicity, allowing to overcome safety issues associated with synthetic

nanocarriers[261,262,270,402]. Some EVs possess inherent targeting ability and display tropism for particular cells or tissues[213,283,284]. In fact, EVs have been recently described to deliver functional RNA more efficiently than state-of-the-art synthetic RNA nanocarriers[403].

Drug loaded EVs can be used to transport and deliver a diverse array of therapeutic cargo to diseased cells and tissues[260,266,268]. Examples of EV-mediated drug delivery include the transport of small molecules (e.g. curcumin or chemotherapeutic drugs), proteins and different RNA molecules (e.g. siRNA, miRNA and mRNA), which have been applied mainly for the treatment of several types of cancer and neurological diseases, but have the potential to deliver drugs to any diseased tissue[257,263–267].

Moreover, EVs can be further engineered to improve specificity and retention on target cells and tissues[283]. Genetic modification of parental cells enables the production of EVs with specific targeting moieties. For example, a protein abundant on the surface of EVs named Lamp2b has been successfully fused to targeting moieties specific for brain, tumor cells and their angiogenic endothelium or IL3 receptors on chronic myeloid leukemia cells to target EVs to these respective tissues and cells[257,287,404].

In spite of several examples successfully targeting EVs to target cells, methods relying on genetic manipulation of EV-producer cells are still challenging and time-consuming, requiring multiple steps of cloning, transfection or viral transduction and selection, which can be particularly challenging in primary cells[405]. In alternative to genetic modification, targeting moieties can be directly anchored to the surface of EVs after EV production and isolation. Several different strategies have been applied in this context (reviewed in Chapter 1), including post-insertion of lipid-conjugated molecules into EV membranes[294,295,297], electrostatic interactions between polymers and EVs[296], protein-lipid interactions[292] and click chemistry[293,298]. Recently, phage display was used to obtain a peptide (named CP05) that binds to the EV surface protein CD63[300]. When this peptide was conjugated with a muscle targeting peptide, EVs were successfully decorated with the conjugated peptide and efficiently delivered therapeutic cargo to muscle tissue in a mouse model of muscular dystrophy.

MSC are a particularly interesting source of EVs for therapeutic application. These cells are regarded as immune evasive and the safety of their administration has already been confirmed in clinical trials[326]. MSC also show great ability for expansion when cultured *ex vivo* and robust expansion platforms have already been established[89,120–124]. In fact, scalable production of MSC-EVs in platforms readily translatable for clinical settings has been recently reported by our group (Chapter 2)[367] and others[333].

In this work, we modified MSC-EVs by anchoring the peptide p28 to their surface, aiming for a targeted anti-cancer drug delivery vehicle. The peptide p28 is a 28 amino acid fragment from the bacterial protein azurin, secreted by *P. aeruginosa*[302,303]. This peptide has been described to show preferential entry into cancer cells when compared to equivalent non-

cancerous cells[306,313]. So we hypothesized that EV decoration with p28 would improve EV targeting to cancer cells. The p28 peptide also has the ability to trigger apoptosis on cancer cells by binding to the tumor suppressor protein p53, stabilizing it and leading to cell-cycle arrest[317,318]. Additionally, p28 is also able to enhance the cytotoxic activity of multiple chemotherapy drugs[319].

Here, we obtained EVs secreted by human BM MSC cultured under S/XF conditions and isolated EVs through a previously described method employing SEC[378]. We fused the cancer-targeting p28 peptide with the CD63-anchoring peptide CP05. This CP05-p28 conjugated peptide was successfully anchored to MSC-EVs and allowed an improved EV uptake by cancer cells.

4.3. Materials and methods

4.3.1. Cell culture

Human breast cancer cells MDA-MB-231 were cultured in DMEM (Gibco) with L-Glutamine (Gibco) supplemented with 10% FBS (Gibco) and 1x Penicillin-Streptomycin (Gibco). Cells were incubated at 37°C and 5% CO_2 in a humidified atmosphere and passaged at 80–90% confluency using 0.25% trypsin digestion[374].

MSC were obtained and isolated from human samples as previously described (Chapter 2)[367]. MSC were cultured as previously described for cell expansion in static conditions as well as to obtain MSC conditioned medium for isolation of MSC-EVs (Chapter 2)[367].

4.3.2. EV isolation from MSC cultures

EVs were isolated from MSC cell culture conditioned medium using TFF combined with SEC, as previously described (Chapter 3).

4.3.3. Peptide synthesis

The conjugated peptide CP05-p28 was synthesized and provided with >95% purity by DGpeptides Co., Ltd. Upon receiving, peptides were dissolved in PBS to a final concentration of 4 mg/mL and stored at -20°C until further use. Detailed peptide sequences are shown in Table 4.1.

Table 4.1 - Nomenclature, sequence and molecular weight of the conjugated peptide used.

Name	Amino acids sequence	Molecular weight (g/mol)
CP05-$(GGGGS)_2$-Myc-p28	CRHSQMTVTSRL-GGGGSGGGGS-EQKLISEEDL-DDPKLYDKDLGSAMGDTVVGQMDAATSL	6130.77

4.3.4. Peptide anchoring to EVs

Previously isolated MSC-EVs were incubated with conjugated peptides for 6 h at 4ºC or for 2 h at room temperature as previously described[300]. Unbound peptides were removed by washing this mixture 3-4 times with 4 mL PBS and filtered until a final volume of c.a. 100 µL, using a 100 kDa MWCO Amicon Ultra-15 centrifugal filter unit (Merck MilliPore). EV-peptide incubation was performed at pre-determined ratios (50 µg peptide/1x10^{10} particles or 5 µg peptide/1x10^{10} particles). EVs were incubated with PBS as controls.

4.3.5. Peptide detection (dot blots)

EV samples were lysed in Triton X100 0.01%, for 10 min at room temperature. Free peptides and EV samples were heated for 10 min at 95ºC. Then, each was spotted on a nitrocellulose membrane using a dot blot apparatus (Bio-Rad). Membranes were blocked with Odyssey Blocking Buffer for 2 h at room temperature, followed by overnight incubation at 4°C with mouse-anti-Myc primary antibody (1:4000, 9E10 from MYC 1-9E10.2 hybridoma, ATCC). Membranes were incubated with IRDye 800CW anti-mouse secondary antibody (1:7500, LI-COR Biosciences, 926-32212) diluted in Odyssey Blocking Buffer for 1 h at room temperature. Membranes were visualized using an Odyssey Infrared Imager at 800 nm. Signal intensity was quantified on ImageJ software using the “Gels” analysis tool.

4.3.6. EV uptake studies

MSC-EVs were labeled with the fluorescent dye AlexaFluor 647 NHS ester (Invitrogen, Thermo Fisher, A37573). Lyophilized dye was dissolved at a concentration of 10 mg/mL in dimethyl sulfoxide (DMSO). EVs were mixed with sodium bicarbonate (pH 8.3, 100 mM final concentration) and 0.625% v/v AlexaFluor 647 NHS ester (10 mg/mL in DMSO), and incubated for 1 hour at 37°C in a shaker incubator at 450 rpm. EVs were then diluted in PBS and quenched in 100 mM Tris-HCl for 20 min at room temperature with regular agitation, in a final volume of 1 mL. EVs were purified from unbound dye through SEC using a XK-16/20 column (GE Healthcare) packed with Sepharose CL-4B (Sigma) according to instructions from the manufacturer[292]. The column was connected to a refrigerated ÄKTA Start chromatography system (GE Healthcare). EV-containing fractions were pooled after elution, sterilized by syringe filtration and concentrated as previously described in the EV isolation section (Chapter 3).

AlexaFluor 647 NHS ester-labeled EVs were decorated with CP05-p28 conjugated peptides as previously described in the “peptide anchoring to EVs” section. Briefly, peptides and EVs were incubated for 2 h at room temperature, at a ratio of 50 µg peptide/1x10^{10} particles and unbound peptides were removed as previously described.

MDA-MB-231 cells were cultured in flat-bottom 96-well plates in their normal growth medium. After 24 h, when a confluency of 80–90% was reached, previously labelled and

peptide-decorated EVs were added and cells were incubated for 4 h at 37°C to allow EV uptake[292]. At the end of this period, cells were imaged on a fluorescent microscope (EVOS FL, Life Technologies). Then, cells were washed once with PBS, trypsinized, resuspended in culture medium and transferred to round-bottom 96-well plates. Plates were centrifuged for 5 min at 350 x *g* to pellet cells, after which cells were resuspended in ice-cold FACS buffer (1 mM EDTA and 2% heat-inactivated FBS in PBS). Cells were analyzed on a CytoFLEX (Beckman Coulter) flow cytometer and further analyzed using FlowJo software.

4.4. Results

4.4.1. Design of an EV anchoring CP05-p28 conjugated peptide

Multiple strategies have been used to engineer EVs in order to deliver therapeutic cargo to diseased cells and tissues, including the display of targeting peptides on the surface of EVs. Here, we designed a conjugated peptide that allows anchoring p28 to the surface of MSC-EVs after their isolation. For this purpose, we used a previously described strategy that enables direct anchoring of peptides to the surface of EVs, which relies on anchoring the CP05 peptide to the EV transmembrane protein CD63[300]. We designed a peptide fusing CP05 and p28, expecting that CP05 would anchor to EVs, thus exposing p28 on their surface (Figure 4.1 A, Table 4.2).

The region comprising the N-terminal 18 amino acids of p28 has been described as the minimal motif for p28 internalization, being expected to be the most influential region for cancer cell uptake[306]. Thus, in order to promote the interaction of this sequence with target cancer cells, the p28 amino acids sequence was placed so that its C-terminal would follow the CP05 sequence, thus allowing its N-terminal to be freely exposed.

Additionally, in order to prevent steric hindrance between CP05 and p28, possibly limiting interaction of p28 with target cancer cells, a $(GGGGS)_2$ linker was included in the peptide design. Myc-tag was inserted in the middle of the peptide sequence, so that it would not compromise the interaction of CP05 with CD63 on the EV side, neither the interaction of p28 with target cancer cells. Although placing Myc in the middle of the peptide sequence could compromise its detection, previous work has been able to successfully detect Myc-tag in the middle of a larger protein sequence[406]. In the end, we obtained the final peptide sequence CP05-$(GGGGS)_2$-Myc-p28 (Figure 4.1 A, Table 4.1).

Peptide detection through immuno-detection of their Myc reporter was tested by dot blot. Peptides were loaded on a dot blot apparatus at different concentrations and Myc was detected by immunoblotting. Different sample preparation conditions were tested. Samples were treated with or without SDS and subjected to heat treatment or not. We were able to detect the conjugated peptide (i.e. CP05-$(GGGGS)_2$-Myc-p28) regardless of sample preparation

conditions (Figure 4.1 B). Generally, higher signal intensities were obtained when more peptide was loaded on the dot blot apparatus, as expected.

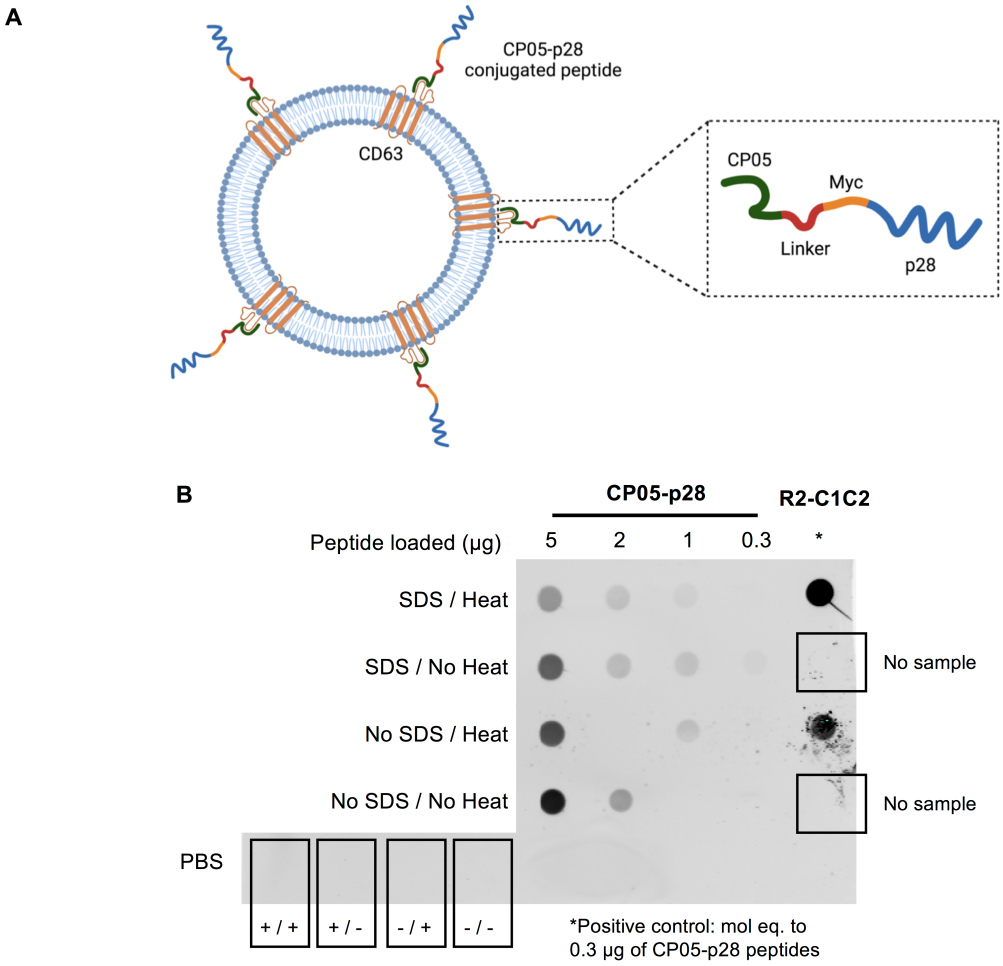

Figure 4.1 - Design of an EV anchoring CP05-p28 conjugated peptide. A) Schematic representation of the surface modification of EVs with a CP05-p28 conjugated peptide (not to scale). The final peptide design contains a peptide sequence (CP05) that anchors to CD63 present on EV surface, a $(GGGGS)_2$ linker a Myc-tag reporter and the p28 peptide (i.e. the 28 amino acid sequence Leu^{50}-Asp^{77} from the protein azurin). Figure created with BioRender.com. **B)** Detection of the previously designed CP05-p28 conjugated peptide through Myc immuno-detection in a dot blot. Different peptide quantities were loaded into the dot blot (i.e. 5, 2, 1 and 0.3 µg). Different sample preparation protocols were tested. Samples were treated with or without 2% SDS and subjected to heat treatment at 95ºC for 10 min or not. PBS was used as a negative control and subjected to the same sample preparation procedures. A previously developed fusion protein (R2-C1C2) containing the same Myc-tag was used as a positive control[292]. R2-C1C2 was loaded into the dot blot at an equivalent amount of peptide molecules as 0.3 µg CP05-p28 conjugated peptides. R2-C1C2 was kindly provided by Sander Kooijmans (UMC Utrecht, The Netherlands).

Table 4.2 - Description of the peptide sequences used to prepare the CP05-p28 conjugated peptide able to anchor to the surface of EVs. Peptides are exhibited from the N-terminal (left) to the C-terminal (right).

Name	Sequence
CP05	CRHSQMTVTSRL
p28	LSTAADMQGVVTDGMASGLDKDYLKPDD
Myc	EQKLISEEDL
Linker	$(GGGGS)_2$

4.4.2. MSC-EV decoration with the CP05-p28 conjugated peptide

The ability of the previously designed CP05-p28 conjugated peptide to anchor to the surface of MSC-EVs was then investigated. Previously isolated BM MSC-EVs (previously characterized by NTA, micro BCA and Western blot in Chapter 3) were incubated with CP05-p28. Unbound peptides were removed through several rounds of washing with PBS followed by ultrafiltration through a 100 kDa MWCO membrane and EVs were analyzed by dot blotting. EVs and peptides were incubated either for 2 h at room temperature or for 6 h at 4ºC, as previously described[300]. CP05-p28 successfully anchored to MSC-EVs (Figure 4.2 A). Indeed, both incubation protocols yielded similar peptide anchoring efficiencies. Peptide anchoring was dose-dependent, since a higher amount of anchored peptide was detected when 50 µg of the peptide was incubated with $1x10^{10}$ EVs than when 5 µg of the peptide was incubated with the same number of EVs. However, estimated peptide anchoring efficiency was lower at the higher peptide to EV incubation ratio of 50 µg peptide/$1x10^{10}$ EVs (4.0% and 3.6%, at 4ºC and at room temperature, respectively), than at 5 µg peptide/$1x10^{10}$ EVs (6.4% and 8.8%, at 4ºC and at room temperature, respectively).

Unbound peptide removal after each washing step was also determined by dot blotting. Free peptide was detected in ultrafiltration washouts, in decreasing quantities after each washing step, as expected (Figure 4.2 B). Most of the free peptide was removed in the first washing step (between 95% and 99%). The remaining free peptide was removed in the second and third washing step, while no free peptide was detected in the fourth washing step. Free peptide was detected in washouts when 50 µg peptide was used in the incubation step, but not when 5 µg peptide was used, probably because it was below the detection limit of the method used.

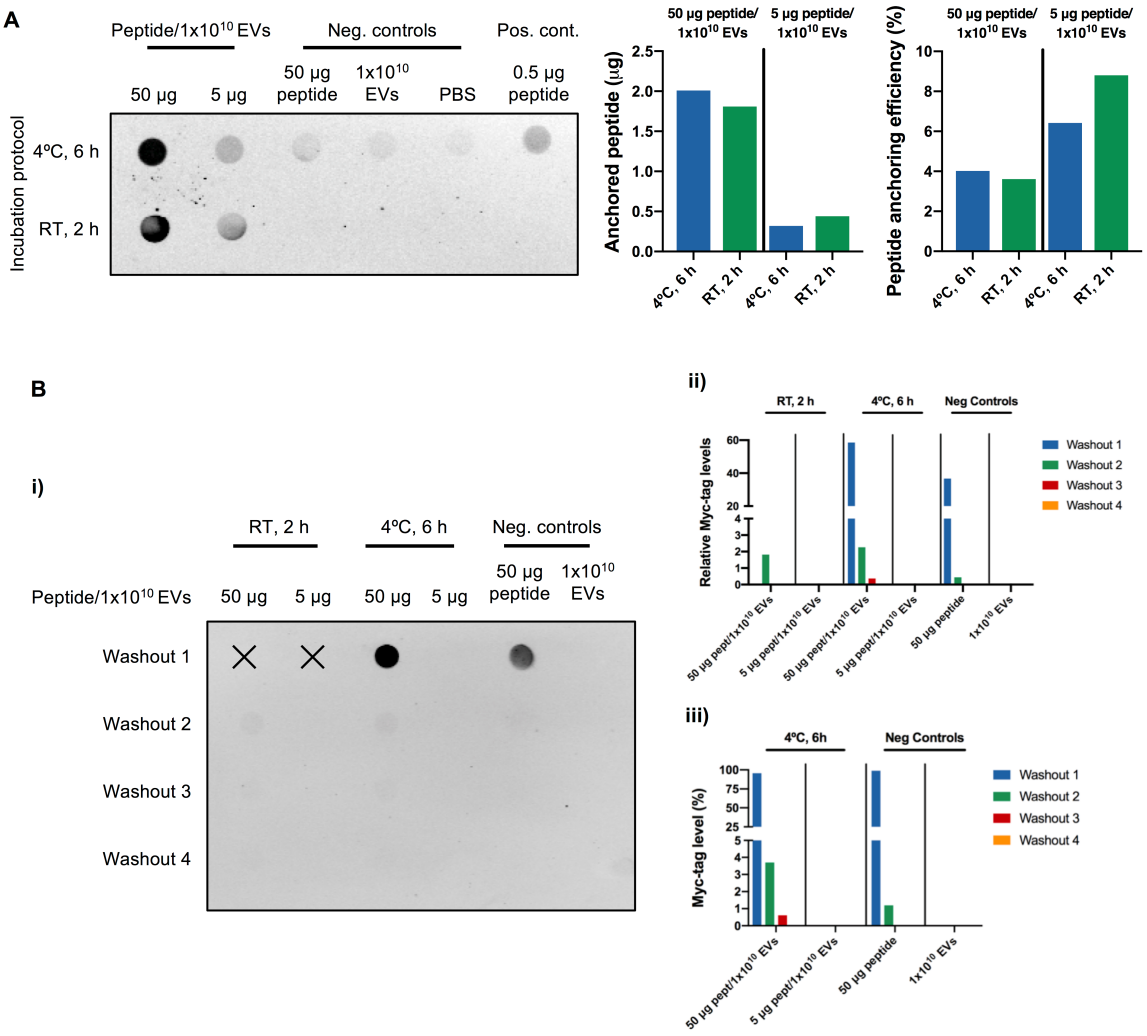

Figure 4.2 - MSC-EV decoration with CP05-p28 conjugated peptides. A) Detection of CP05-p28 conjugated peptides anchored to MSC-EVs through Myc immuno-detection in a dot blot. MSC-EVs were incubated with p28 conjugated peptides either at 4ºC for 6 h or at room temperature for 2 h. Either 50 or 5 µg peptide were incubated with $1x10^{10}$ EV particles (determined by NTA). As controls, both a 50 µg free peptide sample and $1x10^{10}$ EV particles in PBS were subjected to the same processing as the EV-peptide incubated samples. As additional controls, PBS (negative control) and 0.5 µg free peptide (positive control) were loaded directly in the dot blot. Quantifications of peptide mass anchored to EVs as well as peptide anchoring efficiency in each incubation condition estimated by extrapolation from signal intensity of positive control and PBS negative control and corrected for false signal detection in EVs. **B)** Detection of CP05-p28 conjugated peptides present in the filtrate (i.e. washouts) of ultrafiltration operations using 100 kDa MWCO Amicon centrifugal filter units to remove free-peptide from anchoring experiments. Four rounds of washing were performed. i) Peptides were detected through Myc immuno-detection in a dot blot. ii) Relative quantification of peptide detected in the washouts normalized per total Myc signal in the dot blot. iii) Relative quantification of peptide detected in the washouts normalized per condition.

The estimated average number of peptide molecules anchored to each EV ranged between 3000 and 20 000, depending on the incubation conditions (Table 4.3). In order to estimate these values, the total number of anchored peptide molecules was calculated from the estimated mass of anchored peptides, as detected in the dot blots (Figure 4.2 A), considering the molecular weight of this peptide (Table 4.1). This value was divided by the number of EVs used for incubation with peptides (i.e. $1x10^{10}$ particles for all the conditions), based on NTA measurements of EV concentration.

Table 4.3 - Estimated average number of peptide molecules anchored to each EV, depending on the incubation protocol and peptide to EV ratio used.

Incubation protocol	50 µg peptide/1x10^{10} EVs	5 µg peptide/1x10^{10} EVs
4ºC, 6 h	1.97 x 10^{4}	3.15 x 10^{3}
RT, 2 h	1.77 x 10^{4}	4.32 x 10^{3}

4.4.3. EV uptake by cancer cells increased when the CP05-p28 conjugated peptide was anchored to MSC-EVs

We studied the impact of EV surface modification with p28 on EV uptake by breast cancer cells (MDA-MB-231). For this purpose, previously isolated BM MSC-EVs were stained with a fluorescent dye (AlexaFluor 647 NHS ester), followed by free dye removal through SEC. Labeled EVs were then incubated with CP05-p28 as before. Previously cultured MDA-MB-231 cells were exposed to labelled EVs for 4 h at 37ºC. After incubation, cells were observed by fluorescence microscopy and analyzed by flow cytometry.

EV uptake was observed by virtually all cells comparing EV treated conditions with non-EV treated cells, both through fluorescence microscopy and flow cytometry (Figure 4.3). Fluorescence intensity is expected to be proportional to the number of EVs inside each cell. Thus, the median fluorescence intensity (MFI) from each condition was used as a relative measurement of EV uptake. EV uptake by MDA-MB-231 cells increased by 2.4-fold when CP05-p28 was anchored to EVs, compared with peptide-free EVs (Figure 4.3), confirming the ability of p28 to improve EV uptake by cancer cells.

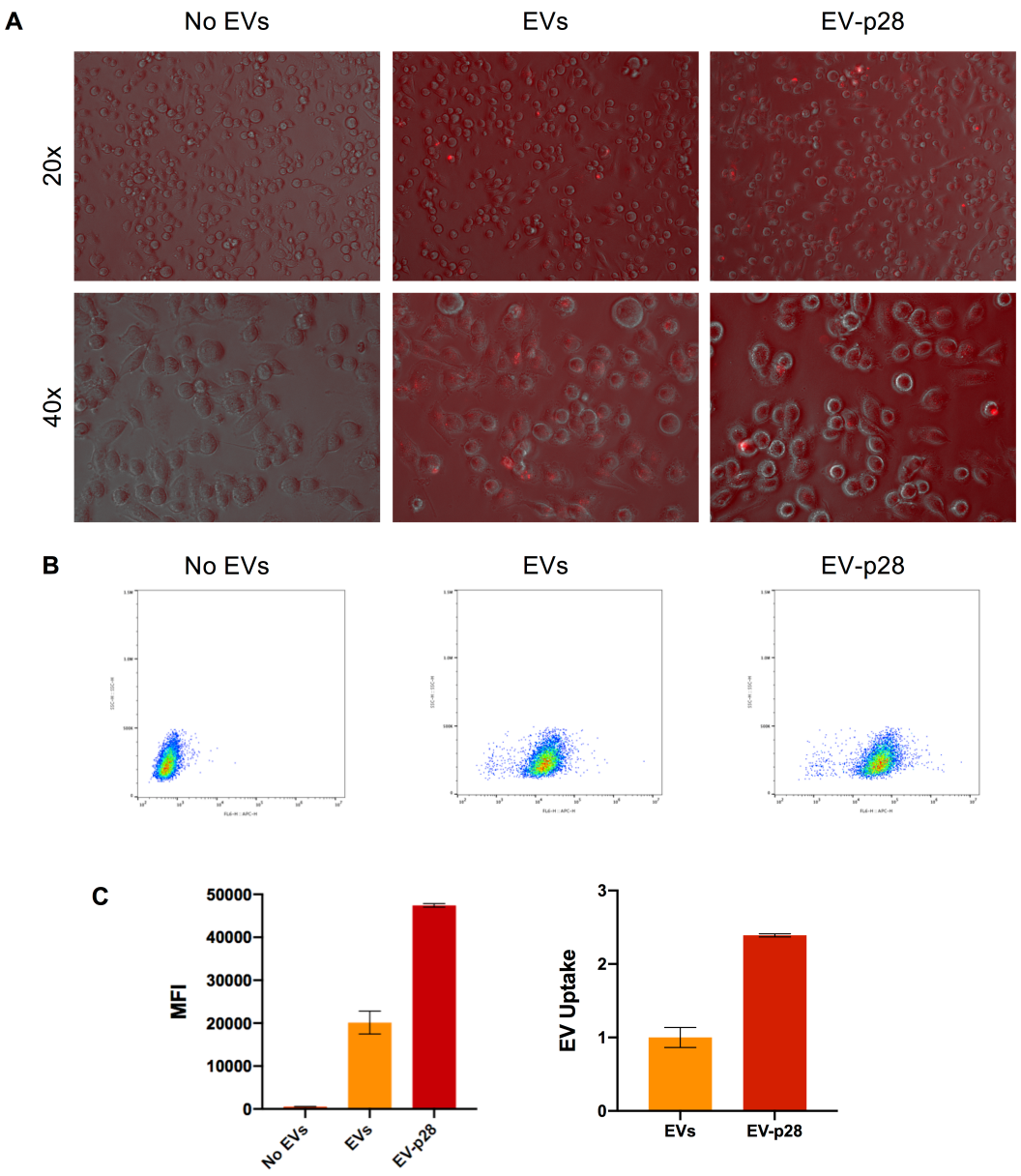

Figure 4.3 - Surface decoration of MSC-EVs with CP05-p28 conjugated peptides improved EV uptake by breast cancer cells. A) Representative images of EV uptake by MDA-MB-231 cells treated with an EV-free PBS control, naive MSC-EVs and MSC-EVs decorated with a CP05-p28 conjugated peptide (in equivalent doses). Merged bright-field and fluorescence microscopy images. AlexaFluor 647 NHS ester-labeled EVs shown in red. Pictures were taken using 20x and 40x objectives. **B)** Flow cytometry analysis of EV uptake by MDA-MB-231 cells. EV fluorescence height (x) vs. side scatter height (y) plots. **C)** Median fluorescence intensities (MFI) of flow cytometry measurements and relative EV uptake based on MFI values. Mean ± SEM (n=2 technical replicates).

4.5. Discussion

EVs have been explored as drug delivery vehicles for the treatment of numerous diseases, relying on their favorable safety profile, intrinsic targeting capacity and ability to transport therapeutic molecules and deliver them to target cells with high efficiency. In particular, a few clinical trials have already been established aiming to study their application for the treatment of different types of cancer using EVs for the delivery of curcumin (NCT01294072), chemotherapeutic agents (NCT01854866) or siRNA (NCT03608631).

In addition to their ability to pack therapeutic molecules, EVs can be engineered to enhance their targeting to specific tissues. This has been achieved either by genetic engineering of parental cells in order to express a targeting moiety fused to an EV transmembrane protein or by anchoring targeting ligands to the surface of EVs after their isolation.

Both strategies present advantages and limitations. While genetic engineering allows to create a cell line stably expressing a certain targeting moiety that will be incorporated on the surface of EVs, the number of successfully modified EVs will be limited by the efficiency of the genetic modification and the number of targeting moieties displayed on the surface of each vesicle will be limited by the availability of the chosen transmembrane protein. In addition, the generation of such cell lines is still time-consuming and particularly challenging in primary cells[405]. Direct anchoring of targeting moieties on the surface of EVs can be faster to obtain and easier to achieve in primary cells, as well as possibly allowing to display targeting moieties at a higher density. However, additional reagents will be necessary, as well as separation processes after EV modification, increasing the complexity of the manufacturing process and possibly limiting its scalability. Therefore, either strategy could be appropriate depending on the therapeutic application and on the EV-secreting cells to be used.

In this work, we sought to enhance the targeting of human MSC-EVs to cancer cells by anchoring the p28 peptide from the bacterial protein azurin to their surface. For that purpose, p28 was conjugated with CP05, a peptide previously found to bind to the EV transmembrane protein CD63[300]. Human BM MSC-EVs were produced in S/XF conditions using hPL as a culture supplement[367] and isolated using a scalable and selective EV isolation method that combines TFF with SEC[378] (as in Chapter 3), establishing this work in conditions that are more readily translatable to a clinical setting.

By employing this EV surface modification strategy, anchoring CP05-p28 conjugated peptides to EVs after they were isolated, we were able to rapidly and easily establish this proof-of-concept study, validating that EV decoration with p28 has the potential to improve EV uptake by cancer cells. However, alternative strategies might present as more useful for the development of a DDS using EVs decorated with p28. In this strategy, CP05 establishes an interaction with CD63 but does not bind covalently to the surface of EVs, which could result in some instability and possible detachment of p28 molecules from the surface of EVs. A strategy allowing to covalently bind targeting moieties to the surface of EVs was recently described, whereby protein ligating enzymes were used to bind an EGFR-targeting peptide or nanobodies targeting EGFR or HER2 to the surface of EVs in order to target cancer cells expressing these receptors[301]. Other previously developed strategies that could be considered include post-insertion of lipid-conjugated molecules into EV membranes[294,295,297] and click chemistry[293,298]. In the future, genetically engineering MSC to stably express p28 conjugated

with an EV surface protein (e.g. Lamp2b[257,287,404], PDGFR[291] or a GPI-anchoring peptide[288]) could be considered, but this is still challenging to perform in primary cells.

Engineering EVs to target cancer cells has usually relied on EV surface modifications with peptides, nanobodies or aptamers targeting receptors overexpressed in specific cancer cells (e.g. HER2[301], IL3 receptor[287], PSMA[297]) or more broadly overexpressed across different cancer types (e.g. EGFR[288,291,292,301]). Here we propose the use of a natural peptide to target cancer cells, which does not have a specific receptor mediating its uptake described yet. Although such a receptor may eventually be disclosed in the future, this peptide is able to preferentially enter a wide range of cancer cells[306], thus showing potential to be applied to target a variety of tumors.

Evidence suggests that p28 may enter both cancerous and normal cells through a receptor-mediated endocytic process including caveolin-1, the ganglioside GM-1, and the Golgi complex[306,307,313]. Considering the p28 uptake kinetics, which evidences that it preferentially accumulates in cancer cells, and that a substantial fraction of p28 penetrates the plasma membrane via caveolae, an increased presence of caveolin-specific proteins (e.g. caveolin-1) on the surface of cancer cells has been proposed to at least partially mediate this preferential entry[306]. Nevertheless, p28 is also able to enter cells through clathrin- and caveolin-independent pathways independent on membrane bound GAGs[306]. Interestingly, chemical inhibition of N-glycosylation reduced p28 penetration across cell membranes[306]. Abnormal glycosylation (including N-glycosylation) on cell surface receptors is associated with changes in cancer progression and metastasis[407–409], suggesting a role of N-glycosylated membrane receptors as a route for preferential entry of p28 into cancer cells.

Azurin and specially its peptide p28 have been proposed for the treatment of different types of cancer[312], with two phase I clinical trials already completed using p28, showing positive outcomes in adult patients with various tumors[321] and in children with tumors from the central nervous system (CNS)[322]. Here we proposed for the first time the use of p28 to decorate EVs, using it as a targeting moiety to direct EV-based DDS to tumors. The results obtained in this work revealed that EV decoration with p28 improved EV uptake by cancer cells, showing the potential of p28 to improve EV targeting to cancer cells and subsequently improve EV-mediated anti-cancer drug delivery.

We observed that CP05-p28 peptides were able to associate with MSC-EVs, in principle by anchoring to their surface. As expected, the amount of peptide anchored to EVs was higher at a higher peptide/EV ratio, since a larger number of peptide molecules was available to interact with the surface of EVs and consequently anchor to them. We also estimated a range of 3000 to 20 000 peptides anchored per EV, depending on incubation conditions. These values seem too high, since each EV surely displays a much smaller number of CD63 proteins on its membrane available for anchoring of the CP05 portion of the conjugated peptides.

Nevertheless, these are rough estimations aiming to help understanding what is happening at the nanoscale where peptide-EV interactions occur and to guide further research. In fact, NTA measurements are prone to underestimate the number of EVs, which could have led to an overestimation of this ratio.

Additionally, we do not know whether the observed peptide anchoring to EVs was mediated by p28 instead of CP05. Further work may allow to study the anchoring of CP05-p28 to MSC-EVs in more detail. Comparing the anchoring of CP05-p28 to EVs with a similar peptide but with a scrambled p28 sequence (p28Scrbl) will allow to determine if the observed anchoring occurred mainly through CP05. If CP05-p28Scrbl would be able to bind to EVs at similar levels compared with Cp05-p28, it would mean that CP05-p28 binds to EVs mainly through an interaction between CP05 and CD63 as expected, and not through p28. Additionally, incubation of Myc-tagged CP05 and p28 peptides with EVs could allow to compare the tendency of each peptide to anchor to EVs and determine if p28 could interfere in the orientation with which CP05-p28 anchors to EVs.

Further work including uptake experiments using MSC-EVs modified with p28Scrbl peptides would allow to validate if the observed improvement of EV uptake by cancer cells was due to the p28 peptide specifically and not just due to an unselective presence of peptides on the surface of EVs. If p28 is required to improve EV uptake by cancer cells, then the uptake of EVs decorated with p28 would be significantly higher than EVs decorated with p28Scrbl.

We observed an improved uptake of p28-decorated EVs by a breast cancer cell line, but p28 could improve the uptake of EVs into multiple cancer cell types. Considering the ability of p28 to preferentially enter a variety of solid tumor cells, compared to equivalent non-cancerous cells[306], further research would benefit from including different cancer cell lines and comparable normal cells. This would allow to determine the specificity of cancer targeting as well as which types of cancer would be more suitable to target using this strategy.

Further research loading p28-decorated EVs with anticancer drugs (e.g. chemotherapeutic agents or siRNA) and delivering them to cancer cells could allow to establish novel EV-based DDS. Interestingly, p28 also has the ability to trigger apoptosis on cancer cells[317,318] and enhance the cytotoxic activity of multiple chemotherapy drugs[319]. Thus, delivering chemotherapy drugs to cancer cells inside p28-decorated EVs could hypothetically boost their anticancer efficacy, due to the synergistic behavior with p28. However, this could be hard to achieve, since p28 would be bound to the outside of EV membranes and therefore may not be released to the cytoplasm and subsequently to the cell nucleus where it exerts its apoptotic effect in cancer cells (i.e. through binding with p53). Additional engineering strategies, reversibly anchoring p28 to the EV surface or even loading p28 into the lumen of EVs could be required for this purpose.

Moreover, p28 may also improve the functional delivery of therapeutic RNA molecules (e.g. siRNA or miRNA) to cancer cells via EVs. A recently established reporter system of EV-mediated functional transfer of RNA revealed that knock-down of caveolin-1 but not flotillin-1 decreased substantially reporter activation[410]. Therefore, p28 could be used to direct EV uptake through caveolin-1, improving the functional transfer of therapeutic RNA molecules into cancer cells. Considering that EVs have been recently described to deliver RNA more efficiently than state-of-the-art synthetic RNA nanocarriers[403], this strategy could considerably improve the efficacy of current RNA-based DDS for cancer therapy and potentially for other conditions.

In conclusion, aiming to develop a DDS for targeted cancer therapy, we hypothesized that decorating EVs with the cancer targeting peptide p28 from the bacterial protein azurin would improve EV uptake by cancer cells. A novel CP05-p28 conjugated peptide was designed and successfully anchored to the surface of MSC-EVs. We manufactured human BM MSC-EVs through a process closely translatable to a clinical setting by employing S/XF conditions and using a scalable and selective EV isolation method that combines TFF with SEC. Indeed, isolated MSC-EVs decorated with p28 revealed an improved EV uptake by breast cancer cells. Further studies elucidating the nature of p28 interaction with cancer cells and subsequent internalization will aid in the application of this peptide for EV-mediated drug delivery. The p28-decorated MSC-EVs obtained through the clinically relevant manufacturing conditions used in this work are promising for the development and application of novel DDS for cancer therapy with improved cancer targeting and eventually more efficient drug delivery capabilities.

5. Concluding remarks and future perspectives

5.1. Concluding remarks

EVs have been the focus of great attention over the last decade due to their promising application both as inherent therapeutics in regenerative medicine and as drug delivery vehicles. In particular, MSC represent a promising source for the production of EVs for therapeutic applications, considering the extensive track record of beneficial therapeutic properties attributed to these cells, as well as to their favorable safety profile already evidenced in numerous clinical trials. In spite of the promising potential of EVs for therapeutic applications, limited efforts have been made in establishing scalable and standardized methods for EV manufacturing.

In Chapter 2, we developed a scalable microcarrier-based bioreactor culture system for the production of MSC-EVs under S/XF conditions. We were able to produce EVs using MSC isolated from three different human tissue sources (BM, AT and UCM). This was the first time that the production of MSC-EVs from different tissue sources were compared using a scalable bioreactor system[411]. We also made a contribution to the field by applying a different bioreactor configuration, featuring easy scalability and available as single-use technology (i.e. a Vertical-Wheel™ bioreactor) for EV production. Production of MSC-EVs in bioreactors improved manufacturing yields compared to static systems and remarkably stimulated the secretion of more EVs per cell. However, the EV isolation method used (i.e. a commercial precipitation kit) presents limitations in terms of selectivity and scalability, prompting further studies using an alternative isolation procedure able to achieve both higher selectivity and scalability.

In Chapter 3, we studied and compared the functional activity of MSC-EVs obtained from two different human tissue sources (BM and UCM) in conditions closely translatable to a clinical setting. We cultured MSC in S/XF conditions and in static systems, and utilized a scalable and selective EV isolation method that combined TFF with SEC. The functional activity of MSC-EVs was studied by investigating their impact on angiogenesis *in vitro*. Both BM and UCM MSC-EVs improved sprouting of endothelial spheroids in a 3D *in vitro* model, validating their pro-angiogenic capacity, in line with previous studies[236,237,327,328,381]. This supports the use of MSC-EVs for regenerative medicine applications using clinically relevant manufacturing conditions. Subtle differences using MSC-EVs from each tissue source suggested different mechanisms involved in their pro-angiogenic activity and are worthy of further investigations.

In Chapter 4, we studied the application of MSC-EVs decorated with the p28 peptide on their surface to develop anti-cancer DDS. This peptide from the bacterial protein azurin is able to preferentially enter a variety of cancer cells and trigger apoptosis[306,317,318]. Although two clinical trials were already completed using p28 for cancer therapy with promising results[321,322], here we proposed for the first time the use of p28 to decorate EVs, using it as a targeting

moiety to direct EV-based DDS to tumors. We observed that EVs decorated with p28 after their isolation showed improved EV uptake by breast cancer cells. As in Chapter 3, MSC were cultured in static systems under S/XF conditions and EVs were isolated by SEC, revealing the possibility to use p28-decorated MSC-EVs, manufactured in conditions closely translatable to a clinical setting, for the development of novel EV-based DDS for cancer therapy.

The work developed in this thesis can be taken to the next level by combining bioreactor culture systems, such as the one used in Chapter 2, with scalable isolation methods like the one used in Chapters 3 and 4 (and keeping S/XF culture conditions used in all chapters), which would allow to establish a fully scalable EV production process (i.e. from upstream to downstream processing), essential for translation into clinical settings.

In particular, it would be relevant to study the angiogenic potential of MSC-EVs (from different MSC tissue sources) manufactured in the bioreactor culture system developed in Chapter 2. EV isolation through SEC would be advantageous for this purpose, since it would allow a scalable process, as well as a selective EV isolation, avoiding limitations presented by the use of commercial precipitation kits.

In addition to the production of EVs using scalable manufacturing systems, complementary strategies can be implemented and optimized in order to increase EV production. Cells respond to stimuli from their environment, which can affect EV secretion. Therefore, it is possible to improve the number of EVs secreted per cell by manipulating cell culture conditions. This could be achieved through manipulation of physicochemical parameters such as oxygen concentration, agitation (i.e. shear stress promoted by fluid flow), temperature, pH or altered nutrient composition. Several studies have demonstrated an increase in EV secretion when different cell types (including MSC) were cultured under low oxygen concentration (i.e. hypoxic conditions) ranging from 0.1% to 3% O_2, compared to controls [327,358,359]. Additionally, previous work from our group revealed that MSC culture in hypoxic conditions (2% O_2) promoted faster cell growth[102] and secretion of pro-angiogenic factors[400] compared with normoxia, supporting the use of hypoxic conditions for the manufacturing of MSC-EVs. Fluid flow has been described to stimulate EV secretion in osteocytes through a Ca^{2+}-mediated response[352]. In Chapter 2 we also observed an improved EV secretion by MSC in our bioreactor system, likely due to fluid flow and resulting shear stress promoted by the bioreactor agitation system[367]. More recently, mechanical stimulation of UCM MSC increased EV secretion in a rotary cell culture system at higher agitation speeds and improved the osteochondral activity of these EVs[412]. A human metastatic melanoma cell line revealed an increased exosome release and uptake at acidic pH (pH 6.0) when compared with neutral pH (pH 7.4)[413]. Exosome secretion was 3-fold higher after 3 days in acidic pH and 8-fold after 4 days. EV secretion also seems to be stimulated by thermal stress, as observed for cancer cells cultured at high temperatures (e.g. 40 - 42ºC)[414,415].

EV secretion can also be stimulated in culture through addition of chemical reagents. Agents that alter the pH of intracellular compartments (e.g. chloroquine and bafilomycin A1) enhance EV secretion by reducing acidification of MVE[416–418], which is required for degradation of internalized components in lysosomes and autophagosomes. Therefore, these agents act as inhibitors of the degradative route of MVE, shifting the balance of the endosomal pathway towards a secretory route, thereby enhancing exosome secretion. EV secretion can also be stimulated by agents that increase intracellular calcium levels such as ionophores (e.g. monensin[419–421], A23187[419] and ionomycin[365]) and inhibitors of calcium-ATPase pump (e.g. thapsigargin[419]). However, the use of these strategies must be addressed with caution since they may alter cell physiology and lead to secretion of EVs with altered composition and functional properties.

Intrinsic EV heterogeneity presents an additional challenge towards EV therapy. Different EV subpopulations, are prone to have different functional effects, depending on their biogenesis, biophysical properties, morphology, intraluminal content or surface components[422–424]. Subpopulation studies, where distinct EV subpopulations are isolated and studied separately, will be relevant to determine the exact contributors for a certain functional effect, such as the pro-angiogenic activity observed in Chapter 3. Then the most relevant subpopulation could be isolated for each therapeutic purpose. This would also allow to obtain a more reproducible and better-defined product, which is important for clinical translation.

In Chapter 3 we assessed the pro-angiogenic activity exerted by MSC-EVs, an effect that has been extensively reported in the literature using different models[236,237,327,328,381]. Considering that the ability to induce angiogenesis is one of the hallmarks of cancer[206], whereby tumor-associated vasculature is generated ensuring a steady supply of oxygen and nutrients to the tumor as it grows, this pro-angiogenic effect must be approached with caution in order to safely apply MSC-EVs as DDS for cancer. The anti-cancer activity of drugs delivered by MSC-EVs must largely outweigh their potential intrinsic pro-angiogenic properties. This could be assessed by combining studies using *in vitro* cancer and angiogenesis models, as well as using *in vivo* models where tumor-associated vasculature could be evaluated. Considering the reconfigurable nature of EVs, a way to circumvent pro-angiogenic effects of MSC-EVs and enhance their anti-cancer activity could include loading these EVs with anti-angiogenic agents (e.g. VEGF or HGF siRNA[295,425,426]) and use them in a combined manner together with additional anti-cancer drugs (e.g. anti-proliferative agents), as previously done with synthetic nanoparticles[427].

In this context, decoration of MSC-EVs with p28 offers additional opportunities regarding tumor-associated angiogenesis. Besides its preferential entry in cancer cells and cancer apoptotic effect, p28 is able to preferentially enter endothelial cells and inhibit angiogenesis within the TME[320]. Thus, p28-decorated MSC-EVs developed in Chapter 4 could also be

loaded with anti-angiogenic drugs targeting tumor-associated vasculature. This would endow p28-decorated EVs with the ability to modulate the TME by disrupting tumor-associated angiogenesis, enhancing the efficiency of these EV-based DDS. Additionally, the ability of p28 to preferentially enter endothelial cells could ultimately improve the ability of p28-decorated MSC-EVs to cross tissue barriers such as the BBB. Once these EVs reached the brain, they could be internalized by brain endothelial cells mediated by p28 and transported across the interior of these cells, crossing the BBB trough transcytosis and then reach target brain tumors to deliver therapeutic cargo.

Overall, in this thesis we demonstrated the possibility of using manufacturing strategies closely translatable to clinical settings to obtain MSC-EVs applicable both for regenerative medicine, by demonstrating their inherent pro-angiogenic capacity, as well as for drug delivery, due to the possibility to modify MSC-EVs to target specific cells and tissues in this case for cancer therapy.

5.2. Future perspectives

In spite of significant advances made in the field of EVs over the last decade, the translation of EV-based therapies into clinical settings still faces several challenges ahead (Figure 5.1). Some of these are common to the challenges faced by cell therapies[339] due to the cellular origin of EVs, while others are specific to the nature of EVs.

Establishing efficient but safe and reproducible methods for EV drug loading and to engineer EV targeting is still challenging and will certainly continue to be the focus of further research. Methods used for exogenous EV loading show low efficiencies, while genetic modification of EV secreting cells for EV modification (either for drug loading or targeting purposes) is still troublesome and difficult in primary cells. Additionally, novel strategies have been developed over the last few years aiming to modify the surface of EVs after their isolation with significant progresses, a trend expected to continue in the following years.

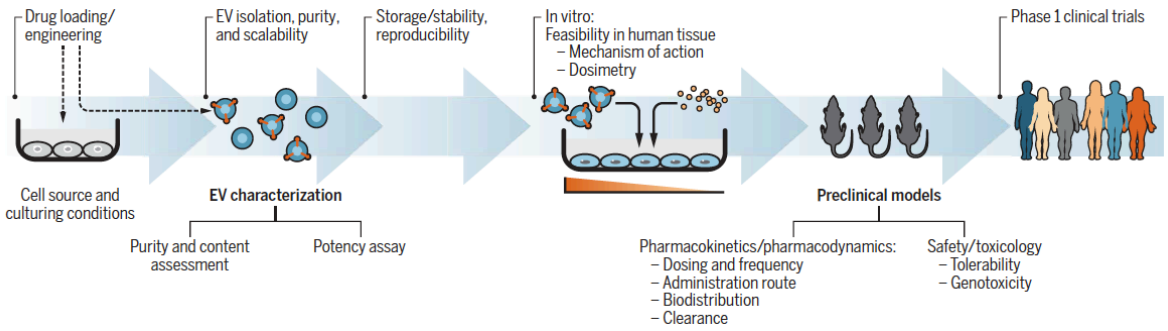

Figure 5.1 - Key factors for translation of EV-based therapeutics into clinical settings. Adapted from [240].

The selection of appropriate EV secreting cells and the tissue where the cells are originated from needs to be carefully considered since each cell type will originate EVs with different properties (e.g. proteins and RNA packaged inside them). In addition, each cell source presents different features including the availability and easiness to isolate from human tissue sources, cell expansion ability and EV secretion capacity.

Appropriate cell culture conditions need to be implemented in order to assure reproducibility and GMP compliance. Scalable processes need to be implemented for EV production in order to achieve production of high numbers of EVs required for clinical application. Bioreactors of different geometries and configurations offer several options in order to achieve this goal[411] (Figure 1.3). The use of S/XF culture conditions, will also be advantageous for clinical translation. Similarly, EV isolation processes will need to assure reproducibility, GMP compliance and scalability, whilst balancing suitable EV purity and yields. Novel strategies with promising application for scalable EV isolation include combining SEC with bind-elute chromatography, whereby smaller contaminants penetrate beads and bind to its core, allowing EVs to flow through at high recovery yields[428]. Affinity methods are also able to recover EVs at high purity and are amenable to be performed in scalable platforms (e.g. affinity chromatography[429,430]). Affinity isolation strategies could include immuno-affinity capture of EVs displaying known protein markers (e.g. tetraspanins[431]) or affinity-binding to lipids present on EVs[432–434]. In the future, EV manufacturing could even benefit from integrated production and isolation processes under continuous operation in order to improve productivity and reduce costs, similarly to other biopharmaceutical products (e.g. monoclonal antibodies)[435–438].

Envisaging their use as off-the-shelf products, appropriate storage conditions for EV products must be clearly defined and their stability must be assured. Strategies may be implemented in order to prolong stability and shelf-life of EVs, such as the addition of trehalose to EV suspensions. This natural sugar that stabilizes proteins, cell membranes and liposomes, decreases intracellular ice formation during freezing and prevents protein aggregation is widely used in food and drug industry and revealed the capacity to prevent aggregation and cryodamage of EVs[439,440].

The translation of EV products to clinical practice will require establishing standardized identity criteria and potency assays for EVs, allowing cross comparison between different laboratories, thereby supporting the development and validation of EV-based therapies and their progression to clinical testing. Motivated by this need, a consortium of researchers recently established identity criteria including quantifiable metrics for MSC-EVs[349] and also presented requirements for the development of standardized potency tests for therapeutic application of these EVs[441]. It is important to clearly define the mechanisms of action of EV-based therapeutics for clinical translation and these should be reflected in suitable potency

assays. However, fully elucidating the therapeutic mechanism of EVs is challenging since it will be multifaceted and vary between disease models.

Afterwards, appropriate preclinical models must be selected to characterize the safety and toxicology of therapeutic EVs as well as their pharmacokinetic and pharmacodynamic profiles[240]. Information from these studies will be relevant to determine proper doses for clinical studies, which will be challenging given the current heterogeneity of EV preparations and their different therapeutic potency depending on the targeted disease. Importantly, pre-clinical studies and current clinical trials indicate that EVs are generally safe and well tolerated[261,262,270,402].

To conclude, there is a long road ahead for the application of EV therapeutics in the clinical setting as the field of EVs is still at its infancy. Nevertheless, it is already clear that EVs will likely give rise to relevant new therapeutic solutions, given their unique set of characteristics compared with synthetic nanocarriers, cell therapies, chemical and biological products. We expect that the work presented in this thesis will contribute to advance the implementation of bioprocessing strategies suitable for clinical application of EV-based products to both regenerative medicine and drug delivery, with a main focus in developing novel therapeutic solutions able to improve healthcare for cancer patients.

6. References

1. Main, J. M. & Prehn, R. T. Successful Skin Homografts After the Administration of High Dosage X Radiation and Homologous Bone Marrow. *J. Natl. Cancer Inst.* **15**, 1023–1029 (1955).
2. Barnes, D. W. H., Corp, M. J., Loutit, J. F. & Neal, F. E. Treatment of Murine Leukaemia With X Rays and Homologous Bone Marrow. *Br. Med. J.* **2**, 626–627 (1956).
3. Thomas, E.-D., Lochte, H. L., Lu, W. C. & Ferreebee, J. W. Intravenous Infusion of Bone Marrow in Patients Receiving Radiation and Chemotherapy. *N. Engl. J. Med.* **257**, 491–496 (1957).
4. Caplan, A. I. Mesenchymal stem cells. *J. Orthop. Res.* **9**, 641–650 (1991).
5. Goujon, E. Recherches expérimentales sur les propriétés de la moelle des os. *J. l'anatomie la Physiol. Norm. Pathol. l'homme des animaux* **6**, 399–412 (1869).
6. Bianco, P., Robey, P. G. & Simmons, P. J. Mesenchymal Stem Cells: Revisiting History, Concepts, and Assays. *Cell Stem Cell* **2**, 313–319 (2008).
7. Tavassoli, M. & Crosby, W. H. Transplantation of Marrow to Extramedullary Sites. *Science* **161**, 54–56 (1968).
8. Friedenstein, A. J., Chailakhjan, R. K. & Lalykin, K. S. The development of fibroblast colonies in marrow and spleen cells. *Cell Tissue Kinet.* **3**, 393–403 (1970).
9. Friedenstein, A. J. Osteogenic stem cells in the bone marrow. in *Bone and Mineral Research* (eds. Heerscbe, J. N. M. & Kanis, J. A.) 243–272 (Elsevier B.V., 1990). doi:10.1016/b978-0-444-81371-8.50012-1
10. Pittenger, M. F. *et al.* Multilineage Potential of Adult Human Mesenchymal Stem Cells. *Science* **284**, 143–147 (1999).
11. Horwitz, E. M. *et al.* Clarification of the nomenclature for MSC: The International Society for Cellular Therapy position statement. *Cytotherapy* **7**, 393–395 (2005).
12. Dominici, M. *et al.* Minimal criteria for defining multipotent mesenchymal stromal cells. The International Society for Cellular Therapy position statement. *Cytotherapy* **8**, 315–317 (2006).
13. Bourin, P. *et al.* Stromal cells from the adipose tissue-derived stromal vascular fraction and culture expanded adipose tissue-derived stromal/stem cells: A joint statement of the International Federation for Adipose Therapeutics and Science (IFATS) and the International So. *Cytotherapy* **15**, 641–648 (2013).
14. Caplan, A. I. & Dennis, J. E. Mesenchymal stem cells as trophic mediators. *J. Cell. Biochem.* **98**, 1076–1084 (2006).
15. da Silva Meirelles, L., Fontes, A. M., Covas, D. T. & Caplan, A. I. Mechanisms involved in the therapeutic properties of mesenchymal stem cells. *Cytokine Growth Factor Rev.* **20**, 419–427 (2009).
16. Heathman, T. R. *et al.* The translation of cell-based therapies: Clinical landscape and

manufacturing challenges. *Regen. Med.* **10**, 49–64 (2015).

17. Cuende, N., Koh, M. B. C., Dominici, M., Rasko, J. E. J. & Ikonomou, L. Cell, tissue and gene products with marketing authorization in 2018 worldwide. *Cytotherapy* **20**, 1401–1413 (2018).
18. European Medicines Agency. Available at: https://www.ema.europa.eu/en. (Accessed: 20th March 2019)
19. United States Food and Drug Administration. Approved Cellular and Gene Therapy Products. Available at: https://www.fda.gov/BiologicsBloodVaccines/CellularGeneTherapyProducts/ApprovedProducts/default.htm. (Accessed: 20th March 2019)
20. Kirouac, D. C. & Zandstra, P. W. The Systematic Production of Cells for Cell Therapies. *Cell Stem Cell* **3**, 369–381 (2008).
21. Blasimme, A. & Rial-Sebbag, E. Regulation of cell-based therapies in Europe: Current challenges and emerging issues. *Stem Cells Dev.* **22**, 14–19 (2013).
22. Dodson, B. P. & Levine, A. D. Challenges in the translation and commercialization of cell therapies. *BMC Biotechnol.* **15**, 1–15 (2015).
23. Chabannon, C. *et al.* Hematopoietic Stem Cell Transplantation in its 60s - A Platform for Cellular Therapies. *Sci. Transl. Med.* **10**, 1–10 (2018).
24. Ährlund-Richter, L. *et al.* Isolation and Production of Cells Suitable for Human Therapy: Challenges Ahead. *Cell Stem Cell* **4**, 20–26 (2009).
25. Lipsitz, Y. Y. *et al.* A roadmap for cost-of-goods planning to guide economic production of cell therapy products. *Cytotherapy* **19**, 1383–1391 (2017).
26. Morrison, S. J. & Scadden, D. T. The bone marrow niche for haematopoietic stem cells. *Nature* **505**, 327–334 (2014).
27. Mueller, S. M. & Glowacki, J. Age-related decline in the osteogenic potential of human bone marrow cells cultured in three-dimensional collagen sponges. *J. Cell. Biochem.* **82**, 583–90 (2001).
28. Kern, S., Eichler, H., Stoeve, J., Klüter, H. & Bieback, K. Comparative Analysis of Mesenchymal Stem Cells from Bone Marrow, Umbilical Cord Blood, or Adipose Tissue. *Stem Cells* **24**, 1294–1301 (2006).
29. Oedayrajsingh-Varma, M. J. *et al.* Adipose tissue-derived mesenchymal stem cell yield and growth characteristics are affected by the tissue-harvesting procedure. *Cytotherapy* **8**, 166–177 (2006).
30. Rubinstein, P. *et al.* Processing and cryopreservation of placental/umbilical cord blood for unrelated bone marrow reconstitution. *Proc. Natl. Acad. Sci. U. S. A.* **92**, 10119–10122 (1995).
31. Wyrsch, A. *et al.* Umbilical cord blood from preterm human fetuses is rich in committed

and primitive hematopoietic progenitors with high proliferative and self-renewal capacity. *Exp. Hematol.* **27**, 1338–1345 (1999).

32. Prindull, G. *et al.* CFU-F circulating in cord blood. *Blut* **54**, 351–359 (1987).
33. Mennan, C. *et al.* Mesenchymal stromal cells derived from whole human umbilical cord exhibit similar properties to those derived from Wharton's jelly and bone marrow. *FEBS Open Bio* **6**, 1054–1066 (2016).
34. Troyer, D. L. & Weiss, M. L. Concise Review: Wharton's Jelly-Derived Cells Are a Primitive Stromal Cell Population. *Stem Cells* **26**, 591–599 (2008).
35. Goodwin, H. S. *et al.* Multilineage differentiation activity by cells isolated from umbilical cord blood: expression of bone, fat, and neural markers. *Biol. Blood Marrow Transplant.* **7**, 581–8 (2001).
36. De Bari, C., Dell'Accio, F., Tylzanowski, P. & Luyten, F. P. Multipotent mesenchymal stem cells from adult human synovial membrane. *Arthritis Rheum.* **44**, 1928–1942 (2001).
37. Fukuchi, Y. *et al.* Human Placenta-Derived Cells Have Mesenchymal Stem/Progenitor Cell Potential. *Stem Cells* **22**, 649–658 (2004).
38. Karaöz, E. *et al.* Isolation and in vitro characterisation of dental pulp stem cells from natal teeth. *Histochem. Cell Biol.* **133**, 95–112 (2010).
39. da Silva Meirelles, L., Chagastelles, P. C. & Nardi, N. B. Mesenchymal stem cells reside in virtually all post-natal organs and tissues. *J. Cell Sci.* **119**, 2204–2213 (2006).
40. Ribeiro, A. *et al.* Mesenchymal stem cells from umbilical cord matrix, adipose tissue and bone marrow exhibit different capability to suppress peripheral blood B, natural killer and T cells. *Stem Cell Res. Ther.* **4**, 125 (2013).
41. Vormittag, P., Gunn, R., Ghorashian, S. & Veraitch, F. S. A guide to manufacturing CAR T cell therapies. *Curr. Opin. Biotechnol.* **53**, 164–181 (2018).
42. Lennon, D. P. & Caplan, A. I. Isolation of rat marrow-derived mesenchymal stem cells. *Exp. Hematol.* **34**, 1606–1607 (2006).
43. Lu, L. L. *et al.* Isolation and characterization of human umbilical cord mesenchymal stem cells with hematopoiesis-supportive function and other potentials. *Haematologica* **91**, 1017–1026 (2006).
44. Nimura, A. *et al.* Increased proliferation of human synovial mesenchymal stem cells with autologous human serum: Comparisons with bone marrow mesenchymal stem cells and with fetal bovine serum. *Arthritis Rheum.* **58**, 501–510 (2008).
45. De Bruyn, C. *et al.* A Rapid, Simple, and Reproducible Method for the Isolation of Mesenchymal Stromal Cells from Wharton's Jelly Without Enzymatic Treatment. *Stem Cells Dev.* **20**, 547–557 (2010).
46. Ghorbani, A., Jalali, S. A. & Varedi, M. Isolation of adipose tissue mesenchymal stem

cells without tissue destruction: A non-enzymatic method. *Tissue Cell* **46**, 54–58 (2014).

47. Zhang, S., Muneta, T., Morito, T., Mochizuki, T. & Sekiya, I. Autologous synovial fluid enhances migration of mesenchymal stem cells from synovium of osteoarthritis patients in tissue culture system. *J. Orthop. Res.* **26**, 1413–1418 (2008).
48. Aktas, M., Radke, T. F., Strauer, B. E., Wernet, P. & Kogler, G. Separation of adult bone marrow mononuclear cells using the automated closed separation system Sepax. *Cytotherapy* **10**, 203–211 (2008).
49. Eyrich, M. *et al.* Development and validation of a fully GMP-compliant production process of autologous, tumor-lysate-pulsed dendritic cells. *Cytotherapy* **16**, 946–964 (2014).
50. Stroncek, D. F. *et al.* Counter-flow elutriation of clinical peripheral blood mononuclear cell concentrates for the production of dendritic and T cell therapies. *J. Transl. Med.* **12**, 241 (2014).
51. Kato, K. & Radbruch, A. Isolation and characterization of CD34+ hematopoietic stem cells from human peripheral blood by high-gradient magnetic cell sorting. *Cytometry* **14**, 384–392 (1993).
52. De Wynter, E. A. *et al.* Comparison of purity and enrichment of CD34+ cells from bone marrow, umbilical cord and peripheral blood (primed for apheresis) using five separation systems. *Stem Cells* **13**, 524–532 (1995).
53. Simmons, P. J. & Torok-Storb, B. Identification of stromal cell precursors in human bone marrow by a novel monoclonal antibody, STRO-1. *Blood* **78**, 55–62 (1991).
54. Gonçalves, R., Lobato da Silva, C., Cabral, J. M. S., Zanjani, E. D. & Almeida-Porada, G. A Stro-1+ human universal stromal feeder layer to expand/maintain human bone marrow hematopoietic stem/progenitor cells in a serum-free culture system. *Exp. Hematol.* **34**, 1353–1359 (2006).
55. Leong, W., Nankervis, B. & Beltzer, J. Automation: what will the cell therapy laboratory of the future look like? *Cell Gene Ther. Insights* **4**, 679–694 (2019).
56. Sutermaster, B. A. & Darling, E. M. Considerations for high-yield, high-throughput cell enrichment: fluorescence versus magnetic sorting. *Sci. Rep.* **9**, 1–9 (2019).
57. Koehl, U. *et al.* IL-2 activated NK cell immunotherapy of three children after haploidentical stem cell transplantation. *Blood Cells, Mol. Dis.* **33**, 261–266 (2004).
58. Neurauter, A. A. *et al.* Cell isolation and expansion using dynabeads. in *Advances in Biochemical Engineering/Biotechnology* **106**, 41–73 (2007).
59. Dai, X., Mei, Y., Nie, J. & Bai, Z. Scaling up the Manufacturing Process of Adoptive T Cell Immunotherapy. *Biotechnol. J.* **14**, 1800239 (2019).
60. McNaughton, B. H., Younger, J. G. & Ostruszka, L. J. Method and System for Buoyant Separation. US 10,195,547 B2. (2019).

61. Liou, Y.-R., Wang, Y.-H., Lee, C.-Y. & Li, P.-C. Buoyancy-Activated Cell Sorting Using Targeted Biotinylated Albumin Microbubbles. *PLoS One* **10**, e0125036 (2015).
62. Aijaz, A. *et al.* Biomanufacturing for clinically advanced cell therapies. *Nat. Biomed. Eng.* **2**, 362–376 (2018).
63. Burgener, A. & Butler, M. Medium Development. in *Cell Culture Technology for Pharmaceutical and Cell-Based Therapies* (eds. Ozturck, S. S. & Hu, W. S.) 41–64 (CRC Press, 2005).
64. Yao, T. & Asayama, Y. Animal-cell culture media: History, characteristics, and current issues. *Reprod. Med. Biol.* **16**, 99–117 (2017).
65. Brunner, D., Appl, H., Pfaller, W. & Gstraunthaler, G. Serum-free cell culture: the serum-free media interactive online database. *ALTEX* **27**, 53–62 (2010).
66. Spees, J. L. *et al.* Internalized antigens must be removed to prepare hypoimmunogenic mesenchymal stem cells for cell and gene therapy. *Mol. Ther.* **9**, 747–756 (2004).
67. European Medicines Agency. *Guideline on human cell-based medicinal products (EMEA/CHMP/410869/ 2006)*. *Official Journal of the European Union* (2007).
68. European Medicines Agency. *Note for guidance on minimising the risk of transmitting animal spongiform encephalopathy agents via human and veterinary medicinal products (EMA/410/01 rev.3)*. *Official Journal of the European Union* (2011).
69. US Food and Drug Administration. *Medical Devices Containing Materials Derived from Animal Sources (Except for In Vitro Diagnostic Devices)*. (2019).
70. Karnieli, O. *et al.* A consensus introduction to serum replacements and serum-free media for cellular therapies. *Cytotherapy* **19**, 155–169 (2017).
71. Hara, Y., Steiner, M. & Baldini, M. G. Platelets as a Source of Growth-Dromotina Factor(s) for Tumor Cells. *Cancer Res.* **40**, 1212–1216 (1980).
72. Umeno, Y., Okuda, A. & Kimura, G. Proliferative behaviour of fibroblasts in plasma-rich culture medium. *J. Cell Sci.* **94**, 567–575 (1989).
73. Burnouf, T., Strunk, D., Koh, M. B. C. & Schallmoser, K. Human platelet lysate: Replacing fetal bovine serum as a gold standard for human cell propagation? *Biomaterials* **76**, 371–387 (2016).
74. van der Valk, J. *et al.* Fetal Bovine Serum (FBS): Past - Present - Future. *ALTEX* **35**, 99–118 (2018).
75. Doucet, C. *et al.* Platelet lysates promote mesenchymal stem cell expansion: A safety substitute for animal serum in cell-based therapy applications. *J. Cell. Physiol.* **205**, 228–236 (2005).
76. Reinisch, A. *et al.* Epigenetic and in vivo comparison of diverse MSC sources reveals an endochondral signature for human hematopoietic niche formation. *Blood* **125**, 249–260 (2015).

77. Kinzebach, S., Dietz, L., Klüter, H., Thierse, H. J. & Bieback, K. Functional and differential proteomic analyses to identify platelet derived factors affecting ex vivo expansion of mesenchymal stromal cells. *BMC Cell Biol.* **14**, 48 (2013).
78. de Soure, A. M. *et al.* Integrated culture platform based on a human platelet lysate supplement for the isolation and scalable manufacturing of umbilical cord matrix-derived mesenchymal stem/stromal cells. *J. Tissue Eng. Regen. Med.* **11**, 1630–1640 (2017).
79. de Sousa Pinto, D. *et al.* Scalable Manufacturing of Human Mesenchymal Stromal Cells in the Vertical-Wheel Bioreactor System: An Experimental and Economic Approach. *Biotechnol. J.* **14**, 1800716 (2019).
80. Schallmoser, K. *et al.* Human platelet lysate can replace fetal bovine serum for clinical-scale expansion of functional mesenchymal stromal cells. *Transfusion* **47**, 1436–1446 (2007).
81. Atashi, F., Jaconi, M. E. E., Pittet-Cuénod, B. & Modarressi, A. Autologous Platelet-Rich Plasma: A Biological Supplement to Enhance Adipose-Derived Mesenchymal Stem Cell Expansion. *Tissue Eng. Part C Methods* **21**, 253–262 (2014).
82. Naveau, A. *et al.* Phenotypic Study of Human Gingival Fibroblasts in a Medium Enriched With Platelet Lysate. *J. Periodontol.* **82**, 632–641 (2010).
83. Hildner, F. *et al.* Human platelet lysate successfully promotes proliferation and subsequent chondrogenic differentiation of adipose-derived stem cells: a comparison with articular chondrocytes. *J. Tissue Eng. Regen. Med.* **9**, 808–818 (2015).
84. Mazzocca, A. D. *et al.* The positive effects of different platelet-rich plasma methods on human muscle, bone, and tendon cells. *Am. J. Sports Med.* **40**, 1742–1749 (2012).
85. Hofbauer, P. *et al.* Human platelet lysate is a feasible candidate to replace fetal calf serum as medium supplement for blood vascular and lymphatic endothelial cells. *Cytotherapy* **16**, 1238–1244 (2014).
86. Hemeda, H., Giebel, B. & Wagner, W. Evaluation of human platelet lysate versus fetal bovine serum for culture of mesenchymal stromal cells. *Cytotherapy* **16**, 170–180 (2014).
87. Huang, C. *et al.* Gamma irradiation of human platelet lysate: validation of efficacy for pathogen reduction and assessment of impacts on hpl performance. *Cytotherapy* **21**, S82–S83 (2019).
88. Simões, I. N. *et al.* Human mesenchymal stem cells from the umbilical cord matrix: Successful isolation and ex vivo expansion using serum-/xeno-free culture media. *Biotechnol. J.* **8**, 448–58 (2013).
89. Carmelo, J. G., Fernandes-Platzgummer, A., Diogo, M. M., da Silva, C. L. & Cabral, J. M. S. A xeno-free microcarrier-based stirred culture system for the scalable expansion

of human mesenchymal stem/stromal cells isolated from bone marrow and adipose tissue. *Biotechnol. J.* **10**, 1235–1247 (2015).

90. Al-Saqi, S. H. *et al.* Defined serum-free media for in vitro expansion of adipose-derived mesenchymal stem cells. *Cytotherapy* **16**, 915–926 (2014).
91. Chen, G. *et al.* Human umbilical cord-derived mesenchymal stem cells do not undergo malignant transformation during long-term culturing in serum-free medium. *PLoS One* **9**, 1–8 (2014).
92. Wang, Y. *et al.* Human mesenchymal stem cells possess different biological characteristics but do not change their therapeutic potential when cultured in serum free medium. *Stem Cell Res. Ther.* **5**, 1–14 (2014).
93. Smith, C. *et al.* Ex vivo expansion of human T cells for adoptive immunotherapy using the novel Xeno-free CTS Immune Cell Serum Replacement. *Clin. Transl. Immunol.* **4**, e31 (2015).
94. Lu, T. L. *et al.* A Rapid Cell Expansion Process for Production of Engineered Autologous CAR-T Cell Therapies. *Hum. Gene Ther. Methods* **27**, 209–218 (2016).
95. Fliefel, R. *et al.* Mesenchymal stem cell proliferation and mineralization but not osteogenic differentiation are strongly affected by extracellular pH. *J. Cranio-Maxillofacial Surg.* **44**, 715–724 (2016).
96. Stolzing, A. & Scutt, A. Effect of reduced culture temperature on antioxidant defences of mesenchymal stem cells. *Free Radic. Biol. Med.* **41**, 326–338 (2006).
97. Waymouth, C. Osmolality of Mammalian Blood and of Media for Culture of Mammalian Cells. *In Vitro* **6**, 109–110 (1970).
98. Mather, J. P. & Roberts, P. E. *Introduction to Cell and Tissue Culture: Theory and Technique*. (Plenun Press, New York, 1998).
99. Eliasson, P. & Jönsson, J. I. The hematopoietic stem cell niche: Low in oxygen but a nice place to be. *J. Cell. Physiol.* **222**, 17–22 (2010).
100. Spencer, J. A. *et al.* Direct measurement of local oxygen concentration in the bone marrow of live animals. *Nature* **508**, 269–273 (2014).
101. Valorani, M. G. *et al.* Pre-culturing human adipose tissue mesenchymal stem cells under hypoxia increases their adipogenic and osteogenic differentiation potentials. *Cell Prolif.* **45**, 225–238 (2012).
102. Dos Santos, F. *et al.* Ex vivo expansion of human mesenchymal stem cells: A more effective cell proliferation kinetics and metabolism under hypoxia. *J. Cell. Physiol.* **223**, 27–35 (2010).
103. Lee, H. H. *et al.* Hypoxia enhances chondrogenesis and prevents terminal differentiation through PI3K/Akt/FoxO dependent anti-apoptotic effect. *Sci. Rep.* **3**, 1–12 (2013).

104. Oliveira, P. H. *et al.* Impact of hypoxia and long-term cultivation on the genomic stability and mitochondrial performance of ex vivo expanded human stem/stromal cells. *Stem Cell Res.* **9**, 225–236 (2012).
105. Guruvenket, S., Rao, G. M., Komath, M. & Raichur, A. M. Plasma surface modification of polystyrene and polyethylene. *Appl. Surf. Sci.* **236**, 278–284 (2004).
106. Jung, S., Sen, A., Rosenberg, L. & Behie, L. A. Identification of growth and attachment factors for the serum-free isolation and expansion of human mesenchymal stromal cells. *Cytotherapy* **12**, 637–657 (2010).
107. Bryhan, M. D., Gagnon, P. E., LaChance, O. V., Shen, Z.-H. & Wang, H. Method for creating a cell growth surface on a polymeric substrate. US6617152B2. (2003).
108. Swistowski, A. *et al.* Xeno-free defined conditions for culture of human embryonic stem cells, neural stem cells and dopaminergic neurons derived from them. *PLoS One* **4**, (2009).
109. de Lima, M. *et al.* Cord-Blood Engraftment with Ex Vivo Mesenchymal-Cell Coculture. *N. Engl. J. Med.* **367**, 2305–2315 (2012).
110. Lee, D. W. *et al.* T cells expressing CD19 chimeric antigen receptors for acute lymphoblastic leukaemia in children and young adults: A phase 1 dose-escalation trial. *Lancet* **385**, 517–528 (2015).
111. Saint-Jean, M. *et al.* Adoptive Cell Therapy with Tumor-Infiltrating Lymphocytes in Advanced Melanoma Patients. *J. Immunol. Res.* **2018**, (2018).
112. Pardo, A. M. P. & Rothenberg, M. E. *Large Scale Expansion of Human Mesenchymal Stem Cells using Corning ® stemgro ® hMSC Medium and Corning CellBIND ® Surface HYPER Stack ® Cell Culture Vessels*. (2013).
113. Blasey, H. D., Isch, C. & Bernard, A. R. Cellcube: A new system for large scale growth of adherent cells. *Biotechnol. Tech.* **9**, 725–728 (1995).
114. Lambrechts, T. *et al.* Evaluation of a monitored multiplate bioreactor for large-scale expansion of human periosteum derived stem cells for bone tissue engineering applications. *Biochem. Eng. J.* **108**, 58–68 (2016).
115. Wikström, K., Blomberg, P. & Islam, K. B. Clinical grade vector production: Analysis of yield, stability, and storage of GMP-produced retroviral vectors for gene therapy. *Biotechnol. Prog.* **20**, 1198–1203 (2004).
116. Wang, H., Kehoe, D., Murrell, J. & Jing, D. Structured Methodology for Process Development in Scalable Stirred Tank Bioreactors Platforms. in *Bioprocessing for Cell-based Therapies* (ed. Connon, C. J.) 35–64 (John Wiley & Sons Ltd., 2017).
117. Bayley, R. *et al.* The productivity limit of manufacturing blood cell therapy in scalable stirred bioreactors. *J. Tissue Eng. Regen. Med.* **12**, e368–e378 (2018).
118. Martin, Y., Eldardiri, M., Lawrence-Watt, D. J. & Sharpe, J. R. Microcarriers and Their

Potential in Tissue Regeneration. *Tissue Eng. Part B Rev.* **17**, 71–80 (2010).

119. Chen, A. K. L., Reuveny, S. & Oh, S. K. W. Application of human mesenchymal and pluripotent stem cell microcarrier cultures in cellular therapy: Achievements and future direction. *Biotechnol. Adv.* **31**, 1032–1046 (2013).
120. dos Santos, F. *et al.* A Xenogeneic-Free Bioreactor System for the Clinical-Scale Expansion of Human Mesenchymal Stem / Stromal Cells. *Biotechnol. Bioeng.* **116**, 1116–1127 (2014).
121. Mizukami, A. *et al.* Stirred tank bioreactor culture combined with serum- / xenogeneic-free culture medium enables an efficient expansion of umbilical cord-derived mesenchymal stem / stromal cells. *Biotechnol. J.* **11**, 1048–1059 (2016).
122. Rafiq, Q. A., Brosnan, K. M., Coopman, K., Nienow, A. W. & Hewitt, C. J. Culture of human mesenchymal stem cells on microcarriers in a 5 l stirred-tank bioreactor. *Biotechnol. Lett.* **35**, 1233–1245 (2013).
123. Lawson, T. *et al.* Process development for expansion of human mesenchymal stromal cells in a 50L single-use stirred tank bioreactor. *Biochem. Eng. J.* **120**, 49–62 (2017).
124. Schirmaier, C. *et al.* Scale-up of adipose tissue-derived mesenchymal stem cell production in stirred single-use bioreactors under low-serum conditions. *Eng. Life Sci.* **14**, 292–303 (2014).
125. Robb, K. P., Fitzgerald, J. C., Barry, F. & Viswanathan, S. Mesenchymal stromal cell therapy: progress in manufacturing and assessments of potency. *Cytotherapy* **21**, 289–306 (2019).
126. Tsai, A. C., Liu, Y. & Ma, T. Expansion of human mesenchymal stem cells in fibrous bed bioreactor. *Biochem. Eng. J.* **108**, 51–57 (2016).
127. Haack-Sørensen, M. *et al.* Culture expansion of adipose derived stromal cells. A closed automated Quantum Cell Expansion System compared with manual flask-based culture. *J. Transl. Med.* **14**, 319 (2016).
128. Mizukami, A. *et al.* A Fully-Closed and Automated Hollow Fiber Bioreactor for Clinical-Grade Manufacturing of Human Mesenchymal Stem / Stromal Cells. *Stem Cell Rev. Reports* **14**, 141–143 (2018).
129. Tirughana, R. *et al.* GMP Production and Scale-Up of Adherent Neural Stem Cells with a Quantum Cell Expansion System. *Mol. Ther. Methods Clin. Dev.* **10**, 48–56 (2018).
130. Lechanteur, C. *et al.* Large-Scale Clinical Expansion of Mesenchymal Stem Cells in the GMP-Compliant, Closed Automated Quantum® Cell Expansion System: Comparison with Expansion in Traditional T-Flasks. *J. Stem Cell Res. Ther.* **4**, 1000222 (2014).
131. Lambrechts, T. *et al.* Large-scale progenitor cell expansion for multiple donors in a monitored hollow fibre bioreactor. *Cytotherapy* **18**, 1219–1233 (2016).
132. Junne, S. & Neubauer, P. How scalable and suitable are single-use bioreactors? *Curr.*

Opin. Biotechnol. **53**, 240–247 (2018).

133. Doran, P. M. *Bioprocess Engineering Principles*. (Academic Press, 2013).
134. Schürch, U., Kramer, H., Einsele, A., Widmer, F. & Eppenberger, H. M. Experimental evaluation of laminar shear stress on the behaviour of hybridoma mass cell cultures, producing monoclonal antibodies against mitochondrial creatine kinase. *J. Biotechnol.* **7**, 179–184 (1988).
135. McQueen, A. & Bailey, J. E. Influence of serum level, cell line, flow type and viscosity on flow-induced lysis of suspended mammalian cells. *Biotechnol. Lett.* **11**, 531–536 (1989).
136. Chisti, Y. Hydrodynamic damage to animal cells. *Crit. Rev. Biotechnol.* **21**, 67–110 (2001).
137. Yourek, G., McCormick, S. M., Mao, J. J. & Reilly, G. C. Shear stress induces osteogenic differentiation of human mesenchymal stem cells. *Regen. Med.* **5**, 713–724 (2010).
138. Hu, K., Sun, H., Gui, B. & Sui, C. TRPV4 functions in flow shear stress induced early osteogenic differentiation of human bone marrow mesenchymal stem cells. *Biomed. Pharmacother.* **91**, 841–848 (2017).
139. Bassaneze, V. *et al.* Shear Stress Induces Nitric Oxide–Mediated Vascular Endothelial Growth Factor Production in Human Adipose Tissue Mesenchymal Stem Cells. *Stem Cells Dev.* **19**, 371–378 (2009).
140. Öncul, A. A., Kalmbach, A., Genzel, Y., Reichl, U. & Thévenin, D. Characterization of flow conditions in 2 L and 20 L wave bioreactors® usingcomputational fluid dynamics. *Biotechnol. Prog.* **26**, 101–110 (2010).
141. Timmins, N. E. *et al.* Clinical scale ex vivo manufacture of neutrophils from hematopoietic progenitor cells. *Biotechnol. Bioeng.* **104**, 832–840 (2009).
142. Sutlu, T. *et al.* Clinical-grade, large-scale, feeder-free expansion of highly active human natural killer cells for adoptive immunotherapy using an automated bioreactor. *Cytotherapy* **12**, 1044–1055 (2010).
143. Croughan, M. S., Giroux, D., Fang, D. & Lee, B. Novel Single-Use Bioreactors for Scale-Up of Anchorage-Dependent Cell Manufacturing for Cell Therapies. in *Stem Cell Manufacturing* (eds. Cabral, J. M. S., da Silva, C. L., Chase, L. G. & Diogo, M. M.) 105–139 (Elsevier, 2016). doi:10.1016/B978-0-444-63265-4.00005-4
144. Sousa, M. F. Q. *et al.* Production of oncolytic adenovirus and human mesenchymal stem cells in a single-use, Vertical-Wheel bioreactor system: Impact of bioreactor design on performance of microcarrier-based cell culture processes. *Biotechnol. Prog.* **31**, 1600–1612 (2015).
145. Rodrigues, C. A. V. *et al.* Scalable culture of human induced pluripotent cells on

microcarriers under xeno-free conditions using single-use vertical-wheel™ bioreactors. *J. Chem. Technol. Biotechnol.* **93**, 3597–3606 (2018).

146. György, B. *et al.* Membrane vesicles, current state-of-the-art: Emerging role of extracellular vesicles. *Cell. Mol. Life Sci.* **68**, 2667–2688 (2011).
147. Chargaff, E. & West, R. The biological significance of the thromboplastic protein of blood. *J. Biol. Chem.* **166**, 189–197 (1946).
148. Wolf, P. The nature and significance of platelet products in human plasma. *Br. J. Haematol.* **13**, 269–288 (1967).
149. Anderson, H. C. Vesicles associated with calcification in the matrix of epiphyseal cartilage. *J. Cell Biol.* **41**, 59–72 (1969).
150. Pan, B. T. & Johnstone, R. M. Fate of the transferrin receptor during maturation of sheep reticulocytes in vitro: Selective externalization of the receptor. *Cell* **33**, 967–978 (1983).
151. Harding, C., Heuser, J. & Stahl, P. Receptor-mediated Endocytosis of Transferrin and of the Transferrin Receptor in Rat Reticulocytes Recycling. *J. Cell. Biol.* **97**, 329–339 (1983).
152. Johnstone, R. M., Adam, M., Hammond, J. R., Orr, L. & Turbide, C. Vesicle formation during reticulocyte maturation. Association of plasma membrane activities with released vesicles (exosomes). *J. Biol. Chem.* **262**, 9412–9420 (1987).
153. Raposo, G. *et al.* B Lymphocytes Secrete Antigen-presenting Vesicles. *J. Exp. Med.* **183**, 1161–1172 (1996).
154. Ratajczak, J. *et al.* Embryonic stem cell-derived microvesicles reprogram hematopoietic progenitors: Evidence for horizontal transfer of mRNA and protein delivery. *Leukemia* **20**, 847–856 (2006).
155. Valadi, H. *et al.* Exosome-mediated transfer of mRNAs and microRNAs is a novel mechanism of genetic exchange between cells. *Nat. Cell Biol.* **9**, 654–659 (2007).
156. Van Niel, G., D'Angelo, G. & Raposo, G. Shedding light on the cell biology of extracellular vesicles. *Nat. Rev. Mol. Cell Biol.* **19**, 213–228 (2018).
157. Mathivanan, S., Ji, H. & Simpson, R. J. Exosomes: Extracellular organelles important in intercellular communication. *J. Proteomics* **73**, 1907–1920 (2010).
158. Mathieu, M., Martin-Jaular, L., Lavieu, G. & Théry, C. Specificities of secretion and uptake of exosomes and other extracellular vesicles for cell-to-cell communication. *Nat. Cell Biol.* **21**, 9–17 (2019).
159. D'Acunzo, P. *et al.* Mitovesicles are a novel population of extracellular vesicles of mitochondrial origin altered in Down syndrome. *Sci. Adv.* **7**, eabe5085 (2021).
160. Karimi, N. *et al.* Detailed analysis of the plasma extracellular vesicle proteome after separation from lipoproteins. *Cell. Mol. Life Sci.* **75**, 2873–2886 (2018).

161. Zhang, H. *et al.* Identification of distinct nanoparticles and subsets of extracellular vesicles by asymmetric flow field-flow fractionation. *Nat. Cell Biol.* **20**, 332–343 (2018).
162. Baietti, M. F. *et al.* Syndecan-syntenin-ALIX regulates the biogenesis of exosomes. *Nat. Cell Biol.* **14**, 677–685 (2012).
163. Trajkovic, K. *et al.* Ceramide Triggers Budding of Exosome Vesicles into Multivesicular Endosomes. *Science* **319**, 1244–1247 (2008).
164. Ira & Johnston, L. J. Sphingomyelinase generation of ceramide promotes clustering of nanoscale domains in supported bilayer membranes. *Biochim. Biophys. Acta - Biomembr.* **1778**, 185–197 (2008).
165. Buschow, S. I. *et al.* MHC II In dendritic cells is targeted to lysosomes or t cell-induced exosomes via distinct multivesicular body pathways. *Traffic* **10**, 1528–1542 (2009).
166. van Niel, G. *et al.* The Tetraspanin CD63 Regulates ESCRT-Independent and -Dependent Endosomal Sorting during Melanogenesis. *Dev. Cell* **21**, 708–721 (2011).
167. Ostrowski, M. *et al.* Rab27a and Rab27b control different steps of the exosome secretion pathway. *Nat. Cell Biol.* **12**, 19–30 (2010).
168. Hsu, C. *et al.* Regulation of exosome secretion by Rab35 and its GTPase-activating proteins TBC1D10A-C. *J. Cell Biol.* **189**, 223–232 (2010).
169. Jahn, R. & Scheller, R. H. SNAREs - Engines for membrane fusion. *Nat. Rev. Mol. Cell Biol.* **7**, 631–643 (2006).
170. Piccin, A., Murphy, W. G. & Smith, O. P. Circulating microparticles: pathophysiology and clinical implications. *Blood Rev.* **21**, 157–171 (2007).
171. Mulcahy, L. A., Pink, R. C. & Carter, D. R. F. Routes and mechanisms of extracellular vesicle uptake. *J. Extracell. Vesicles* **3**, 24641 (2014).
172. Escrevente, C., Keller, S., Altevogt, P. & Costa, J. Interaction and uptake of exosomes by ovarian cancer cells. *BMC Cancer* **11**, 1–10 (2011).
173. Kirchhausen, T. Clathrin. *Annu. Rev. Biochem.* **69**, 699–727 (2000).
174. Nanbo, A., Kawanishi, E., Yoshida, R. & Yoshiyama, H. Exosomes Derived from Epstein-Barr Virus-Infected Cells Are Internalized via Caveola-Dependent Endocytosis and Promote Phenotypic Modulation in Target Cells. *J. Virol.* **87**, 10334–10347 (2013).
175. Svensson, K. J. *et al.* Exosome uptake depends on ERK1/2-heat shock protein 27 signaling and lipid raft-mediated endocytosis negatively regulated by caveolin-1. *J. Biol. Chem.* **288**, 17713–17724 (2013).
176. Feng, D. *et al.* Cellular internalization of exosomes occurs through phagocytosis. *Traffic* **11**, 675–687 (2010).
177. Costa Verdera, H., Gitz-Francois, J. J., Schiffelers, R. M. & Vader, P. Cellular uptake of extracellular vesicles is mediated by clathrin-independent endocytosis and macropinocytosis. *J. Control. Release* **266**, 100–108 (2017).

178. Doherty, G. J. & McMahon, H. T. Mechanisms of endocytosis. *Annu. Rev. Biochem.* **78**, 857–902 (2009).
179. Stephens, L., Ellson, C. & Hawkins, P. Roles of PI3Ks in leukocyte chemotaxis and phagocytosis. *Curr. Opin. Cell Biol.* **14**, 203–213 (2002).
180. Heusermann, W. *et al.* Exosomes surf on filopodia to enter cells at endocytic hot spots, traffic within endosomes, and are targeted to the ER. *J. Cell Biol.* **213**, 173–184 (2016).
181. Santos, M. F. *et al.* VAMP-associated protein-A and oxysterol-binding protein–related protein 3 promote the entry of late endosomes into the nucleoplasmic reticulum. *J. Biol. Chem.* **293**, 13834–13848 (2018).
182. Corbeil, D. *et al.* Uptake and Fate of Extracellular Membrane Vesicles: Nucleoplasmic Reticulum-Associated Late Endosomes as a New Gate to Intercellular Communication. *Cells* **9**, 1931 (2020).
183. Lo Cicero, A., Stahl, P. D. & Raposo, G. Extracellular vesicles shuffling intercellular messages: For good or for bad. *Curr. Opin. Cell Biol.* **35**, 69–77 (2015).
184. Maas, S. L. N., Breakefield, X. O. & Weaver, A. M. Extracellular Vesicles: Unique Intercellular Delivery Vehicles. *Trends Cell Biol.* **27**, 172–188 (2017).
185. Miyado, K. *et al.* The fusing ability of sperm is bestowed by CD9-containing vesicles released from eggs in mice. *Proc. Natl. Acad. Sci. U. S. A.* **105**, 12921–12926 (2008).
186. Desrochers, L. M., Bordeleau, F., Reinhart-King, C. A., Cerione, R. A. & Antonyak, M. A. Microvesicles provide a mechanism for intercellular communication by embryonic stem cells during embryo implantation. *Nat. Commun.* **7**, 11958 (2016).
187. Gross, J. C., Chaudhary, V., Bartscherer, K. & Boutros, M. Active Wnt proteins are secreted on exosomes. *Nat. Cell Biol.* **14**, 1036–1045 (2012).
188. Beckett, K. *et al.* Drosophila S2 cells secrete wingless on exosome-like vesicles but the wingless gradient forms independently of exosomes. *Traffic* **14**, 82–96 (2013).
189. Vyas, N. *et al.* Vertebrate Hedgehog is secreted on two types of extracellular vesicles with different signaling properties. *Sci. Rep.* **4**, 1–12 (2014).
190. Corrigan, L. *et al.* BMP-regulated exosomes from Drosophila male reproductive glands reprogram female behavior. *J. Cell Biol.* **206**, 671–688 (2014).
191. Gassama, Y. & Favereaux, A. Emerging Roles of Extracellular Vesicles in the Central Nervous System: Physiology, Pathology, and Therapeutic Perspectives. *Front. Cell. Neurosci.* **15**, 1–7 (2021).
192. Fauré, J. *et al.* Exosomes are released by cultured cortical neurones. *Mol. Cell. Neurosci.* **31**, 642–648 (2006).
193. Korkut, C. *et al.* Trans-Synaptic Transmission of Vesicular Wnt Signals through Evi/Wntless. *Cell* **139**, 393–404 (2009).
194. Korkut, C. *et al.* Regulation of Postsynaptic Retrograde Signaling by Presynaptic

Exosome Release. *Neuron* **77**, 1039–1046 (2013).

195. Frühbeis, C. *et al.* Neurotransmitter-Triggered Transfer of Exosomes Mediates Oligodendrocyte-Neuron Communication. *PLoS Biol.* **11**, e1001604 (2013).
196. Lopez-Verrilli, M. A., Picou, F. & Court, F. A. Schwann cell-derived exosomes enhance axonal regeneration in the peripheral nervous system. *Glia* **61**, 1795–1806 (2013).
197. Théry, C. *et al.* Indirect activation of naïve CD4+ T cells by dendritic cell-derived exosomes. *Nat. Immunol.* **3**, 1156–1162 (2002).
198. Segura, E. *et al.* ICAM-1 on exosomes from mature dendritic cells is critical for efficient naive T-cell priming. *Blood* **106**, 216–223 (2005).
199. Qazi, K. R., Gehrmann, U., Jordö, E. D., Karlsson, M. C. I. & Gabrielsson, S. Antigen-loaded exosomes alone induce Thl-type memory through a B cell dependent mechanism. *Blood* **113**, 2673–2683 (2009).
200. Mittelbrunn, M. *et al.* Unidirectional transfer of microRNA-loaded exosomes from T cells to antigen-presenting cells. *Nat. Commun.* **2**, 282 (2011).
201. Montecalvo, A. *et al.* Mechanism of transfer of functional microRNAs between mouse dendritic cells via exosomes. *Blood* **119**, 756–766 (2012).
202. Okoye, I. S. *et al.* MicroRNA-Containing T-Regulatory-Cell-Derived Exosomes Suppress Pathogenic T Helper 1 Cells. *Immunity* **41**, 89–103 (2014).
203. Hergenreider, E. *et al.* Atheroprotective communication between endothelial cells and smooth muscle cells through miRNAs. *Nat. Cell Biol.* **14**, 249–256 (2012).
204. Borges, F. T. *et al.* TGF-β1-Containing exosomes from injured epithelial cells activate fibroblasts to initiate tissue regenerative responses and fibrosis. *J. Am. Soc. Nephrol.* **24**, 385–392 (2013).
205. Shah, R., Patel, T. & Freedman, J. E. Circulating Extracellular Vesicles in Human Disease. *N. Engl. J. Med.* **379**, 958–966 (2018).
206. Hanahan, D. & Weinberg, R. A. Hallmarks of cancer: the next generation. *Cell* **144**, 646–674 (2011).
207. Kucharzewska, P. *et al.* Exosomes reflect the hypoxic status of glioma cells and mediate hypoxia-dependent activation of vascular cells during tumor development. *Proc. Natl. Acad. Sci. U. S. A.* **110**, 7312–7317 (2013).
208. De Vrij, J. *et al.* Glioblastoma-derived extracellular vesicles modify the phenotype of monocytic cells. *Int. J. Cancer* **137**, 1630–1642 (2015).
209. Pucci, F. *et al.* SCS macrophages suppress melanoma by restricting tumor-derived vesicle-B cell interactions. *Science* **352**, 242–246 (2016).
210. Wieckowski, E. U. *et al.* Tumor-Derived Microvesicles Promote Regulatory T Cell Expansion and Induce Apoptosis in Tumor-Reactive Activated CD8 + T Lymphocytes . *J. Immunol.* **183**, 3720–3730 (2009).

211. Peinado, H. *et al.* Melanoma exosomes educate bone marrow progenitor cells toward a pro-metastatic phenotype through MET. *Nat. Med.* **18**, 883–891 (2012).
212. Costa-Silva, B. *et al.* Pancreatic cancer exosomes initiate pre-metastatic niche formation in the liver. *Nat. Cell Biol.* **17**, 816–826 (2015).
213. Hoshino, A. *et al.* Tumour exosome integrins determine organotropic metastasis. *Nature* **527**, 329–335 (2015).
214. Zhang, L. *et al.* Microenvironment-induced PTEN loss by exosomal microRNA primes brain metastasis outgrowth. *Nature* **527**, 100–104 (2015).
215. Muralidharan-Chari, V. *et al.* Microvesicle removal of anticancer drugs contributes to drug resistance in human pancreatic cancer cells. *Oncotarget* **7**, 50365–50379 (2016).
216. Au Yeung, C. L. *et al.* Exosomal transfer of stroma-derived miR21 confers paclitaxel resistance in ovarian cancer cells through targeting APAF1. *Nat. Commun.* **7**, 11150 (2016).
217. Vella, L. J., Hill, A. F. & Cheng, L. Focus on extracellular vesicles: Exosomes and their role in protein trafficking and biomarker potential in Alzheimer's and Parkinson's disease. *Int. J. Mol. Sci.* **17**, 173 (2016).
218. Quek, C. & Hill, A. F. The role of extracellular vesicles in neurodegenerative diseases. *Biochem. Biophys. Res. Commun.* **483**, 1178–1186 (2017).
219. Yuyama, K., Sun, H., Mitsutake, S. & Igarashi, Y. Sphingolipid-modulated exosome secretion promotes clearance of amyloid-β by microglia. *J. Biol. Chem.* **287**, 10977–10989 (2012).
220. Falker, C. *et al.* Exosomal cellular prion protein drives fibrillization of amyloid beta and counteracts amyloid beta-mediated neurotoxicity. *J. Neurochem.* **137**, 88–100 (2016).
221. Lyu, L. *et al.* A critical role of cardiac fibroblast-derived exosomes in activating renin angiotensin system in cardiomyocytes. *J. Mol. Cell. Cardiol.* **89**, 268–279 (2015).
222. Wang, C. *et al.* Macrophage-derived mir-155-containing exosomes suppress fibroblast proliferation and promote fibroblast inflammation during cardiac injury. *Mol. Ther.* **25**, 192–204 (2017).
223. Raab-Traub, N. & Dittmer, D. P. Viral effects on the content and function of extracellular vesicles. *Nat. Rev. Microbiol.* **15**, 559–572 (2017).
224. Ramakrishnaiah, V. *et al.* Exosome-mediated transmission of hepatitis C virus between human hepatoma Huh7.5 cells. *PNAS* **110**, 13109–13113 (2013).
225. Katsuda, T., Kosaka, N. & Ochiya, T. The roles of extracellular vesicles in cancer biology: Toward the development of novel cancer biomarkers. *Proteomics* **14**, 412–425 (2014).
226. Thompson, A. G. *et al.* Extracellular vesicles in neurodegenerative disease-pathogenesis to biomarkers. *Nat. Rev. Neurol.* **12**, 346–357 (2016).

227. Szabo, G. & Momen-Heravi, F. Extracellular vesicles in liver disease and potential as biomarkers and therapeutic targets. *Nat. Rev. Gastroenterol. Hepatol.* **14**, 455–466 (2017).
228. Vader, P., Breakefield, X. O. & Wood, M. J. A. Extracellular vesicles: Emerging targets for cancer therapy. *Trends Mol. Med.* **20**, 385–393 (2014).
229. Urabe, F. *et al.* Extracellular vesicles as biomarkers and therapeutic targets for cancer. *Am. J. Physiol. - Cell Physiol.* **318**, C29–C39 (2020).
230. Lee, C. *et al.* Exosomes Mediate the Cytoprotective Action of Mesenchymal Stromal Cells on Hypoxia-Induced Pulmonary Hypertension. *Circulation* **126**, 2601–2611 (2012).
231. Ruppert, K. A. *et al.* Human Mesenchymal Stromal Cell-Derived Extracellular Vesicles Modify Microglial Response and Improve Clinical Outcomes in Experimental Spinal Cord Injury. *Sci. Rep.* **8**, 480 (2018).
232. Song, Y. *et al.* Exosomal miR-146a Contributes to the Enhanced Therapeutic Efficacy of Interleukin-1β-Primed Mesenchymal Stem Cells Against Sepsis. *Stem Cells* **35**, 1208–1221 (2017).
233. Seo, Y., Kim, H. S. & Hong, I. S. Stem cell-derived extracellular vesicles as immunomodulatory therapeutics. *Stem Cells Int.* **2019**, 10–15 (2019).
234. Herrera, M. B. *et al.* Human liver stem cell-derived microvesicles accelerate hepatic regeneration in hepatectomized rats. *J. Cell. Mol. Med.* **14**, 1605–1618 (2010).
235. Gatti, S. *et al.* Microvesicles derived from human adult mesenchymal stem cells protect against ischaemia-reperfusion-induced acute and chronic kidney injury. *Nephrol. Dial. Transplant.* **26**, 1474–1483 (2011).
236. Bian, S. *et al.* Extracellular vesicles derived from human bone marrow mesenchymal stem cells promote angiogenesis in a rat myocardial infarction model. *J. Mol. Med.* **92**, 387–397 (2014).
237. Vrijsen, K. R. *et al.* Exosomes from Cardiomyocyte Progenitor Cells and Mesenchymal Stem Cells Stimulate Angiogenesis Via EMMPRIN. *Adv. Healthc. Mater.* **5**, 2555–2565 (2016).
238. Zhang, B. *et al.* HucMSC-Exosome Mediated-Wnt4 Signaling Is Required for Cutaneous Wound Healing. *Stem Cells* **33**, 2158–2168 (2015).
239. Fang, S. *et al.* Umbilical Cord-Derived Mesenchymal Stem Cell-Derived Exosomal MicroRNAs Suppress Myofibroblast Differentiation by Inhibiting the Transforming Growth Factor-β/SMAD2 Pathway During Wound Healing. *Stem Cells Transl. Med.* **5**, 1425–1439 (2016).
240. Wiklander, O. P. B., Brennan, M., Lötvall, J., Breakefield, X. O. & Andaloussi, S. E. L. Advances in therapeutic applications of extracellular vesicles. *Sci. Transl. Med.* **11**, 1–

16 (2019).

241. Gnecchi, M. *et al.* Paracrine action accounts for marked protection of ischemic heart by Akt-modified mesenchymal stem cells. *Nat. Med.* **11**, 367–368 (2005).
242. Gnecchi, M. *et al.* Evidence supporting paracrine hypothesis for Akt-modified mesenchymal stem cell-mediated cardiac protection and functional improvement. *FASEB J.* **20**, 661–669 (2006).
243. Timmers, L. *et al.* Reduction of myocardial infarct size by human mesenchymal stem cell conditioned medium. *Stem Cell Res.* **1**, 129–137 (2008).
244. Timmers, L. *et al.* Human mesenchymal stem cell-conditioned medium improves cardiac function following myocardial infarction. *Stem Cell Res.* **6**, 206–214 (2011).
245. Bi, B., Schmitt, R., Israilova, M., Nishio, H. & Cantley, L. G. Stromal Cells Protect against Acute Tubular Injury via an Endocrine Effect. *J. Am. Soc. Nephrol.* **18**, 2486–2496 (2007).
246. Lai, R. C. *et al.* Exosome secreted by MSC reduces myocardial ischemia/reperfusion injury. *Stem Cell Res.* **4**, 214–222 (2010).
247. Bruno, S. *et al.* Mesenchymal stem cell-derived microvesicles protect against acute tubular injury. *J. Am. Soc. Nephrol.* **20**, 1053–1067 (2009).
248. Bruno, S. *et al.* Microvesicles derived from mesenchymal stem cells enhance survival in a lethal model of acute kidney injury. *PLoS One* **7**, e33115 (2012).
249. Doeppner, T. R. *et al.* Extracellular Vesicles Improve Post-Stroke Neuroregeneration and Prevent Postischemic Immunosuppression. *Stem Cells Transl. Med.* **4**, 1131–1143 (2015).
250. Kim, D. *et al.* Chromatographically isolated CD63 + CD81 + extracellular vesicles from mesenchymal stromal cells rescue cognitive impairments after TBI. *PNAS* **113**, 170–175 (2016).
251. Li, T. *et al.* Exosomes Derived from Human Umbilical Cord Mesenchymal Stem Cells Alleviate Liver Fibrosis. *Stem Cells Dev.* **22**, 845–854 (2013).
252. Haga, H., Yan, I. K., Takahashi, K., Matsuda, A. & Patel, T. Extracellular Vesicles from Bone Marrow-Derived Mesenchymal Stem Cells Improve Survival from Lethal Hepatic Failure in Mice. *Stem Cells Transl. Med. Med.* **6**, 1262–1272 (2017).
253. Nassar, W. *et al.* Umbilical cord mesenchymal stem cells derived extracellular vesicles can safely ameliorate the progression of chronic kidney diseases. *Biomater. Res.* **20**, 1–11 (2016).
254. Börger, V. *et al.* International Society for Extracellular Vesicles and International Society for Cell and Gene Therapy statement on extracellular vesicles from mesenchymal stromal cells and other cells: considerations for potential therapeutic agents to suppress coronavirus disease-19. *Cytotherapy* **22**, 482–485 (2020).

255. Monsel, A. *et al.* Therapeutic effects of human mesenchymal stem cell-derived microvesicles in severe pneumonia in mice. *Am. J. Respir. Crit. Care Med.* **192**, 324–336 (2015).
256. Morrison, T. J. *et al.* Mesenchymal stromal cells modulate macrophages in clinically relevant lung injury models by extracellular vesicle mitochondrial transfer. *Am. J. Respir. Crit. Care Med.* **196**, 1275–1286 (2017).
257. Alvarez-Erviti, L. *et al.* Delivery of siRNA to the mouse brain by systemic injection of targeted exosomes. *Nat. Biotechnol.* **29**, 341–345 (2011).
258. Zhuang, X. *et al.* Treatment of brain inflammatory diseases by delivering exosome encapsulated anti-inflammatory drugs from the nasal region to the brain. *Mol. Ther.* **19**, 1769–1779 (2011).
259. Elsharkasy, O. M. *et al.* Extracellular vesicles as drug delivery systems: Why and how? *Adv. Drug Deliv. Rev.* **159**, 332–343 (2020).
260. Batrakova, E. V & Kim, M. S. Using exosomes, naturally-equipped nanocarriers, for drug delivery. *J. Control. Release* **219**, 396–405 (2015).
261. Zhu, X. *et al.* Comprehensive toxicity and immunogenicity studies reveal minimal effects in mice following sustained dosing of extracellular vesicles derived from HEK293T cells. *J. Extracell. Vesicles* **6**, 1324730 (2017).
262. Saleh, A. F. *et al.* Extracellular vesicles induce minimal hepatotoxicity and immunogenicity. *Nanoscale* **11**, 6990–7001 (2019).
263. Sun, D. *et al.* A novel nanoparticle drug delivery system: The anti-inflammatory activity of curcumin is enhanced when encapsulated in exosomes. *Mol. Ther.* **18**, 1606–1614 (2010).
264. Toffoli, G. *et al.* Exosomal doxorubicin reduces the cardiac toxicity of doxorubicin. *Nanomedicine* **10**, 2963–2971 (2015).
265. Kim, M. S. *et al.* Development of exosome-encapsulated paclitaxel to overcome MDR in cancer cells. *Nanomedicine Nanotechnology, Biol. Med.* **12**, 655–664 (2016).
266. Kugeratski, F. G., McAndrews, K. M. & Kalluri, R. Multifunctional Applications of Engineered Extracellular Vesicles in the Treatment of Cancer. *Endocrinol. (United States)* **162**, 1–15 (2021).
267. Kooijmans, S. A. A., de Jong, O. G. & Schiffelers, R. M. Exploring interactions between extracellular vesicles and cells for innovative drug delivery system design. *Adv. Drug Deliv. Rev.* **173**, 252–278 (2021).
268. Vader, P., Mol, E. A., Pasterkamp, G. & Schiffelers, R. M. Extracellular vesicles for drug delivery. *Adv. Drug Deliv. Rev.* **106**, 148–156 (2016).
269. Aqil, F., Munagala, R., Jeyabalan, J., Agrawal, A. K. & Gupta, R. Exosomes for the Enhanced Tissue Bioavailability and Efficacy of Curcumin. *AAPS J.* **19**, 1691–1702

(2017).

270. Kamerkar, S. *et al.* Exosomes facilitate therapeutic targeting of oncogenic KRAS in pancreatic cancer. *Nature* **546**, 498–503 (2017).
271. Tian, Y. *et al.* A doxorubicin delivery platform using engineered natural membrane vesicle exosomes for targeted tumor therapy. *Biomaterials* **35**, 2383–2390 (2014).
272. Hadla, M. *et al.* Exosomes increase the therapeutic index of doxorubicin in breast and ovarian cancer mouse models. *Nanomedicine* **11**, 2431–2441 (2016).
273. Fuhrmann, G., Serio, A., Mazo, M., Nair, R. & Stevens, M. M. Active loading into extracellular vesicles significantly improves the cellular uptake and photodynamic effect of porphyrins. *J. Control. Release* **205**, 35–44 (2015).
274. Haney, M. J. *et al.* Exosomes as drug delivery vehicles for Parkinson's disease therapy. *J. Control. Release* **207**, 18–30 (2015).
275. Kooijmans, S. A. A. *et al.* Electroporation-induced siRNA precipitation obscures the efficiency of siRNA loading into extracellular vesicles. *J. Control. Release* **172**, 229–238 (2013).
276. Reshke, R. *et al.* Reduction of the therapeutic dose of silencing RNA by packaging it in extracellular vesicles via a pre-microRNA backbone. *Nat. Biomed. Eng.* **4**, 52–68 (2020).
277. Sato, Y. T. *et al.* Engineering hybrid exosomes by membrane fusion with liposomes. *Sci. Rep.* **6**, 1–11 (2016).
278. Piffoux, M., Silva, A. K. A., Wilhelm, C., Gazeau, F. & Tareste, D. Modification of Extracellular Vesicles by Fusion with Liposomes for the Design of Personalized Biogenic Drug Delivery Systems. *ACS Nano* **12**, 6830–6842 (2018).
279. Pascucci, L. *et al.* Paclitaxel is incorporated by mesenchymal stromal cells and released in exosomes that inhibit in vitro tumor growth: A new approach for drug delivery. *J. Control. Release* **192**, 262–270 (2014).
280. Lou, G. *et al.* Exosomes derived from MIR-122-modified adipose tissue-derived MSCs increase chemosensitivity of hepatocellular carcinoma. *J. Hematol. Oncol.* **8**, 1–11 (2015).
281. Yim, N. *et al.* Exosome engineering for efficient intracellular delivery of soluble proteins using optically reversible protein-protein interaction module. *Nat. Commun.* **7**, 1–9 (2016).
282. Choi, H. *et al.* Exosome-based delivery of super-repressor IκBα relieves sepsis-associated organ damage and mortality. *Sci. Adv.* **6**, 1–10 (2020).
283. Murphy, D. E. *et al.* Extracellular vesicle-based therapeutics: natural versus engineered targeting and trafficking. *Exp. Mol. Med.* **51**, 1–12 (2019).
284. Matsumoto, A. *et al.* Role of Phosphatidylserine-Derived Negative Surface Charges in

the Recognition and Uptake of Intravenously Injected B16BL6-Derived Exosomes by Macrophages. *J. Pharm. Sci.* **106**, 168–175 (2017).

285. El-Andaloussi, S. *et al.* Exosome-mediated delivery of siRNA in vitro and in vivo. *Nat. Protoc.* **7**, 2112–2126 (2012).
286. Tian, Y. *et al.* A doxorubicin delivery platform using engineered natural membrane vesicle exosomes for targeted tumor therapy. *Biomaterials* **35**, 2383–2390 (2014).
287. Bellavia, D. *et al.* Interleukin 3- receptor targeted exosomes inhibit in vitro and in vivo chronic myelogenous Leukemia cell growth. *Theranostics* **7**, 1333–1345 (2017).
288. Kooijmans, S. A. A. *et al.* Display of GPI-anchored anti-EGFR nanobodies on extracellular vesicles promotes tumour cell targeting. *J. Extracell. Vesicles* **5**, 31053 (2016).
289. Yang, J., Zhang, X., Chen, X., Wang, L. & Yang, G. Exosome Mediated Delivery of miR-124 Promotes Neurogenesis after Ischemia. *Mol. Ther. Nucleic Acids* **7**, 278–287 (2017).
290. Mentkowski, K. I. & Lang, J. K. Exosomes Engineered to Express a Cardiomyocyte Binding Peptide Demonstrate Improved Cardiac Retention in Vivo. *Sci. Rep.* **9**, 1–13 (2019).
291. Ohno, S. I. *et al.* Systemically injected exosomes targeted to EGFR deliver antitumor microrna to breast cancer cells. *Mol. Ther.* **21**, 185–191 (2013).
292. Kooijmans, S. A. A., Gitz-Francois, J. J. J. M., Schiffelers, R. M. & Vader, P. Recombinant phosphatidylserine-binding nanobodies for targeting of extracellular vesicles to tumor cells: A plug-and-play approach. *Nanoscale* **10**, 2413–2426 (2018).
293. Jia, G. *et al.* Biomaterials NRP-1 targeted and cargo-loaded exosomes facilitate simultaneous imaging and therapy of glioma in vitro and in vivo. *Biomaterials* **178**, 302–316 (2018).
294. Kooijmans, S. A. A. *et al.* PEGylated and targeted extracellular vesicles display enhanced cell specificity and circulation time. *J. Control. Release* **224**, 77–85 (2016).
295. Wang, Y. *et al.* Nucleolin-targeted Extracellular Vesicles as a Versatile Platform for Biologics Delivery to Breast Cancer. *Theranostics* **7**, 1360–1372 (2017).
296. Tamura, R., Uemoto, S. & Tabata, Y. Augmented liver targeting of exosomes by surface modification with cationized pullulan. *Acta Biomater.* **57**, 274–284 (2017).
297. Pi, F. *et al.* Nanoparticle orientation to control RNA loading and ligand display on extracellular vesicles for cancer regression. *Nat. Nanotechnol.* **13**, 82–89 (2018).
298. Tian, T. *et al.* Surface functionalized exosomes as targeted drug delivery vehicles for cerebral ischemia therapy. *Biomaterials* **150**, 137–149 (2018).
299. Ye, Z. *et al.* Methotrexate-Loaded Extracellular Vesicles Functionalized with Therapeutic and Targeted Peptides for the Treatment of Glioblastoma Multiforme. *ACS*

Appl. Mater. Interfaces **10**, 12341–12350 (2018).

300. Gao, X. *et al.* Anchor peptide captures, targets, and loads exosomes of diverse origins for diagnostics and therapy. *Sci. Transl. Med.* **10**, eaat0195 (2018).
301. Pham, T. C. *et al.* Covalent conjugation of extracellular vesicles with peptides and nanobodies for targeted therapeutic delivery. *J. Extracell. Vesicles* **10**, e12057 (2021).
302. M. Fialho, A., Bernardes, N. & M Chakrabarty, A. Exploring the anticancer potential of the bacterial protein azurin. *AIMS Microbiol.* **2**, 292–303 (2016).
303. Bernardes, N. & Fialho, A. M. Perturbing the dynamics and organization of cell membrane components: A new paradigm for cancer-targeted therapies. *Int. J. Mol. Sci.* **19**, 3871 (2018).
304. Yamada, T. *et al.* Bacterial redox protein azurin, tumor suppressor protein p53, and regression of cancer. *Proc. Natl. Acad. Sci. U. S. A.* **99**, 14098–14103 (2002).
305. Yamada, T. *et al.* Apoptosis or growth arrest: Modulation of tumor suppressor p53's specificity by bacterial redox protein azurin. *Proc. Natl. Acad. Sci. U. S. A.* **101**, 4770–4775 (2004).
306. Taylor, B. N. *et al.* Noncationic Peptides Obtained From Azurin Preferentially Enter Cancer Cells. *Cancer Res.* **69**, 537–546 (2009).
307. Bernardes, N. *et al.* Azurin interaction with the lipid raft components ganglioside GM-1 and caveolin-1 increases membrane fluidity and sensitivity to anti-cancer drugs. *Cell Cycle* **17**, 1649–1666 (2018).
308. Apiyo, D. & Wittung-Stafshede, P. Unique complex between bacterial azurin and tumor-suppressor protein p53. *Biochem. Biophys. Res. Commun.* **332**, 965–968 (2005).
309. Taranta, M., Bizzarri, A. R. & Cannistraro, S. Probing the interaction between p53 and the bacterial protein azurin by single molecule force spectroscopy. *J. Mol. Recognit.* **21**, 63–70 (2008).
310. Chaudhari, A. *et al.* Cupredoxin-cancer interrelationship: Azurin binding with EphB2, interference in EphB2 tyrosine phosphorylation, and inhibition of cancer growth. *Biochemistry* **46**, 1799–1810 (2007).
311. Bernardes, N. *et al.* Modulation of membrane properties of lung cancer cells by azurin enhances the sensitivity to EGFR-targeted therapy and decreased β1 integrin-mediated adhesion. *Cell Cycle* **15**, 1415–1424 (2016).
312. Yaghoubi, A. *et al.* p28 Bacterial Peptide, as an Anticancer Agent. *Front. Oncol.* **10**, 1303 (2020).
313. Yamada, T. *et al.* Internalization of bacterial redox protein azurin in mammalian cells: Entry domain and specificity. *Cell. Microbiol.* **7**, 1418–1431 (2005).
314. Wang, J. *et al.* ICn3D, a web-based 3D viewer for sharing 1D/2D/3D representations of biomolecular structures. *Bioinformatics* **36**, 131–135 (2020).

315. Berman, H. M. *et al.* The protein data bank. *Acta Crystallogr. Sect. D Biol. Crystallogr.* **58**, 899–907 (2002).
316. Crane, B. R., Di Bilio, A. J., Winkler, J. R. & Gray, H. B. Electron Tunneling in Single Crystals of Pseudomonas aeruginosa Azurins. *J. Am. Chem. Soc.* **123**, 11623–11631 (2001).
317. Yamada, T. *et al.* P28, A first in class peptide inhibitor of cop1 binding to p53. *Br. J. Cancer* **108**, 2495–2504 (2013).
318. Yamada, T., Das Gupta, T. K. & Beattie, C. W. P28, an anionic cell-penetrating peptide, increases the activity of wild type and mutated p53 without altering its conformation. *Mol. Pharm.* **10**, 3375–3383 (2013).
319. Yamada, T., Das Gupta, T. K. & Beattie, C. W. P28-Mediated activation of p53 in G2-M phase of the cell cycle enhances the efficacy of DNA damaging and antimitotic chemotherapy. *Cancer Res.* **76**, 2354–2365 (2016).
320. Mehta, R. R. *et al.* A cell penetrating peptide derived from azurin inhibits angiogenesis and tumor growth by inhibiting phosphorylation of VEGFR-2, FAK and Akt. *Angiogenesis* **14**, 355–369 (2011).
321. Warso, M. A. *et al.* A first-in-class, first-in-human, phase i trial of p28, a non-HDM2-mediated peptide inhibitor of p53 ubiquitination in patients with advanced solid tumours. *Br. J. Cancer* **108**, 1061–1070 (2013).
322. Lulla, R. R. *et al.* Phase i trial of p28 (NSC745104), a non-HDM2-mediated peptide inhibitor of p53 ubiquitination in pediatric patients with recurrent or progressive central nervous system tumors: A Pediatric Brain Tumor Consortium Study. *Neuro. Oncol.* **18**, 1319–1325 (2016).
323. Ferlay, J. *et al.* Global Cancer Observatory: Cancer Today. Lyon, France: International Agency for Research on Cancer. (2020). Available at: https://gco.iarc.fr/today/about. (Accessed: 3rd July 2021)
324. Sasieni, P. D., Shelton, J., Ormiston-Smith, N., Thomson, C. S. & Silcocks, P. B. What is the lifetime risk of developing cancer?: the effect of adjusting for multiple primaries. *Br. J. Cancer* **105**, 460 (2011).
325. Peer, D. *et al.* Nanocarriers as an emerging platform for cancer therapy. *Nat. Nanotechnol.* **2**, 751–760 (2007).
326. Lalu, M. M. *et al.* Safety of Cell Therapy with Mesenchymal Stromal Cells (SafeCell): A Systematic Review and Meta-Analysis of Clinical Trials. *PLoS One* **7**, (2012).
327. Salomon, C. *et al.* Exosomal Signaling during Hypoxia Mediates Microvascular Endothelial Cell Migration and Vasculogenesis. *PLoS One* **8**, 1–24 (2013).
328. Lopatina, T. *et al.* Platelet-derived growth factor regulates the secretion of extracellular vesicles by adipose mesenchymal stem cells and enhances their angiogenic potential.

Cell Commun. Signal. **12**, 1–12 (2014).

329. Lener, T. *et al.* Applying extracellular vesicles based therapeutics in clinical trials - An ISEV position paper. *J. Extracell. Vesicles* **4**, 30087 (2015).
330. Börger, V. *et al.* Mesenchymal stem/stromal cell-derived extracellular vesicles and their potential as novel immunomodulatory therapeutic agents. *Int. J. Mol. Sci.* **18**, 1450 (2017).
331. EL Andaloussi, S., Lakhal, S., Mäger, I. & Wood, M. J. A. Exosomes for targeted siRNA delivery across biological barriers. *Adv. Drug Deliv. Rev.* **65**, 391–397 (2013).
332. Elahi, F. M., Farwell, D. G., Nolta, J. A. & Anderson, J. D. Preclinical translation of exosomes derived from mesenchymal stem/stromal cells. *Stem Cells* **38**, 15–21 (2020).
333. Mendt, M. *et al.* Generation and testing of clinical-grade exosomes for pancreatic cancer. *JCI insight* **3**, e99263 (2018).
334. Phinney, D. G. & Pittenger, M. F. Concise Review: MSC-Derived Exosomes for Cell-Free Therapy. *Stem Cells* **35**, 851–858 (2017).
335. Ren, G. *et al.* Concise Review: Mesenchymal Stem Cells and Translational Medicine: Emerging Issues. *Stem Cells Translational Medicine* **1**, 51–58 (2012).
336. Golpanian, S. *et al.* Concise Review: Review and Perspective of Cell Dosage and Routes of Administration From Preclinical and Clinical Studies of Stem Cell Therapy for Heart Disease. *Stem Cells Transl. Med.* **5**, 186–191 (2016).
337. Wysoczynski, M., Khan, A. & Bolli, R. New Paradigms in Cell Therapy: Repeated Dosing, Intravenous Delivery, Immunomodulatory Actions, and New Cell Types. *Circ. Res.* **123**, 138–158 (2018).
338. Kordelas, L. *et al.* MSC-derived exosomes: A novel tool to treat therapy-refractory graft-versus-host disease. *Leukemia* **28**, 970–973 (2014).
339. de Almeida Fuzeta, M., Branco, A. D. M., Fernandes-Platzgummer, A., Lobato da Silva, C. & Cabral, J. M. S. Addressing the Manufacturing Challenges of Cell-Based Therapies. in *Advances in biochemical engineering/biotechnology* (eds. Silva, A., Moreira, J., Lobo, J. & Almeida, H.) **171**, 225–278 (Springer, 2019).
340. de Soure, A. M., Fernandes-Platzgummer, A., da Silva, C. L. & Cabral, J. M. S. Scalable microcarrier-based manufacturing of mesenchymal stem/stromal cells. *J. Biotechnol.* **236**, 88–109 (2016).
341. Nogueira, D. E. S. *et al.* Strategies for the expansion of human induced pluripotent stem cells as aggregates in single-use Vertical-Wheel™ bioreactors. *J. Biol. Eng.* **13**, 1–14 (2019).
342. Gardiner, C., Ferreira, Y. J., Dragovic, R. A., Redman, C. W. G. & Sargent, I. L. Extracellular vesicle sizing and enumeration by nanoparticle tracking analysis. *J. Extracell. Vesicles* **2**, 19671 (2013).

343. Racher, A. J., Looby, D. & Griffiths, J. B. Use of lactate dehydrogenase release to assess changes in culture viability. *Cytotechnology* **3**, 301–307 (1990).
344. Webber, J. & Clayton, A. How pure are your vesicles? *J. Extracell. Vesicles* **2**, 1–6 (2013).
345. Conlan, R. S., Pisano, S., Oliveira, M. I., Ferrari, M. & Mendes Pinto, I. Exosomes as Reconfigurable Therapeutic Systems. *Trends Mol. Med.* **23**, 636–650 (2017).
346. Keshtkar, S., Azarpira, N. & Ghahremani, M. H. Mesenchymal stem cell-derived extracellular vesicles: novel frontiers in regenerative medicine. *Stem Cell Res. Ther.* **9**, 63 (2018).
347. Li, Y. *et al.* A33 antibody-functionalized exosomes for targeted delivery of doxorubicin against colorectal cancer. *Nanomedicine Nanotechnology, Biol. Med.* **14**, 1973–1985 (2018).
348. Kim, M. S. *et al.* Engineering macrophage-derived exosomes for targeted paclitaxel delivery to pulmonary metastases: in vitro and in vivo evaluations. *Nanomedicine Nanotechnology, Biol. Med.* **14**, 195–204 (2018).
349. Witwer, K. W. *et al.* Defining mesenchymal stromal cell (MSC)-derived small extracellular vesicles for therapeutic applications. *J. Extracell. Vesicles* **8**, 1609206 (2019).
350. Viswanathan, S. *et al.* Mesenchymal stem versus stromal cells: International Society for Cell & Gene Therapy (ISCT®) Mesenchymal Stromal Cell committee position statement on nomenclature. *Cytotherapy* **21**, 1019–1024 (2019).
351. Haraszti, R. A. *et al.* Exosomes Produced from 3D Cultures of MSCs by Tangential Flow Filtration Show Higher Yield and Improved Activity. *Mol. Ther.* **26**, 2838–2847 (2018).
352. Morrell, A. E. *et al.* Mechanically induced Ca2+ oscillations in osteocytes release extracellular vesicles and enhance bone formation. *Bone Res.* **6**, 1–11 (2018).
353. Frauenschuh, S. *et al.* A microcarrier-based cultivation system for expansion of primary mesenchymal stem cells. *Biotechnol. Prog.* **23**, 187–193 (2007).
354. Eibes, G. *et al.* Maximizing the ex vivo expansion of human mesenchymal stem cells using a microcarrier-based stirred culture system. *J. Biotechnol.* **146**, 194–197 (2010).
355. Bhang, S. H. *et al.* Angiogenesis in ischemic tissue produced by spheroid grafting of human adipose-derived stromal cells. *Biomaterials* **32**, 2734–2747 (2011).
356. Costa, M. H. G., McDevitt, T. C., Cabral, J. M. S., da Silva, C. L. & Ferreira, F. C. Tridimensional configurations of human mesenchymal stem/stromal cells to enhance cell paracrine potential towards wound healing processes. *J. Biotechnol.* **262**, 28–39 (2017).
357. Cha, J. M. *et al.* Efficient scalable production of therapeutic microvesicles derived from

human mesenchymal stem cells. *Sci. Rep.* **8**, 1–16 (2018).

358. King, H. W., Michael, M. Z. & Gleadle, J. M. Hypoxic enhancement of exosome release by breast cancer cells. *BMC Cancer* **12**, 421 (2012).
359. Panigrahi, G. K. *et al.* Hypoxia-induced exosome secretion promotes survival of African-American and Caucasian prostate cancer cells. *Sci. Rep.* **8**, 1–13 (2018).
360. Rupert, D. L. M., Claudio, V., Lässer, C. & Bally, M. Methods for the physical characterization and quantification of extracellular vesicles in biological samples. *Biochim. Biophys. Acta - Gen. Subj.* **1861**, 3164–3179 (2017).
361. Hood, J. L., Scott, M. J. & Wickline, S. A. Maximizing exosome colloidal stability following electroporation. *Anal. Biochem.* **448**, 41–49 (2014).
362. Akagi, T., Kato, K., Hanamura, N., Kobayashi, M. & Ichiki, T. Evaluation of desialylation effect on zeta potential of extracellular vesicles secreted from human prostate cancer cells by on-chip microcapillary electrophoresis. *Jpn. J. Appl. Phys.* **53**, 06JL01 (2014).
363. Kesimer, M. & Gupta, R. Physical characterization and profiling of airway epithelial derived exosomes using light scattering. *Methods* **87**, 59–63 (2015).
364. Mitchell, J. P., Court, J., Mason, M. D., Tabi, Z. & Clayton, A. Increased exosome production from tumour cell cultures using the Integra CELLine Culture System. *J. Immunol. Methods* **335**, 98–105 (2008).
365. Jeppesen, D. K. *et al.* Quantitative proteomics of fractionated membrane and lumen exosome proteins from isogenic metastatic and nonmetastatic bladder cancer cells reveal differential expression of EMT factors. *Proteomics* **14**, 699–712 (2014).
366. Watson, D. C. *et al.* Efficient production and enhanced tumor delivery of engineered extracellular vesicles. *Biomaterials* **105**, 195–205 (2016).
367. de Almeida Fuzeta, M. *et al.* Scalable Production of Human Mesenchymal Stromal Cell-Derived Extracellular Vesicles Under Serum-/Xeno-Free Conditions in a Microcarrier-Based Bioreactor Culture System. *Front. Cell Dev. Biol.* **8**, 553444 (2020).
368. Du, W. J. *et al.* Heterogeneity of proangiogenic features in mesenchymal stem cells derived from bone marrow, adipose tissue, umbilical cord, and placenta. *Stem Cell Res. Ther.* **7**, 163 (2016).
369. Mol, E. A., Goumans, M. J., Doevendans, P. A., Sluijter, J. P. G. & Vader, P. Higher functionality of extracellular vesicles isolated using size-exclusion chromatography compared to ultracentrifugation. *Nanomedicine Nanotechnology, Biol. Med.* **13**, 2061–2065 (2017).
370. Van Mil, A. *et al.* MicroRNA-214 inhibits angiogenesis by targeting Quaking and reducing angiogenic growth factor release. *Cardiovasc. Res.* **93**, 655–665 (2012).
371. Eliceiri, B. P., Klemke, R., Strömblad, S. & Cheresh, D. A. Integrin αvβ3 requirement for sustained mitogen-activated protein kinase activity during angiogenesis. *J. Cell Biol.*

140, 1255–1263 (1998).

372. Ballif, B. A. & Blenis, J. Molecular mechanisms mediating mammalian mitogen-activated protein kinase (MAPK) kinase (MEK)-MAPK cell survival signals. *Cell Growth Differ.* **12**, 397–408 (2001).
373. Manning, B. D. & Cantley, L. C. AKT/PKB Signaling: Navigating Downstream. *Cell* **129**, 1261–1274 (2007).
374. Mol, E. A. *et al.* Injectable Supramolecular Ureidopyrimidinone Hydrogels Provide Sustained Release of Extracellular Vesicle Therapeutics. *Adv. Healthc. Mater.* **8**, 1900847 (2019).
375. Théry, C. *et al.* Minimal information for studies of extracellular vesicles 2018 (MISEV2018): a position statement of the International Society for Extracellular Vesicles and update of the MISEV2014 guidelines. *J. Extracell. Vesicles* **7**, 1535750 (2018).
376. Lötvall, J. *et al.* Minimal experimental requirements for definition of extracellular vesicles and their functions: A position statement from the International Society for Extracellular Vesicles. *J. Extracell. Vesicles* **3**, 26913 (2014).
377. Linares, R., Tan, S., Gounou, C., Arraud, N. & Brisson, A. R. High-speed centrifugation induces aggregation of extracellular vesicles. *J. Extracell. Vesicles* **4**, 29509 (2015).
378. Nordin, J. Z. *et al.* Ultrafiltration with size-exclusion liquid chromatography for high yield isolation of extracellular vesicles preserving intact biophysical and functional properties. *Nanomedicine Nanotechnology, Biol. Med.* **11**, 879–883 (2015).
379. Gardiner, C. *et al.* Techniques used for the isolation and characterization of extracellular vesicles: Results of a worldwide survey. *J. Extracell. Vesicles* **5**, 32945 (2016).
380. Gualerzi, A. *et al.* Raman spectroscopy as a quick tool to assess purity of extracellular vesicle preparations and predict their functionality. *J. Extracell. Vesicles* **8**, 1568780 (2019).
381. Zhu, W. *et al.* Exosomes derived from human bone marrow mesenchymal stem cells promote tumor growth in vivo. *Cancer Lett.* **315**, 28–37 (2012).
382. Lee, J.-K. *et al.* Exosomes Derived from Mesenchymal Stem Cells Suppress Angiogenesis by Down-Regulating VEGF Expression in Breast Cancer Cells. *PLoS One* **8**, e84256 (2013).
383. Rosenberger, L. *et al.* Stem cell exosomes inhibit angiogenesis and tumor growth of oral squamous cell carcinoma. *Sci. Rep.* **9**, 1–12 (2019).
384. Todorova, D., Simoncini, S., Lacroix, R., Sabatier, F. & Dignat-George, F. Extracellular vesicles in angiogenesis. *Circ. Res.* **120**, 1658–1673 (2017).
385. Liang, X., Zhang, L., Wang, S., Han, Q. & Zhao, R. C. Exosomes secreted by mesenchymal stem cells promote endothelial cell angiogenesis by transferring miR-125a. *J. Cell Sci.* **129**, 2182–2189 (2016).

386. Kang, T. *et al.* Adipose-Derived Stem Cells Induce Angiogenesis via Microvesicle Transport of miRNA-31. *Stem Cells Transl. Med.* **5**, 440–450 (2016).
387. Zou, X. *et al.* Human mesenchymal stromal cell-derived extracellular vesicles alleviate renal ischemic reperfusion injury and enhance angiogenesis in rats. *Am. J. Transl. Res.* **8**, 4289–4299 (2016).
388. Ma, J. *et al.* Exosomes Derived from Akt -Modified Human Umbilical Cord Mesenchymal Stem Cells Improve Cardiac Regeneration and Promote Angiogenesis via Activating Platelet-Derived Growth Factor D . *Stem Cells Transl. Med.* **6**, 51–59 (2017).
389. Shabbir, A., Cox, A., Rodriguez-Menocal, L., Salgado, M. & Van Badiavas, E. Mesenchymal Stem Cell Exosomes Induce Proliferation and Migration of Normal and Chronic Wound Fibroblasts, and Enhance Angiogenesis in Vitro. *Stem Cells Dev.* **24**, 1635–1647 (2015).
390. Anderson, J. D. *et al.* Comprehensive proteomic analysis of mesenchymal stem cell exosomes reveals modulation of angiogenesis via nuclear factor-kappaB signaling. *Stem Cells* **34**, 601–613 (2016).
391. Zhang, B. *et al.* Human Umbilical Cord Mesenchymal Stem Cell Exosomes Enhance Angiogenesis Through the Wnt4/β-Catenin Pathway. *Stem Cells Transl. Med.* **4**, 513–522 (2015).
392. Taraboletti, G. *et al.* Shedding of the matrix metalloproteinases MMP-2, MMP-9, and MT1-MMP as membrane vesicle-associated components by endothelial cells. *Am. J. Pathol.* **160**, 673–680 (2002).
393. Lombardo, G. *et al.* Activated Stat5 trafficking Via Endothelial Cell-derived Extracellular Vesicles Controls IL-3 Pro-angiogenic Paracrine Action. *Sci. Rep.* **6**, 1–14 (2016).
394. Kim, H. K., Song, K. S., Chung, J. H., Lee, K. R. & Lee, S. N. Platelet microparticles induce angiogenesis in vitro. *Br. J. Haematol.* **124**, 376–384 (2004).
395. Brill, A., Dashevsky, O., Rivo, J., Gozal, Y. & Varon, D. Platelet-derived microparticles induce angiogenesis and stimulate post-ischemic revascularization. *Cardiovasc. Res.* **67**, 30–38 (2005).
396. Vrijsen, K. R. *et al.* Cardiomyocyte progenitor cell-derived exosomes stimulate migration of endothelial cells. *J. Cell. Mol. Med.* **14**, 1064–1070 (2010).
397. Wiklander, O. P. B. *et al.* Extracellular vesicle in vivo biodistribution is determined by cell source, route of administration and targeting. *J. Extracell. Vesicles* **4**, 1–13 (2015).
398. Potapova, I. A. *et al.* Mesenchymal Stem Cells Support Migration, Extracellular Matrix Invasion, Proliferation, and Survival of Endothelial Cells In Vitro. *Stem Cells* **25**, 1761–1768 (2007).
399. Teixeira, F. G. *et al.* Modulation of the Mesenchymal Stem Cell Secretome Using

Computer-Controlled Bioreactors: Impact on Neuronal Cell Proliferation, Survival and Differentiation. *Sci. Rep.* **6**, 1–14 (2016).

400. Pinto, D. S. *et al.* Modulation of the in vitro angiogenic potential of human mesenchymal stromal cells from different tissue sources. *J. Cell. Physiol.* **235**, 7224–7238 (2020).
401. Hung, S.-C., Pochampally, R. R., Chen, S.-C., Hsu, S.-C. & Prockop, D. J. Angiogenic Effects of Human Multipotent Stromal Cell Conditioned Medium Activate the PI3K-Akt Pathway in Hypoxic Endothelial Cells to Inhibit Apoptosis, Increase Survival, and Stimulate Angiogenesis. *Stem Cells* **25**, 2363–2370 (2007).
402. Guo, M. *et al.* Autologous tumor cell–derived microparticle-based targeted chemotherapy in lung cancer patients with malignant pleural effusion. *Sci. Transl. Med.* **11**, 1–16 (2019).
403. Murphy, D. E. *et al.* Natural or Synthetic RNA Delivery: A Stoichiometric Comparison of Extracellular Vesicles and Synthetic Nanoparticles. *Nano Lett.* **21**, 1888–1895 (2021).
404. Tian, Y. *et al.* Biomaterials A doxorubicin delivery platform using engineered natural membrane vesicle exosomes for targeted tumor therapy. *Biomaterials* **35**, 2383–2390 (2014).
405. Kooijmans, S. A. A., Schiffelers, R. M., Zarovni, N. & Vago, R. Modulation of tissue tropism and biological activity of exosomes and other extracellular vesicles: New nanotools for cancer treatment. *Pharmacol. Res.* **111**, 487–500 (2016).
406. Morlacchi, S. *et al.* Insertion of a myc-tag within α-dystroglycan domains improves its biochemical and microscopic detection. *BMC Biochem.* **13**, 14 (2012).
407. Pinho, S. S. & Reis, C. A. Glycosylation in cancer: Mechanisms and clinical implications. *Nat. Rev. Cancer* **15**, 540–555 (2015).
408. Partridge, E. A. *et al.* Regulation of cytokine receptors by golgi N-glycan processing and endocytosis. *Science* **306**, 120–124 (2004).
409. Seales, E. C. *et al.* Hypersialylation of β1 integrins, observed in colon adenocarcinoma, may contribute to cancer progression by up-regulating cell motility. *Cancer Res.* **65**, 4645–4652 (2005).
410. de Jong, O. G. *et al.* A CRISPR-Cas9-based reporter system for single-cell detection of extracellular vesicle-mediated functional transfer of RNA. *Nat. Commun.* **11**, 1–13 (2020).
411. Grangier, A. *et al.* Technological advances towards extracellular vesicles mass production. *Adv. Drug Deliv. Rev.* 113843 (2021). doi:10.1016/j.addr.2021.113843
412. Yan, L., Liu, G. & Wu, X. Exosomes derived from umbilical cord mesenchymal stem cells in mechanical environment show improved osteochondral activity via upregulation of LncRNA H19. *J. Orthop. Transl.* **26**, 111–120 (2021).
413. Parolini, I. *et al.* Microenvironmental pH is a key factor for exosome traffic in tumor cells.

J. Biol. Chem. **284**, 34211–34222 (2009).

414. Chen, T., Guo, J., Yang, M., Zhu, X. & Cao, X. Chemokine-Containing Exosomes Are Released from Heat-Stressed Tumor Cells via Lipid Raft-Dependent Pathway and Act as Efficient Tumor Vaccine. *J. Immunol.* **186**, 2219–2228 (2011).
415. Hedlund, M., Nagaeva, O., Kargl, D., Baranov, V. & Mincheva-Nilsson, L. Thermal- and oxidative stress causes enhanced release of NKG2D ligand-bearing immunosuppressive exosomes in leukemia/lymphoma T and B cells. *PLoS One* **6**, e16899 (2011).
416. Scott, C. C. & Gruenberg, J. Ion flux and the function of endosomes and lysosomes: PH is just the start: The flux of ions across endosomal membranes influences endosome function not only through regulation of the luminal pH. *BioEssays* **33**, 103–110 (2011).
417. Edgar, J. R., Manna, P. T., Nishimura, S., Banting, G. & Robinson, M. S. Tetherin is an exosomal tether. *Elife* **5**, 1–19 (2016).
418. Ortega, F. G. *et al.* Interfering with endolysosomal trafficking enhances release of bioactive exosomes. *Nanomedicine Nanotechnology, Biol. Med.* **20**, 102014 (2019).
419. Savina, A., Furlán, M., Vidal, M. & Colombo, M. I. Exosome release is regulated by a calcium-dependent mechanism in K562 cells. *J. Biol. Chem.* **278**, 20083–20090 (2003).
420. Haneklaus, M. *et al.* Cutting Edge: miR-223 and EBV miR-BART15 Regulate the NLRP3 Inflammasome and IL-1 Production. *J. Immunol.* **189**, 3795–3799 (2012).
421. Guo, B. B., Bellingham, S. A. & Hill, A. F. Stimulating the release of exosomes increases the intercellular transfer of prions. *J. Biol. Chem.* **291**, 5128–5137 (2016).
422. Bobrie, A., Colombo, M., Krumeich, S., Raposo, G. & Théry, C. Diverse subpopulations of vesicles secreted by different intracellular mechanisms are present in exosome preparations obtained by differential ultracentrifugation. *J. Extracell. Vesicles* **1**, 18397 (2012).
423. Willms, E. *et al.* Cells release subpopulations of exosomes with distinct molecular and biological properties. *Sci. Rep.* **6**, 1–12 (2016).
424. Lässer, C., Jang, S. C. & Lötvall, J. Subpopulations of extracellular vesicles and their therapeutic potential. *Mol. Aspects Med.* **60**, 1–14 (2018).
425. Yang, T. *et al.* Delivery of Small Interfering RNA to Inhibit Vascular Endothelial Growth Factor in Zebrafish Using Natural Brain Endothelia Cell-Secreted Exosome Nanovesicles for the Treatment of Brain Cancer. *AAPS J.* **19**, 475–486 (2017).
426. Zhang, H. *et al.* Exosomes serve as nanoparticles to suppress tumor growth and angiogenesis in gastric cancer by delivering hepatocyte growth factor siRNA. *Cancer Sci.* **109**, 629–641 (2018).
427. Feng, Q. *et al.* Synergistic inhibition of breast cancer by co-delivery of VEGF siRNA

and paclitaxel via vapreotide-modified core-shell nanoparticles. *Biomaterials* **35**, 5028–5038 (2014).

428. Corso, G. *et al.* Reproducible and scalable purification of extracellular vesicles using combined bind-elute and size exclusion chromatography. *Sci. Rep.* **7**, 1–10 (2017).
429. Mathivanan, S. *et al.* Proteomics analysis of A33 immunoaffinity-purified exosomes released from the human colon tumor cell line LIM1215 reveals a tissue-specific protein signature. *Mol. Cell. Proteomics* **9**, 197–208 (2010).
430. Tengattini, S. Chromatographic Approaches for Purification and Analytical Characterization of Extracellular Vesicles: Recent Advancements. *Chromatographia* **82**, 415–424 (2019).
431. Jørgensen, M. *et al.* Extracellular Vesicle (EV) array: Microarray capturing of exosomes and other extracellular vesicles for multiplexed phenotyping. *J. Extracell. Vesicles* **2**, 20920 (2013).
432. Nakai, W. *et al.* A novel affinity-based method for the isolation of highly purified extracellular vesicles. *Sci. Rep.* **6**, 1–11 (2016).
433. Wan, Y. *et al.* Rapid magnetic isolation of extracellular vesicles via lipid-based nanoprobes. *Nat. Biomed. Eng.* **1**, 1–11 (2017).
434. Ishida, T. *et al.* Application of peptides with an affinity for phospholipid membranes during the automated purification of extracellular vesicles. *Sci. Rep.* **10**, 1–12 (2020).
435. Castilho, L. R., Anspach, F. B. & Deckwer, W. D. An integrated process for mammalian cell perfusion cultivation and product purification using a dynamic filter. *Biotechnol. Prog.* **18**, 776–781 (2002).
436. Godawat, R., Konstantinov, K., Rohani, M. & Warikoo, V. End-to-end integrated fully continuous production of recombinant monoclonal antibodies. *J. Biotechnol.* **213**, 13–19 (2015).
437. Carvalho, R. J. & Castilho, L. R. Tools Enabling Continuous and Integrated Upstream and Downstream Processes in the Manufacturing of Biologicals. in *Continuous Biomanufacturing - Innovative Technologies and Methods* (ed. Subramanian, G.) 31–68 (John Wiley & Sons, Inc., 2017). doi:10.1002/9783527699902.ch2
438. Gronemeyer, P., Thiess, H., Zobel-Roos, S., Ditz, R. & Strube, J. Integration of Upstream and Downstream in Continuous Biomanufacturing. in *Continuous Biomanufacturing - Innovative Technologies and Methods* (ed. Subramanian, G.) 481–510 (John Wiley & Sons, Inc., 2017). doi:10.1002/9783527699902.ch17
439. Bosch, S. *et al.* Trehalose prevents aggregation of exosomes and cryodamage. *Sci. Rep.* **6**, 1–11 (2016).
440. Jain, N. K. & Roy, I. Effect of trehalose on protein structure. *Protein Sci.* **18**, 24–36 (2009).

441. Gimona, M. *et al.* Critical considerations for the development of potency tests for therapeutic applications of mesenchymal stromal cell-derived small extracellular vesicles. *Cytotherapy* **23**, 373–380 (2021).

Research outputs

Publications in Scientific Journals

de Almeida Fuzeta, M., Bernardes, N., Oliveira, F.D., Costa, A.C., Fernandes-Platzgummer, A., Farinha, J.P., Rodrigues, C.A.V., Jung, S., Tseng, R.-J., Milligan, W., Lee, B., Castanho, M.A.R.B., Gaspar, D., Cabral, J.M.S., da Silva, C.L. (2020) Scalable Production of Human Mesenchymal Stromal Cell-Derived Extracellular Vesicles Under Serum-/Xeno-Free Conditions in a Microcarrier-Based Bioreactor Culture System. Front Cell Dev Biol 8:553444

de Almeida Fuzeta M., de Matos Branco A.D., Fernandes-Platzgummer A., da Silva C.L., Cabral J.M.S. (2019) Addressing the Manufacturing Challenges of Cell-Based Therapies. In: Advances in Biochemical Engineering/Biotechnology. Springer, Berlin, Heidelberg.

Pinto, D. , Bandeiras, C. , de Almeida Fuzeta, M. , Rodrigues, C. A., Jung, S. , Hashimura, Y. , Tseng, R. , Milligan, W. , Lee, B. , Ferreira, F. C., Silva, C. and Cabral, J. M. (2019), Scalable Manufacturing of Human Mesenchymal Stromal Cells in the Vertical-Wheel Bioreactor System: An Experimental and Economic Approach. Biotechnol. J. 14:1800716. doi:10.1002/biot.201800716

Oral Presentations in Conferences

Fuzeta MA, Milligan W, da Silva CL. (2021), Scalable Xeno-free Production of MSC-Derived EVs in Single-use Bioreactors. AventaCell Global Showcase. International Society for Cell and Gene Therapy Meeting 2021. New Orleans, Louisiana, USA.

Fuzeta MA, Oliveira FD, Costa AC, Fernandes-Platzgummer A, Jung S, Tseng RJ , Milligan W, Lee B, Bernardes N, Gaspar D, Cabral JMS, Lobato da Silva C. (2020), Scalable Production of Human Mesenchymal Stromal Cell (MSC)-Derived Extracellular Vesicles in Microcarrier-based Bioreactors under Xeno(geneic)-free Conditions. International Society for Cell and Gene Therapy Meeting 2020. Paris, France.

Fuzeta MA, Oliveira FD, Costa AC, Fernandes-Platzgummer A, Bernardes N, Gaspar D, Cabral JMS, Lobato da Silva C. (2019), Scalable Production of Human Mesenchymal Stem/Stromal Cell (MSC)-Derived Extracellular Vesicles in Vertical-Wheel Bioreactors. 11th International Meeting of the Portuguese Society for Stem Cells and Cell Therapies. Lisbon, Portugal.

Fuzeta MA, Oliveira FD, Costa AC, Fernandes-Platzgummer A, Bernardes N, Gaspar D, Cabral JMS, Lobato da Silva C. (2019), Manufacturing Human Mesenchymal Stem/Stromal Cell (MSC)-Derived Extracellular Vesicles in Vertical-Wheel Bioreactors for Cancer Therapy. EACR conference on Nanotechnology in Cancer. Cambridge, United Kingdom.

Poster Presentations in Conferences

Fuzeta MA, Bernardes N, van de Wakker SI, Roefs MT, Olijve W, Fernandes-Platzgummer A, Vader P, Sluijter JPG, Cabral JMS, da Silva CL (2021) Scalable bioreactor production and angiogenic potential of extracellular vesicles derived from human mesenchymal stromal cells. International Society for Extracellular Vesicles Meeting 2021 (Virtual).

Fuzeta MA, Oliveira FD, Costa AC, Fernandes-Platzgummer A, Jung S, Tseng RJ , Milligan W, Lee B, Bernardes N, Gaspar D, Cabral JMS, Lobato da Silva C. (2020), Manufacturing Extracellular Vesicles Derived from Human Mesenchymal Stromal Cells (MSC) in Bioreactors for Cancer Therapy. International Society for Extracellular Vesicles Meeting 2020. Philadelphia, Pennsylvania, USA.

Fuzeta, M.A., Bernardes, N., Oliveira, F.D., Costa, A.C., Fernandes-Platzgummer, A., Farinha, J.P., Rodrigues, C.A.V., Jung, S., Tseng, R.-J., Milligan, W., Lee, B., Castanho, M.A.R.B., Gaspar, D., Cabral, J.M.S., da Silva, C.L. (2020) Scalable Production of Human Mesenchymal Stromal Cell-Derived Extracellular Vesicles Under Serum-/Xeno-Free Conditions in a Microcarrier-Based Bioreactor Culture System. IST PhD Open Days. Lisbon, Portugal.

Fuzeta MA, Oliveira FD, Costa AC, Fernandes-Platzgummer A, Bernardes N, Gaspar D, Cabral JMS, Lobato da Silva C. (2019), Scalable Production of Human Mesenchymal Stem/Stromal Cell (MSC)-Derived Extracellular Vesicles in Vertical-Wheel Bioreactors for Cancer Therapy. Stem Cell Community Day. Lisbon, Portugal.

Fuzeta MA, Oliveira FD, Fernandes-Platzgummer A, Bernardes N, Gaspar D, Cabral JMS, Lobato da Silva C. (2019), Manufacturing Extracellular Vesicles Derived from Human Mesenchymal Stem/Stromal Cells (MSC) in Vertical-Wheel Bioreactors. Encontro Ciência 2019. Lisbon, Portugal.

Fuzeta MA, Oliveira FD, Fernandes-Platzgummer A, Bernardes N, Gaspar D, Cabral JMS, Lobato da Silva C. (2019), Manufacturing Human Mesenchymal Stem/Stromal Cell (MSC)-

Derived Extracellular Vesicles in Vertical-Wheel Bioreactors. XIII Annual CAML PhD Students Meeting. Lisbon, Portugal.

Fuzeta MA. Supervisors: Bernardes N, Gaspar D, Lobato da Silva C. (2019), Manufacturing Human Mesenchymal Stem/Stromal Cell (MSC)-Derived Extracellular Vesicles in Vertical-Wheel Bioreactors. IST PhD Open Days. Lisbon, Portugal.

Fuzeta MA, Pinto DS, Oliveira FD, Rodrigues CAV, Fernandes-Platzgummer A, Jung SH, Tseng RJ, Milligan W, Lee B, Bernardes N, Gaspar D, Lobato da Silva C, Cabral JMS. (2019), Manufacturing Human Mesenchymal Stem/Stromal Cells (MSC) and MSC-Derived Extracellular Vesicles in Vertical-Wheel Bioreactors. Advancing Manufacture of Cell and Gene Therapies VI. Coronado, California, USA.

Fuzeta MA, Pinto DS, Oliveira FD, Rodrigues CAV, Fernandes-Platzgummer A, Jung SH, Lee B, Bernardes N, Gaspar D, Lobato da Silva C, Cabral JMS. (2018), Manufacturing Human Mesenchymal Stem/Stromal Cells and Derived Extracellular Vesicles in Single-use Vertical-Wheel Bioreactors. Secretome Without Borders 2018. Braga, Portugal.